Micrometeoroid and Orbital Debris (MMOD) Shield Ballistic Limit Analysis Program

Shannon Ryan
USRA Lunar and Planetary Institute
Johnson Space Center, Houston, Texas

Eric L. Christiansen
Johnson Space Center, Houston, Texas

NASA STI Program ... in Profile

Since its founding, NASA has been dedicated to the advancement of aeronautics and space science. The NASA scientific and technical information (STI) program plays a key part in helping NASA maintain this important role.

The NASA STI program operates under the auspices of the Agency Chief Information Officer. It collects, organizes, provides for archiving, and disseminates NASA's STI. The NASA STI program provides access to the NASA Aeronautics and Space Database and its public interface, the NASA Technical Report Server, thus providing one of the largest collections of aeronautical and space science STI in the world. Results are published in both non-NASA channels and by NASA in the NASA STI Report Series, which includes the following report types:
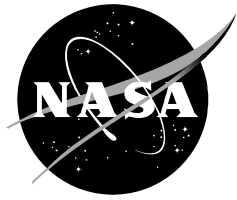
- TECHNICAL PUBLICATION. Reports of completed research or a major significant phase of research that present the results of NASA Programs and include extensive data or theoretical analysis. Includes compilations of significant scientific and technical data and information deemed to be of continuing reference value. NASA counterpart of peer-reviewed formal professional papers but has less stringent limitations on manuscript length and extent of graphic presentations.

- TECHNICAL MEMORANDUM. Scientific and technical findings that are preliminary or of specialized interest, e.g., quick release reports, working papers, and bibliographies that contain minimal annotation. Does not contain extensive analysis.

- CONTRACTOR REPORT. Scientific and technical findings by NASA-sponsored contractors and grantees.

- CONFERENCE PUBLICATION. Collected papers from scientific and technical conferences, symposia, seminars, or other meetings sponsored or co-sponsored by NASA.

- SPECIAL PUBLICATION. Scientific, technical, or historical information from NASA programs, projects, and missions, often concerned with subjects having substantial public interest.

- TECHNICAL TRANSLATION. English-language translations of foreign scientific and technical material pertinent to NASA's mission.

Specialized services also include creating custom thesauri, building customized databases, and organizing and publishing research results.

For more information about the NASA STI program, see the following:

- Access the NASA STI program home page at *http://www.sti.nasa.gov*

- E-mail your question via the Internet to help@sti.nasa.gov

- Fax your question to the NASA STI Help Desk at 443-757-5803

- Phone the NASA STI Help Desk at 443-757-5802

- Write to:
  NASA STI Help Desk
  NASA Center for AeroSpace Information
  7115 Standard Drive
  Hanover, MD 21076-1320

Micrometeoroid and Orbital Debris (MMOD) Shield Ballistic Limit Analysis Program

Shannon Ryan
USRA Lunar and Planetary Institute
Johnson Space Center, Houston, Texas

Eric L. Christiansen
Johnson Space Center, Houston, Texas

Available from:

Contents

Figures

Tables

Glossary of Terms and Abbreviations

AETB	aluminum enhanced thermal barrier
BLC	ballistic limit curve
BLE	ballistic limit equation
CFRP	carbon fiber reinforced plastic
CRV	crew return vehicle
EMI	Ernst-Mach-Institute
ESA	European Space Agency
GUI	graphical user interface
HC	honeycomb
HV	hypervelocity
HVI	hypervelocity impact
ISS	International Space Station
JSC	Johnson Space Center
JWST	James Webb Space Telescope
LV	low velocity
MDB	mesh double-bumper
MLI	multilayer insulation
MMOD	micrometeoroid and orbital debris
MS	multi-shock
NRL	Naval Research Laboratory
PICA	phenolic impregnated carbon ablator
RCC	Reinforced Carbon-Carbon
RTV	room temperature vulcanizing
S/d_p	standoff-to-projectile-diameter ratio
SiC	silicon carbide
SIP	strain isolation pad
SP	sandwich panel
SRL	Schaefer Ryan Lambert

Notations

AD   Areal density (g/cm^2)
c   Coefficient
C   Coefficient
d   Diameter (cm)
D_c Crater diameter (cm)
D_e Entry hole diameter (cm)
D_h Clear hole diameter (cm)
E   Modulus of elasticity (Pa)
g_i Failure coefficient
HB   Brinell hardness (HB)
k   Failure coefficient
K   Coefficient
K_{3s} Low-velocity coefficient
K_{3d} High-velocity coefficient
m   Mass
P_∞ Penetration depth (cm)
S   Spacing (cm)
t   Thickness (cm)
V   Projectile velocity (km/s)
ε Elongation to fail (%)
ρ Density (g/cm^3)
θ Impact angle measured from target normal to velocity vector (radians)
σ Rear wall yield stress (ksi) (Note: 1 ksi = 1,000 lb/in^2 = 6.895 MPa)

Subscripts:
b   Bumper
c   Critical
max   Maximum
n   Normal
p   Projectile
s   Shield
w   Rear wall
1..3   Individual bumpers, layers or spacing

Disclaimer

The Micrometeoroid and Orbital Debris (MMOD) Shield Ballistic Limit Analysis Program, which is herein referred to as "the program," that is described in this report is provided as a tool to aid in MMOD shield design and impact performance assessment. While every effort has been made to ensure accuracy of program calculations, the results should be used *only as a guide*. Furthermore, ballistic limit equations (BLEs) that were implemented in the program were selected as a result of their correct form for: implementation into the NASA MMOD risk analysis software (BUMPER-II), common acceptance and application in the MMOD field, and preliminary assessments of predictive accuracy. The selection of the BLEs that were implemented within the program should not be considered either an endorsement or a recommendation by NASA or the Johnson Space Center Hypervelocity Impact Technology Facility. Updates to the BLEs that are implemented within the program will be provided in light of new test data and validation assessments.

Introduction

A software program has been developed that enables the user to quickly and simply perform ballistic limit calculations for shield configurations that are subject to hypervelocity meteoroid/orbital debris (MMOD) impacts. This analysis program consists of two core modules: a design module and a performance module. The design module enables a user to calculate preliminary dimensions of a shield configuration (e.g., thicknesses/areal densities, spacing, etc.) for a "design" particle (diameter, density, impact velocity, incidence). The performance module enables a more detailed shielding analysis, providing the performance of a user-defined shielding configuration over the range of relevant in-orbit impact conditions.

Installation

The analysis program, which operates as an add-in to Microsoft Excel®, is distributed as an executable setup file (setup.exe). During installation, the user is prompted to enter the desired location of the program folder (the default is C:\Program Files\BLE Program\). To enable the program help to function correctly, a registry key is also installed. To include the analysis program in the list of Excel® add-ins, double-click on the .xla file. Once installed, the add-in is accessible through any Excel® workbook by clicking on the shield analysis program icon (Figure 1), which is located either in a new "Custom" toolbar for Excel® 2003, or within the add-ins tab of Excel® 2007. To deactivate/reactivate the add-in in Excel® 2003, use the Tools > Add-ins > Browse dialog. For Excel® 2007, the add-in is activated via the Excel® Options, which are accessed through the "Office Button." Within the Add-Ins tab of the Options window, the user should select "Go" to manage "Excel Add-ins." From there, the file can be located by browsing the local system.
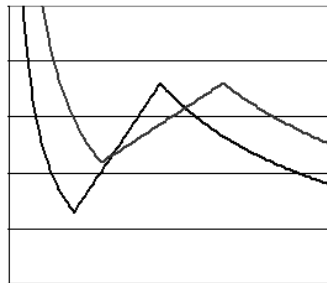
Figure 1: Ballistic limit analysis program icon.

Operation

Within the program, the design module is accessed via the "Shield design" tab at the top of the graphical user interface (GUI), and the performance module is accessed via the "Shield performance" tab. The main screen for the design and performance modules is shown in Figure 2. In both the design and the performance module, the user is requested to select a shield type (single-wall, dual-wall, Thermal Protection System (TPS), Advanced) and configuration (e.g., Advanced shield configurations include stuffed Whipple shield, multi-shock (MS), etc.). After selecting a shield configuration, the user clicks "Analyze" to enter the specific analysis sub-module. An example of the shield design window is shown in Figure 3 for a metallic Whipple shield configuration. To exit the program at any time, the user may click on the "Exit" button.
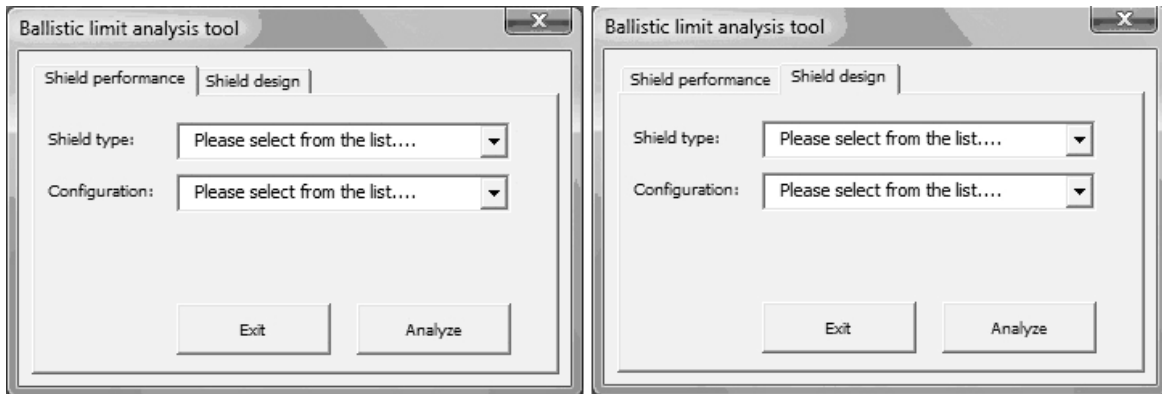
Figure 2: Main screen for the design and performance modules.
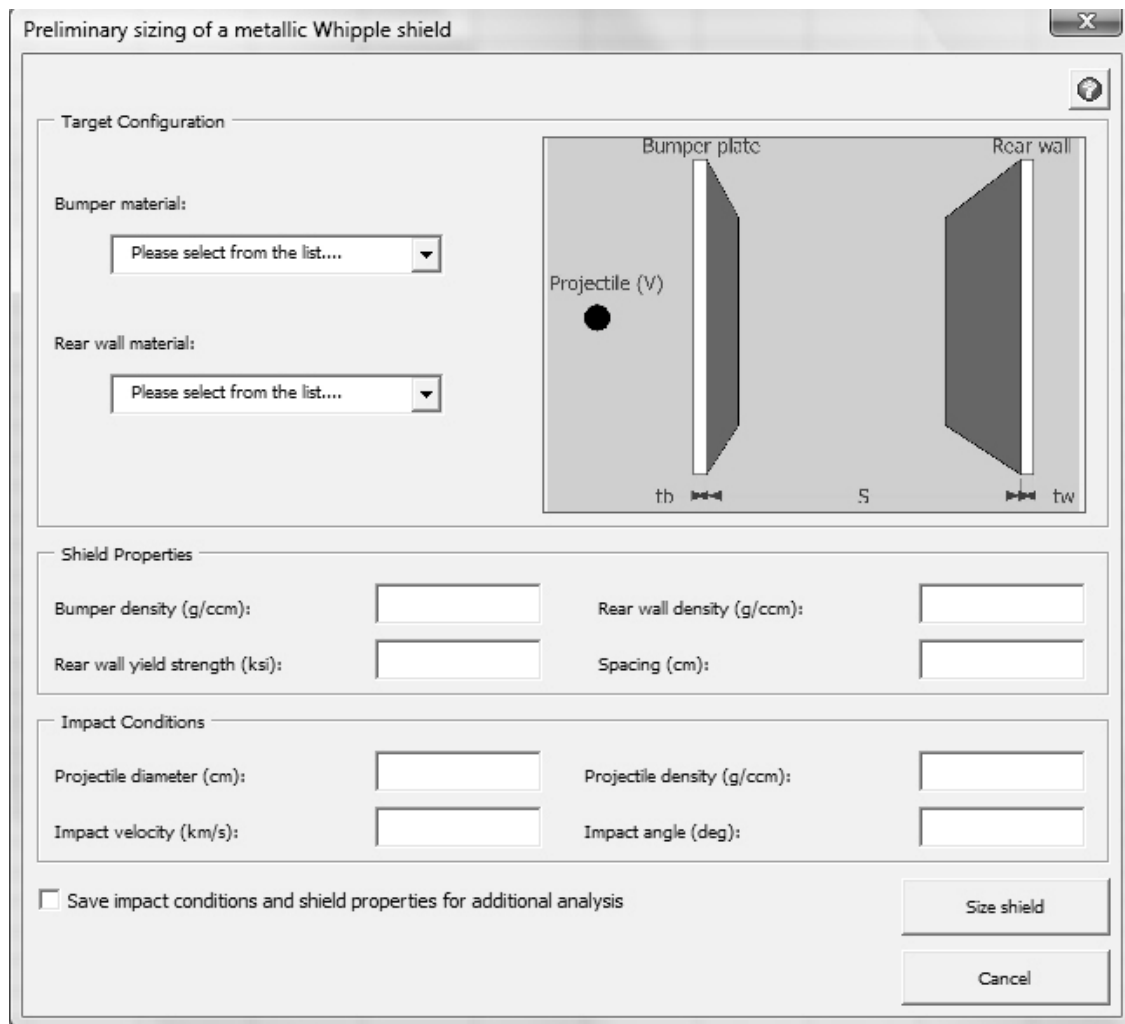
Figure 3: Metallic Whipple shield sizing window.

A schematic of the shield configuration is provided at the top of the GUI, along with the symbols for target components and spacing. The user can find help on the specific ballistic limit equation (BLE) that was selected by clicking on the help icon in the upper right corner of the window. For each shielding configuration, the input window takes on the same basic appearance. If the user would like to store the inputs

(shield properties, impact conditions) for further analysis, this can be achieved by checking the tick box in the lower left corner of the page. If the tick box is selected, the impact conditions and shield properties will be automatically entered when the user performs additional analyses on a matching configuration. The results of the analysis are written to the active Microsoft Excel® workbook. Each analysis is written to an individual worksheet that is renamed according to the format *configuration(number)*. For instance, if after initializing the analysis program the user performs a design analysis on a metallic Whipple shield, the resulting worksheet will be titled Whipple(1).

User Inputs, Material Properties, and Calculation Notes and Warnings

After selecting an analysis approach (i.e., design or performance) and a specific shielding configuration, the user is taken to the configuration sub-module where he/she is required to input shield parameters and impact conditions. For some shield types (e.g., metallic Whipple shield, triple-wall shield), the user is required to select component materials from a drop-down box (Figure 4). Included within the Shield Analysis program is a material properties database that includes density, yield strength, sound speed, and Brinell hardness values for a range of metals that are commonly used in space hardware. In Table 1, the list of materials that are included in the database and the corresponding material properties is provided (from [1], except where noted). When the user selects one of these materials from the drop-down menu, the relevant values are directly input into the user form (Figure 5).

Material	Density (g/cm^3)	Yield strength (ksi)	Sound speed (km/s)	Brinell hardness (BN)
Al 1100-O	2.71	5	5.05	23
Al 1100-H14	2.71	17	5.05	32
Al 2024-T3	2.77	50	5.11	120
Al 2024-T4	2.77	47	5.11	120
Al 2024-T351	2.77	47	5.11	120
Al 2219-T87	2.84	57	5.10	130
Al 2219-T851	2.84	51	5.10	130
Al 2219-T852	2.84	54	5.10	115
Al 3003-O	2.73	6	5.06	28
Al 3003-H12	2.73	18	5.06	35
Al 3003-H14	2.73	21	5.06	40
Al 6061-O	2.70	8	5.05	30
Al 6061-T6	2.70	40	5.05	95
Al 7075-T6	2.80	73	5.04	150
Al 7075-T73	2.80	63	5.04	135
Al 7178-T6	2.83	78	5.03	160
AMg6 aluminum	2.63	35	5.07	73
Ti-15V-3Cr-3Al-3Sn [2]	4.73	-	4.26	257
SS (CRES 15-5PH) [2]	7.80	-	-	-

Table 1: Material Properties Included in the Database
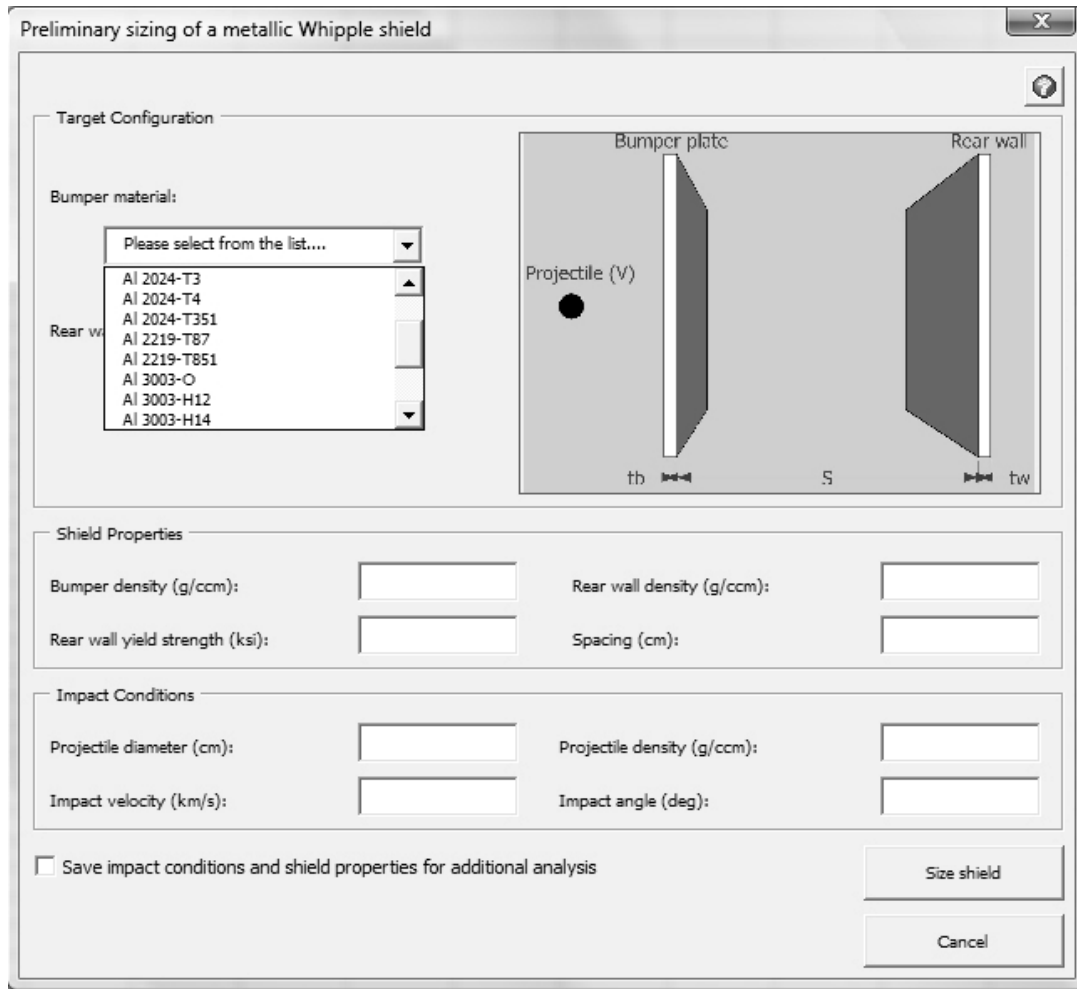
Figure 4: Selecting a material from the drop-down menu (metallic Whipple shield design module).
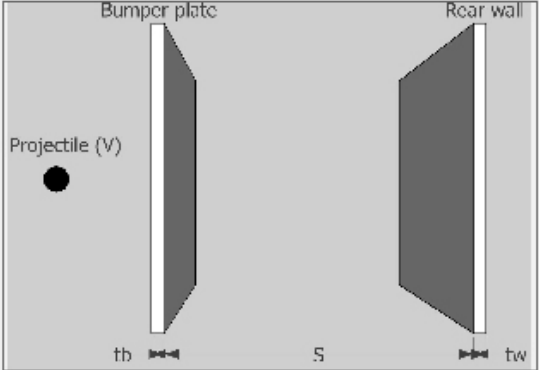
In Figure 5, a green "?" is shown beside the bumper material selection and a red "!" is found beside the rear wall material selection. These icons indicate the notes (in the case of question marks) and warnings (in the case of exclamation marks) that are relevant to the selection that can be viewed by clicking on the icon. An example warning dialog window is shown in Figure 6.

Figure 5: Direct insertion of material properties from the material property database (metallic Whipple shield design module).
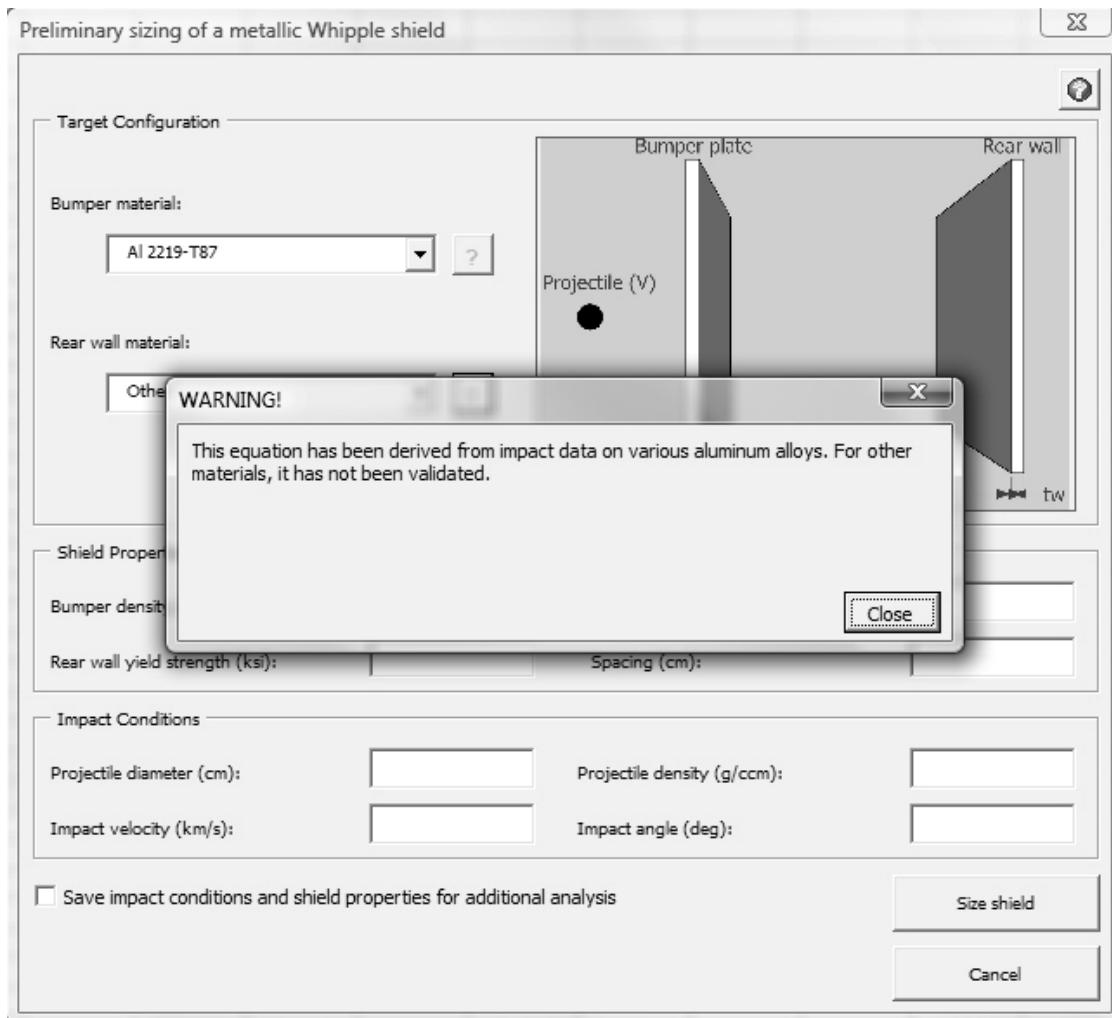
Figure 6: Example of warning dialog (metallic Whipple shield design module).

Ballistic limit curves

The performance module is used to assess the shielding capability of a specific shielding configuration over a complete range of impact conditions. Generally, this is presented as a curve that defines the failure (e.g., perforation) limits of the structure in terms of projectile diameter and impact velocity and that is known as a ballistic limit curve (BLC). For impact conditions that are below the curve, the shield is predicted to successfully defeat the impactor, while those impact conditions that are above the curve indicate predicted failure. Once the user has input all shield properties and impact conditions into the performance analysis window, a ballistic limit curve is generated by clicking on "Calculate and Plot." An example of the generated ballistic limit curve is shown in Figure 7. When multiple performance analyses are made, the ballistic limit curves are shown together on the same chart. The legend entries correspond to the worksheets containing the performance data.
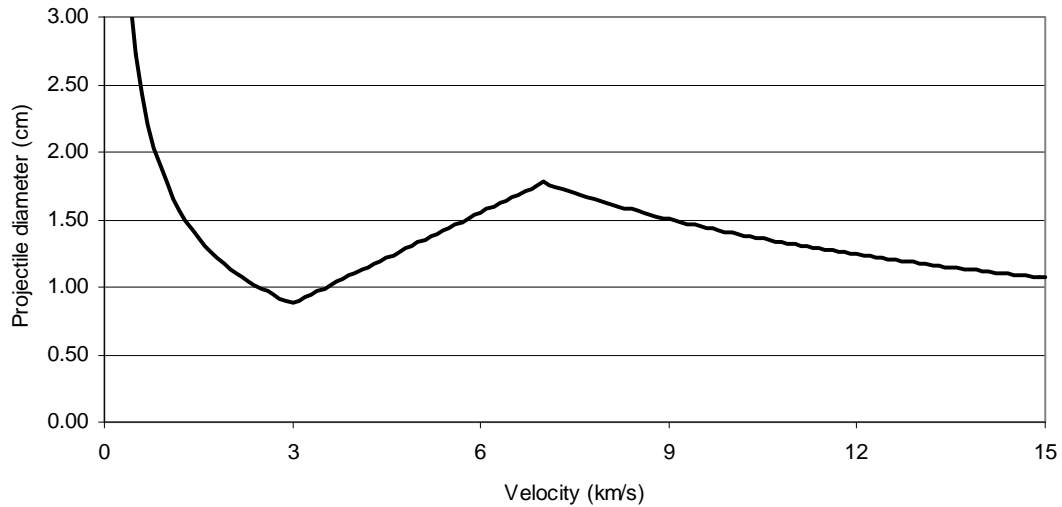
Figure 7: Output of the performance module-ballistic limit curve (metallic Whipple shield).

Ballistic Limit Equations

BLEs are expressed as either

- design equations, which can be used to size a shield to defend against a specific particle threat; or
- performance equations that define the failure limits of a shield configuration over the range of the impact conditions that are expected in orbit. These are commonly expressed in a form that is suitable for direct insertion in to risk assessment codes such as the NASA BUMPER code.

An overview of implemented design and performance BLEs for a range of common shielding and TPSs is made in this chapter. A technique for considering shielding performance against non-spherical projectiles is also reviewed, as well as techniques that enable the effect of multilayer insulation (MLI) to be accounted for.

Single wall

Metallic single wall

The Cour-Palais semi-infinite plate equation considers that the impact of a projectile into a semi-infinite plate that results in the formation of a hemispherical crater. As the thickness of the plate is decreased, the plate undergoes internal fracturing (incipient spallation), detachment of spalled material, and, finally, perforation when the entry crater and spallation area overlap. The metallic single-wall configuration is shown in Figure 8.
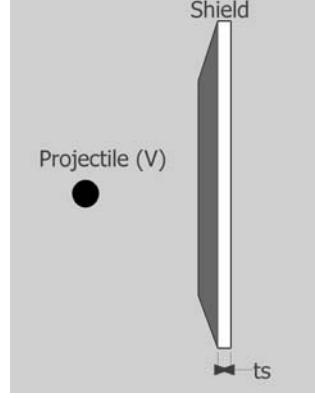
Figure 8: Metallic single-wall target schematic for application of the Cour-Palais semi-infinite plate equation.

The penetration depth into a semi-infinite target is calculated as

$$P_\infty = 5.24 d_p^{\,19/18} HB^{-0.25} \left(\rho_p / \rho_s\right)^{0.5} \left(V \cos\theta / C\right)^{2/3} \qquad \text{If } \left(\rho_p / \rho_s\right) < 1.5 \text{ (from [1])} \qquad (1)$$

$$P_\infty = 5.24 d_p^{\,19/18} HB^{-0.25} \left(\rho_p / \rho_s\right)^{2/3} \left(V \cos\theta / C\right)^{2/3} \qquad \text{If } \left(\rho_p / \rho_s\right) \geq 1.5 \text{ (from [4])} \qquad (2)$$

Required shielding thickness can be determined for a design particle, depending on the failure mode (from [3]),

$$\text{to prevent incipient spallation:} \qquad t_s \geq 3.0 P_\infty \qquad (3)$$

$$\text{to prevent detached spallation:} \qquad t_s \geq 2.2 P_\infty \qquad (4)$$

$$\text{to prevent perforation:} \qquad t_s \geq 1.8 P_\infty \qquad (5)$$

For a specific shielding configuration, the ballistic limit can be determined using

$$d_c = \left[\frac{t_s}{k} \cdot \frac{HB^{0.25}\left(\rho_s / \rho_p\right)^{0.5}}{5.24\left(V \cos\theta / C\right)^{2/3}} \right]^{18/19} \qquad \text{If } \left(\rho_p / \rho_s\right) < 1.5 \qquad (6)$$

$$d_c = \left[\frac{t_s}{k} \cdot \frac{HB^{0.25}\left(\rho_s / \rho_p\right)^{3/2}}{5.24\left(V \cos\theta / C\right)^{2/3}} \right]^{18/19} \qquad \text{If } \left(\rho_p / \rho_s\right) \geq 1.5 \qquad (7)$$

where $k = 3.0$; 2.2; 1.8 for incipient spallation, detached spallation, and perforation, respectively.

The validation overview is shown in Table 2.

	Validated for	Applied to	Comments
Materials	Aluminum	Aluminum	Failure parameter k derived for Al 2024-T3, is interchangeable with other alloys.
Impact angles	0° to 85°	Normal, oblique	Equation appears to slightly over-predict penetration depth for impact angles >45° [5]
Impact velocities	< 8 km/s	All	For velocities > 8 km/s, the equation is expected to be conservative.
Projectile diameters	0.05–1.27 cm	All	None.
Projectile materials	Aluminum, glass, steel, copper	All	None.

Table 2: Valid Application of the Cour-Palais Single-plate BLE

Titanium single wall

Penetration into a monolithic titanium shield is calculated with a slightly modified version of the Cour-Palais semi-infinite relationship, from [5]

$$P_\infty = 5.24 d_p HB^{-0.25} \left(\rho_p / \rho_s \right)^{0.5} \left(V \cos \theta / C \right)^{2/3} \tag{8}$$

Required shielding thickness can be determined for a design particle, depending on the failure mode,

to prevent incipient spallation: $\quad\quad t_s \geq 3.0 P_\infty \quad\quad\quad\quad\quad (9)$

to prevent detached spallation: $\quad\quad t_s \geq 2.4 P_\infty \quad\quad\quad\quad\quad (10)$

to prevent perforation: $\quad\quad\quad\quad\quad t_s \geq 1.8 P_\infty \quad\quad\quad\quad\quad (11)$

For a specific shielding configuration, the ballistic limit can be determined using

$$d_c = \frac{t_s}{k} \cdot \frac{HB^{0.25} \left(\rho_s / \rho_p \right)^{0.5}}{5.24 \left(V \cos \theta / C \right)^{2/3}} \tag{12}$$

where k = 3.0; 2.4; 1.8 for incipient spallation; detached spallation, and perforation, respectively.

Modifications to the Cour-Palais semi-infinite plate cratering relationship were made for monolithic titanium based on testing for the James Webb Space Telescope (JWST). Derivation was made from test data on rod and sheet stock Ti 15-3-3-3 at normal incidence and impact velocities that were between 6.4 and 7.0 km/s. Additional numerical simulation data were used for verification [5]. The validation overview is shown in Table 3.

Stainless-steel single wall

Penetration relationships for monolithic stainless-steel targets are provided in [1], which is derived from cratering experiments into CRES 15-5PH stainless steel. Material properties used in the aluminum and titanium alloy relationships (i.e., Brinell hardness and sound speed) are included in the material parameter, K, which is given as 0.345 in. [1].

	Validated for	Applied to	Comments
Materials	Titanium alloys	Titanium alloys	Baseline Ti alloy used for derivation of BLE is Ti-15V-3Cr-3Al-3Sn (bar and sheet form)
Impact angles	0°	Normal, oblique	Modified semi-infinite plate angle dependence (2/3rd power instead of 12/19)
Impact velocities	6.4-7.0 km/s	All	Modified semi-infinite plate velocity dependence (2/3rd power instead of 12/19)
Projectile diameters	mm-sized	All	None
Projectile materials	Aluminum	All	None

Table 3: Valid Application of the Titanium Single-plate BLE

Penetration depth is calculated as

$$P_\infty = K \cdot d_p \left(\rho_p / \rho_s \right)^{0.5} \left(V \cos\theta / C \right)^{2/3} \tag{13}$$

To prevent perforation, the required thickness of the panel is given as

$$t_s \geq 1.8 P_\infty \tag{14}$$

For a specific shielding configuration, the ballistic limit can be determined using

$$d_c = \left[\frac{t_s}{k} \cdot \frac{\left(\rho_s / \rho_p \right)^{0.5}}{K \left(V \cos\theta \right)^{2/3}} \right]^{18/19} \tag{15}$$

where $k = 1.8$ for perforation and $K = 0.345$.

A series of cratering experiments was performed on monolithic CRES 15-5PH stainless-steel targets to determine modifications to the Cour-Palais semi-infinite plate relationship [1]. Non-penetrating impacts were performed at normal and oblique incidence at high velocity to investigate crater formation in International Space Station (ISS) handrails that were impacted by MMOD projectiles. Additional test data remain unpublished. The validation overview is shown in Table 4.

	Validated for	Applied to	Comments
Materials	Stainless steel	Stainless steel	Derived from test data on CRES 15-5PH
Impact angles	0°, 45°, 60°, 75°	Normal, oblique	Maintains Cour-Palais semi-infinite plate angle dependence
Impact velocities	7.0±0.2 km/s	All	Maintains semi-infinite plate velocity dependence
Projectile diameters	mm-sized	All	None
Projectile materials	Aluminum	All	None

Table 4: Valid Application of the Stainless-steel Single-plate BLE

Carbon fiber reinforced plastic (CFRP) single wall

Crater formation and shock transmission in multilayer, non-isotropic materials such as CFRP is considerably different to that seen in metals. Schaefer et al. [7] propose a modification of the cratering equation that uses a single material parameter (K_{CFRP}) to describe the effect of material properties (e.g., Brinell hardness, density, sound speed). This factor is empirically adjusted to impact test data.

The penetration depth into a semi-infinite CFRP plate is given by Schaefer et al. as

$$P_\infty = K_{CFRP} \cdot d_p \cdot \rho_p^{0.5} \cdot \left(V \cos\theta \right)^{2/3} \tag{16}$$

where K_{CFRP} - Material constant $= 0.52$.

Eq. (16) was derived from testing on a single laminate and, as such, does not include the effect of shield density. To extend the application of this equation, a modified version is presented which includes the effect of density (based on the cratering relationship for aluminum alloys). The material parameter K_{CFRP} has been adjusted to fit the predictions of the existing equation for the tested material (i.e. $\rho_s = 1.42$ g/cm^3) as follows:

$$P_\infty = K_{CFRP} \cdot d_p \cdot \left(\rho_p / \rho_s \right)^{0.5} \cdot \left(V \cos\theta \right)^{2/3} \tag{17}$$

where K_{CFRP} - Material constant $= 0.62$

Required shielding thickness can be determined for a design particle depending on the failure mode as follows:

$$\text{to prevent detached spallation:} \qquad t_s \geq 3 P_\infty \tag{18}$$
$$\text{to prevent perforation:} \qquad t_s \geq 1.8 P_\infty \tag{19}$$

For a specific shielding configuration, the ballistic limit can be determined using

$$d_c = \frac{t_s \left(\rho_s / \rho_p \right)^{0.5}}{k \cdot K_{CFRP} \cdot \left(V \cos\theta \right)^{2/3}} \tag{20}$$

where $k = 3.0$; 1.8 for detached spallation and perforation, respectively.

The validation overview is shown in Table 5.

Fiberglass single wall

Similar to the stainless-steel penetration equation, a relationship has been derived from tests on e-glass/epoxy fiberglass composites (from [2]) as follows:

$$P_\infty = K \cdot d_p \left(\rho_p / \rho_s \right)^{0.5} \left(V \cos\theta / C \right)^{2/3} \tag{21}$$

For the fiberglass laminate that was tested ($\rho_s = 1.8$ g/cm3), the material constant K is given in [2] as 0.434.

	Validated for	Applied to	Comments
Materials	CFRP	CFRP	The dependence of ballistic limit on fiber/epoxy type, fiber volume content, weave type, lay-up, etc. are included in the parameter K_{CFRP} that has been validated for a 3.8-mm-thick quasi-isotropic laminate. For different configurations, this parameter may require empirical adjustment.
Impact angle	0°	Normal, oblique	None.
Impact velocities	5.8-6.6 km/s	All	None.
Projectile diameters	0.71-1.22 cm	All	None.
Projectile materials	Aluminum	All	None.

Table 5: Valid Application of the Schaefer BLE for CFRP Plates

To prevent perforation, the required thickness of the panel is calculated as

$$t_s \geq 1.8 P_\infty \tag{22}$$

For a specific shielding configuration, the ballistic limit can be determined using

$$d_c = \frac{t_s}{k} \cdot \frac{\left(\rho_s / \rho_p\right)^{0.5}}{K\left(V \cos\theta\right)^{2/3}} \tag{23}$$

where $k = 1.8$ for perforation and $K = 0.434$.

The fiberglass BLE was derived from testing on fiberglass replicates of shuttle Reinforced Carbon-Carbon (RCC) panels as part of the Return to Flight hypervelocity impact testing.

The validation overview is shown in Table 6.

	Validated for	Applied to	Comments
Materials	Fiberglass	Fiberglass	Material constant K is derived for an e-glass/epoxy composite with density, $\rho_s = 1.8$ g/cm^3. For other configurations, the equation is not validated.
Impact angles	0°, 30°, 45°, 60°, 90°	Normal, oblique	None
Impact velocities	6.8 km/s	All	None
Projectile diameters	mm-sized	All	None
Projectile materials	Aluminum	All	None

Table 6: Valid Application of the Fiberglass Single-plate BLE

Fused silica glass

BLEs for fused silica were developed during the Apollo Program to assess the risk that was associated with the crew module windows. The low tensile strength and brittle nature of glass leads to comparatively extensive internal fracturing and surface spallation with comparatively shallow crater depths. Impact craters generally have a central area of high damage that can appear white in color, surrounded by circular fracture patterns. Internal fracturing can also be observed within glass targets that are below the crater limits, the depth of which is of interest for fracture analysis. Crater diameter and depth measurements are defined in Figure 9 on a fused silica glass target with typical high-velocity impact damage features.

The penetration depth into semi-infinite glass is calculated as (from [3])

$$P_\infty = 0.53 \rho_p^{\,0.5} d^{19/18} \left(V \cos\theta \right)^{2/3} \tag{24}$$

Required shielding thickness can be determined for a design particle depending on the failure mode [2]

to prevent perforation:	$t_s \geq 2.0 P_\infty$	(25)
to prevent spallation:	$t_s \geq 3.0 P_\infty$	(26)
to prevent cracking:	$t_s \geq 7.0 P_\infty$	(27)
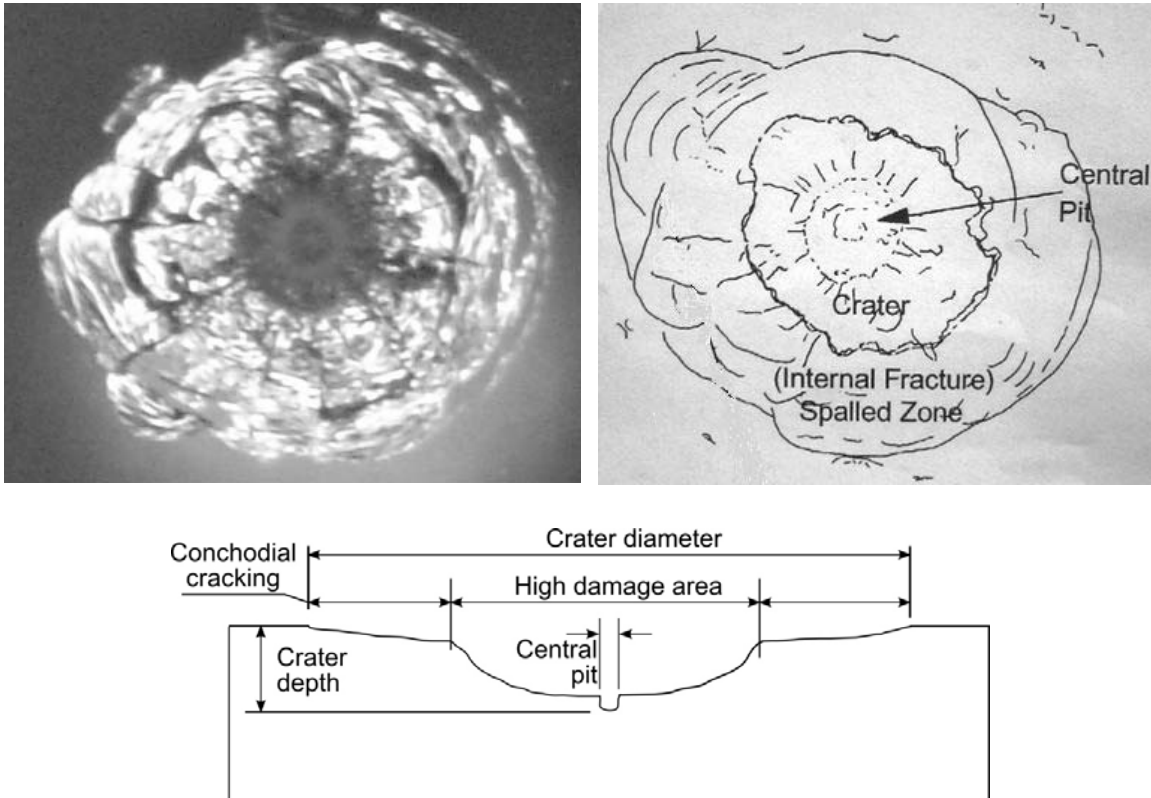
Figure 9: Damage characteristics and measurements in glass targets. Top: front view (photograph and schematic); bottom: damage measurement schematic (side view).

For a specific shielding configuration, the ballistic limit can be determined using

13

$$d_c = \left[1.89 \frac{t_s}{k \cdot \rho_p^{\,0.5} \cdot (V \cos\theta)^{2/3}} \right]^{18/19} \tag{28}$$

where $k = 3$; 2 for spallation and perforation, respectively.

Hypervelocity impact (HVI) on brittle glass targets results in front-side craters with large diameters relative to crater depth. The diameter of an impact crater in fused silica is calculated using (from [8])

$$D_c = 30.9 \rho_p^{\,0.44} d_p^{\,1.33} (V \cos\theta)^{0.44} \tag{29}$$

Non-perforating damages on glass structures (e.g., an optical measurement device) can also be considered as a failure criterion if the local surface damage exceeds an operational requirement. For calculating the critical particle size based on allowable impact crater diameter ($D_{c,max}$), Eq. (29) is rearranged as follows:

$$d_c = \left(\frac{D_{c,max}}{30.9 \cdot \rho_p^{\,0.44} (V \cos\theta)^{0.44}} \right)^{1/1.33} \tag{30}$$

A considerable amount of test data for HVI on fused silica glass exist as a result of the application of fused silica glass on NASA spacecraft (e.g., Apollo, shuttle, ISS, etc.). Impact tests data cover a range of projectile materials, impact velocities, and impact angles (e.g., [9]).

The validation overview is shown in Table 7.

	Validated for	Applied to	Comments
Materials	Fused silica glass	Fused silica glass	None.
Impact angle	~0°, 30°, 45°, 60°	Normal, oblique	None.
Impact velocities	~2.7–12 km/s	All	None.
Projectile diameters	0.14–0.40 cm	All	Documentation of impact test data limited.
Projectile materials	Aluminum, glass, steel, Nylon, aluminum-oxide, copper	All	Impact tests using borosilicate glass and Pyrex glass projectiles followed different velocity dependence; however. the two-thirds power was selected based on applicable projectile diameters.

Table 7: Valid Application of the Cratering Equation for Fused Silica Glass Targets

Fused Quartz Glass

Fused quartz glass is used, for instance, in place of fused silica glass on Russian components of the ISS. The primary difference between the two materials arises from the difference in manufacturing techniques where fused quartz is manufactured from quartz crystals, and fused silica glass is produced using high-purity silica sand. The penetration characteristics of the two glasses are slightly different, and as such, a modification to the semi-infinite silica glass equation is proposed (from [10]).

$$P_\infty = 0.758\rho_p{}^{0.5}d^{19/18}\left(V\cos\theta\right)^{2/3} \qquad (31)$$

Required shielding thickness can be determined for a design particle depending on the failure mode, similar to that for fused silica glass.

To prevent perforation: $\quad t_s \geq 2.0P_\infty \qquad (32)$

To prevent spallation: $\quad t_s \geq 3.0P_\infty \qquad (33)$

To prevent cracking: $\quad t_s \geq 7.0P_\infty \qquad (34)$

For a specific shielding configuration, the ballistic limit can be determined using

$$d_c = \left[1.32\frac{t_s}{k\cdot\rho_p{}^{0.5}\cdot\left(V\cos\theta\right)^{2/3}}\right]^{18/19} \qquad (35)$$

where $\quad k = 3; 2$ for spallation and perforation, respectively.

The diameter of a crater that is produced by impact on a semi-infinite fused quartz glass target is calculated using

$$D_c = 15.1\rho_p{}^{0.44}d_p{}^{1.33}\left(V\cos\theta\right)^{0.44} \qquad (36)$$

Expressed in terms of shield performance,

$$d_c = \left(\frac{D_{c,\text{max}}}{15.1\cdot\rho_p{}^{0.44}\left(V\cos\theta\right)^{0.44}}\right)^{1/1.33} \qquad (37)$$

A series of nine HVI tests performed at the NASA Johnson Space Center (JSC) on fused quartz glass that was manufactured by the Russian Institute of Technical Glass (Moscow), was used to modify the semi-infinite cratering equation coefficient (0.758) and front side crater diameter equation coefficient (15.1) using a method of least squares regression fit.

The validation overview is shown in Table 8.

Polycarbonate

Polycarbonates are commonly used as protective covers for more fragile glass windows (e.g., ISS hatch windows) due to its significantly higher impact strength. Subsequently, the penetration depth into polycarbonate is less than that of glass or acrylic, and is calculated (from [2]) as

$$P_\infty = d_p\rho_p{}^{1/3}V^{2/3}\left(V\cos\theta\right)^{1/3} \qquad (38)$$

15

	Validated for	Applied to	Comments
Materials	Fused quartz glass	Fused quartz glass	Modifications to the fused silica glass penetration depth and crater diameter equation were made using data from nine HVI tests performed at the NASA JSC. Density, projectile diameter, and impact velocity dependence were all maintained.
Impact angle	0°, 45°, 60°	Normal, oblique	None.
Impact velocities	6.61–6.97 km/s	All	None.
Projectile diameters	0.07–0.20 cm	All	None.
Projectile materials	Aluminum	All	None.

Table 8: Valid Application of the Cratering Equation for Fused Quartz Glass Targets

Required shielding thickness can be determined for a design particle depending on the failure mode, the same as those considered for fused silica glass.

To prevent perforation: $\quad t_s \geq P_\infty / 1.04$ (39)

To prevent detached spallation: $\quad t_s \geq P_\infty / 0.98$ (40)

To prevent attached spallation: $\quad t_s \geq P_\infty / 0.65$ (41)

For a specific shielding configuration, the ballistic limit can be determined using

$$d_c = \frac{k \cdot t_s}{\rho_p^{1/3} \cdot V^{2/3} \cdot (\cos\theta)^{1/3}}$$ (42)

where $\quad k = 0.65; 0.98; 1.04$ for attached spallation; detached spallation, and perforation, respectively

The validation overview is shown in Table 9.

	Validated for	Applied to	Comments
Materials	Polycarbonate	Polycarbonate	Equations derived for Hyzod AR, an amorphous thermoplastic with a hard coated surface (manufactured by Sheffield Plastics, Inc.).
Impact angle	0°, 45°	Normal, oblique	None
Impact velocities	4.02–7.09 km/s	All	None
Projectile diameters	1.0–3.0 cm	All	None
Projectile materials	Aluminum	All	None

Table 9: Valid Application of the Cratering Equation for Polycarbonate Targets

Dual wall

Metallic Whipple shield

A Whipple shield consists of a thin sacrificial bumper and rear wall, with some interior spacing (shown in Figure 10).
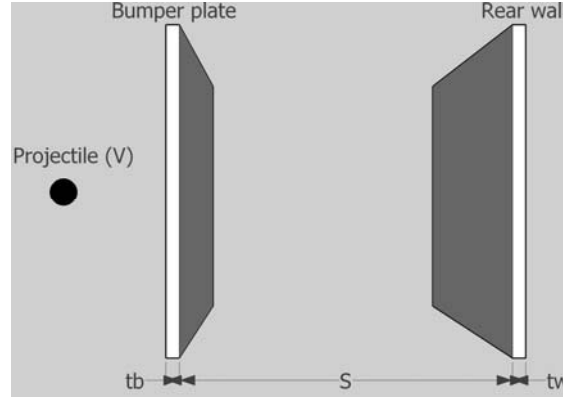
Figure 10: Metallic Whipple shield configuration for application of the Whipple shield BLE.

Bumper and rear wall thicknesses for defeating a design particle are sized with the JSC Whipple shield equation for a bumper-thickness-to-projectile-diameter ratio that is optimized for projectile fragmentation and dispersion (only valid for impact velocities > 7 km/s).

$$t_b = c_b d_p \frac{\rho_p}{\rho_b} \tag{43}$$

where $c_b = 0.25$ when $15 > S/d_p < 30$ and $c_b = 0.20$ when $S/d_p \geq 30$ (for aluminum on aluminum impacts)

$$t_w = c_w d_p^{0.5} \left(\rho_p \rho_b\right)^{1/6} m_p^{1/3} \left(V \cos\theta / S^{0.5}\right) \left(70/\sigma_y\right)^{0.5} \tag{44}$$

where $c_w = 0.16$ cm^2-sec/g$^{2/3}$-km (for aluminum on aluminum impacts)

The ballistic limit of a specific shielding configuration is defined by the JSC Whipple shield equation in three parts, each of which corresponds to conditions of the projectile following impact with the bumper plate. The low-velocity (LV) regime is defined for impacts in which the projectile perforates the bumper plate without fragmenting, leading to impact of an intact (albeit deformed) projectile on the shield rear wall. Once impact velocities are increased such that shock amplitudes are sufficient to induce projectile fragmentation, this is termed the intermediate (or shatter) regime. Further increases in velocity lead to additional projectile fragmentation (and eventually melting), providing a more equally dispersed fragment cloud of smaller particles with increasing velocity that is progressively less lethal to the shield rear wall (shielding performance thus increases with impact velocity in the intermediate regime). The onset of the hypervelocity (HV) regime is defined as the point at which further increases in impact velocity lead to a reduction in performance of the Whipple shield (i.e., increased fragment cloud lethality).

In the HV regime, Gehrig [11] found that for (tb/dp) ratios above 0.25, the required thickness of a Whipple shield rear wall was nearly constant, as shown in Figure 11. However, thinner bumpers lead to a sharp increase in rear wall thickness due to incomplete projectile fragmentation.

For sufficiently thick bumpers, i.e.,

$$\frac{t_b}{d_p} \geq 0.25 \qquad\qquad \text{for } 15 < S/d_p < 30 \qquad\qquad (45)$$

$$\frac{t_b}{d_p} \geq 0.20 \qquad\qquad \text{for } S/d_p \geq 30 \qquad\qquad (46)$$

the JSC Whipple shield equation (new non-optimum) is applied.
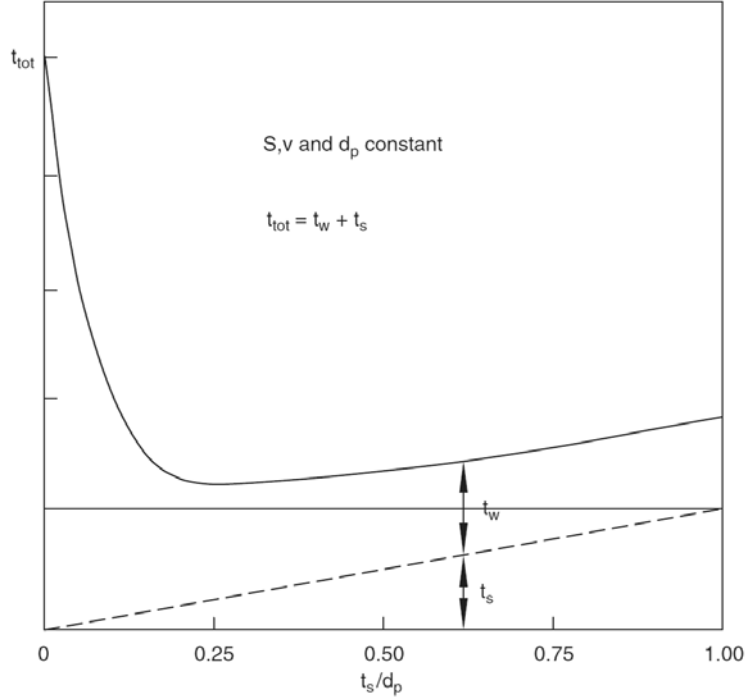
Figure 11: The effect of bumper thickness to projectile diameter ratio on required total Whipple shield thickness [12] (note: t_s indicates bumper thickness).

For the LV regime ($V/\cos\theta \leq V_{LV}$),

$$d_c = \left[\frac{t_w \left(\dfrac{\sigma_y}{40} \right)^{0.5} + t_b}{0.6 \left(\cos\theta \right)^{5/3} \rho_p^{0.5} V^{2/3}} \right]^{18/19} \qquad\qquad (47)$$

For the HV regime ($V/\cos\theta \geq V_{HV}$),

$$d_c = 3.918 \frac{t_w^{2/3} S^{1/3} \left(\sigma/70 \right)^{1/3}}{\rho_p^{1/3} \rho_b^{1/9} \left(V \cos\theta \right)^{2/3}} \qquad\qquad (48)$$

18

For the intermediate-velocity regime ($V_{LV} < V/\cos\theta < V_{HV}$),

$$d_c = d_c\left(V_{LV}\right)\times\left(1.75-\left(V\cos\theta\right)/4\right)+d_c\left(V_{HV}\right)\times\left(\left(V\cos\theta\right)/4-0.75\right)$$

(49)

For aluminum on aluminum impact, the transition from low-intermediate (V_{LV}) and intermediate-HV (V_{HV}) regimes occurs at 3 and 7 km/s, respectively.

To extend the application of the JSC Whipple shield equation to configurations with under-sized bumper plates, Reimerdes et al. [12] proposed a modification of shield performance based on the degradation of projectile fragmentation efficiency, F_2^*; i.e.,

$$d_c = 3.918\,F_2^* \frac{t_w^{2/3}S^{1/3}\left(\sigma/70\right)^{1/3}}{\rho_p^{1/3}\rho_b^{1/9}\left(V\cos\theta\right)^{2/3}}$$

(50)

where $\quad V_{HV} = 7$ km/s

The formulation of factor F_2^* is given as

$$F_2^* = \begin{cases} 1 & ,\left(t_b/d_p\right)\geq\left(t_b/d_p\right)_{crit} \\ r_{S/D}-2\dfrac{\left(t_b/d_p\right)}{\left(t_b/d_p\right)_{crit}}\left(r_{S/D}-1\right)+\left(\dfrac{\left(t_b/d_p\right)}{\left(t_b/d_p\right)_{crit}}\right)^2\left(r_{S/D}-1\right) & ,\left(t_b/d_p\right)<\left(t_b/d_p\right)_{crit} \end{cases}$$

(51)

where $\quad \left(t_b/d_p\right)_{crit} = 0.25$

The term $r_{S/D}$ in Eq. (51) is the ratio between required rear wall thickness for the condition when no bumper is present (i.e., $t_b = 0$), and the rear wall thickness when the bumper is properly sized according to Eq. (43) (i.e., $t_b/d_p = (t_b/d_p)_{crit}$).

$$r_{S/D} = \frac{t_w\left(t_b=0\right)}{t_w\left(t_b/d_p=\left(t_b/d_p\right)_{crit}\right)}$$

(52)

The term $r_{S/D}$ is evaluated once at $V = V_{HV}$, from which the values of F_2^* and d_p are found iteratively using Eq. (51) and Eq. (50), respectively. To automate the iterative procedure, a minimization function (type: golden section search) has been implemented. For more details, see [13].

In the LV regime (i.e., $V/\cos\theta \leq V_{LV}$), the Reimerdes-modified Whipple shield equation is given as

$$d_c = \left[\frac{t_w/k+t_s}{0.796K_\infty\rho_p^{0.518}V_n^{2/3}}\right]^{18/19}$$

(53)

19

The onset of projectile fragmentation (i.e., LV to shatter regime limit) was found by Maiden et al [14] to depend on bumper thickness to projectile diameter ratio (t_b/d_p), a finding that was visually confirmed by Piekutowsi in [15]. Reimerdes defined the onset of projectile fragmentation (i.e., V_{LV}) by the linear regression fit that is shown in Figure 12; and equal to

$$V_{LV} = 1.853 + 0.397 \left(\frac{t_b}{d_p} \right)^{-0.565} \tag{54}$$
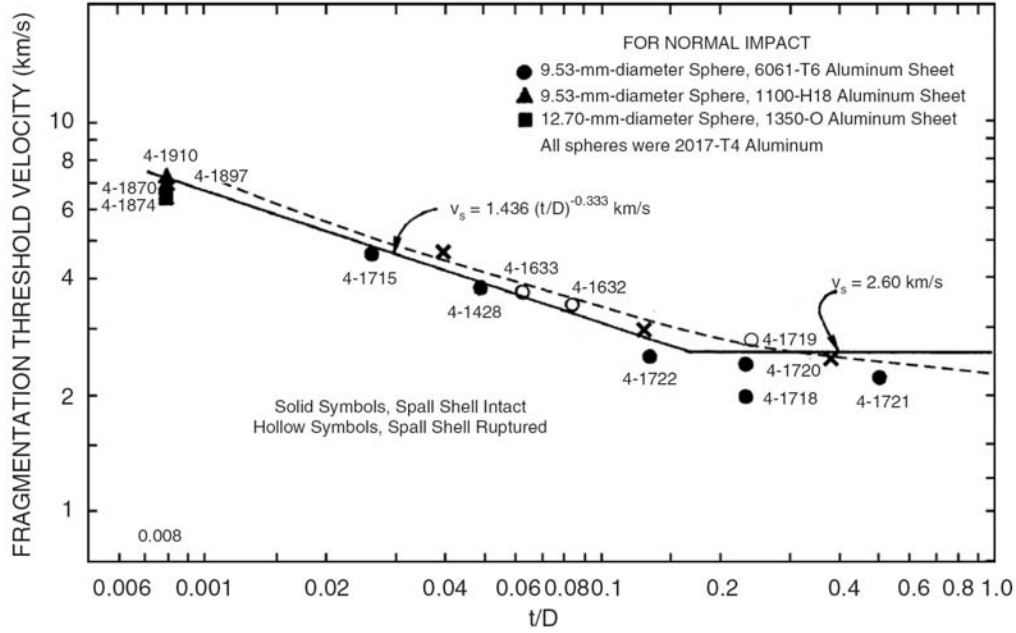
Figure 12: The onset of spherical projectile fragmentation for aluminum-on-aluminum impacts depending on the ratio of bumper plate thickness (t) to projectile diameter (D). Dashed curve is linear regression from [12].

For oblique impact, Christiansen [4] found that at angles that are above 65°, the majority of rear wall damage is induced by bumper fragments. As such, for higher angles of obliquity, the critical particle size should be constrained to that at 65°; i.e.,

$$d_c \left(\theta > 65^\circ \right) = d_c \left(\theta = 65^\circ \right) \tag{55}$$

Given its application during the Apollo mission and the fact that the metallic Whipple shield is the baseline of most MMOD shielding configurations, a considerable database of HV impact test results exists. The results of just under 200 tests that were either performed at, or funded by, NASA JSC on a wide variety of aluminum Whipple shield configurations are reported in [10]. These experiments cover a range of projectile diameters (0.04 to 1.9 cm), projectile materials (Nylon, glass, aluminum), impact velocities (6.7 to 7.5 km/s), bumper thickness to projectile diameter ratios (0.08 to 0.64), shield spacing to projectile diameter ratios (13 to 96). All tests were performed on aluminum alloys at normal incidence ($\theta=0°$), at or close to the target ballistic limit. For the Reimerdes-modified equations, eight additional tests were performed for conditions below the $(t_b/d_p)_{crit}$ limit. The validation overview is shown in Table 10.

	Validated for	Applied to	Comments
Materials	Aluminum	Aluminum	HV performance normalized to Al7075-T6 data, LV performance normalized to Al6061-T6
Impact angles	0°-85°	Normal, oblique	The Reimerdes modification was derived from tests at normal incidence only.
Impact velocities	2.5–8 km/s	All	None,
Projectile diameters	Up to 1.9 cm	All	For projectile-diameter-to-shield-spacing ratios $(d_p/S) < 15$, the critical projectile diameter in the HV regime may be non-conservatively predicted.
Projectile materials	Copper, glass, Aluminum, Nylon	All	None,

Table 10: Valid Application of the Whipple Shield BLE

Honeycomb sandwich panel

The Schaefer Ryan Lambert (SRL) triple-wall BLE [17][18] is applicable with dual- and triple-wall structures. To enable this, the equation converges to a dual-wall solution in the case of zero rear wall thickness ($t_w = 0$) or zero spacing between the bumper plate and the rear wall ($S_2 = 0$). The equation incorporates fit factors (K_{3S}, K_{3D}) from the European Space Agency (ESA) triple-wall equation [19] to account for inclusion of honeycomb sandwich panels (Figure 13).
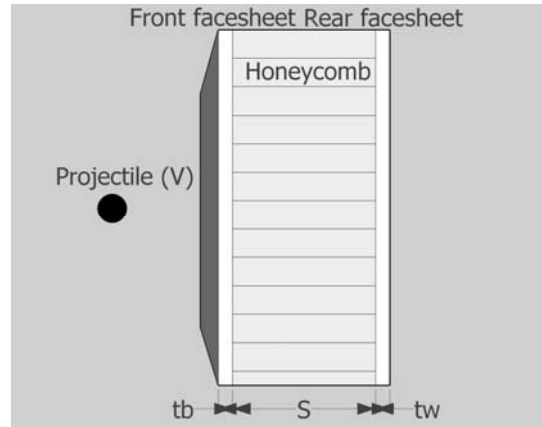
Figure 13: Honeycomb sandwich panel configurations applicable for application of the SRL triple-wall BLE.

Calculations are made using aluminum thicknesses, which are calculated for non-aluminum materials using equivalent areal densities; i.e.,

$$t_{al,eq} = t_{CFRP} \cdot \frac{\rho_{CFRP}}{\rho_{al}} \tag{56}$$

For sizing the facesheets of a honeycomb sandwich panel, an equal thickness of the front and rear facesheet is assumed. Facesheet sizing is performed using

$$t_b = t_w = 0.8056 \cdot d_p^{3/2} K_{3D} \rho_p^{1/2} \rho_b^{1/6} S^{-1/2} V \left(\cos\theta\right)^{3\delta/2} \left(70/\sigma_y\right)^{1/2} \tag{57}$$

In a manner that is similar to that of the JSC Whipple shield equation, the SRL triple-wall equation calculates the ballistic limit of a structure in three parts.

In the LV regime, $V/\cos\theta \leq V_{LV}$:

$$d_c = \left[\frac{t_w/K_{3S} \cdot (\sigma/40)^{1/2} + t_b}{0.6(\cos\theta)^\delta \rho_p^{1/2} V^{2/3}} \right]^{18/19} \tag{58}$$

In the HV regime, $V/\cos\theta \geq V_{HV}$:

$$d_c = \frac{1.155 \cdot S^{1/3} t_w^{2/3} \cdot \left(\dfrac{\sigma_y}{70} \right)^{1/3}}{K_{3D}^{2/3} \rho_p^{1/3} \rho_b^{1/9} V^{2/3} (\cos\theta)^\delta} \tag{59}$$

For $V_{LV} < V/\cos\theta < V_{HV}$, linear interpolation is used; i.e.,

$$d_c = d_c(V_{LV}) + \frac{[d_c(V_{HV}) - d_c(V_{LV})]}{V_{HV} - V_{LV}} \times (V - V_{LV}) \tag{60}$$

Impact regime transition velocities (V_{LV}, V_{HV}) are dependent on the outer bumper and projectile material. In [17], a one-dimensional shock impedance match analysis was performed to determine transition velocities for impact of aluminum on CFRP. An overview of parameters that are applicable with the SRL triple-wall equation is given in Table 11.

Outer bumper	V_{LV}	V_{HV}	K_{3S}	K_{3D}	δ
Aluminum*	3	7	1.4	0.4	4/3 if $45 \geq \theta \leq 65°$ 5/4 if $45 < \theta > 65°$
CFRP	4.2	8.4	1.1	0.4	4/3
Other	3	7	1.4	0.4	4/3 if $45 \geq \theta \leq 65°$ 5/4 if $45 < \theta > 65°$

* For K3S=1.0, K3D=0.16, $\delta = 5/3$ the SRL equation is equivalent to the JSC Whipple shield equation

Table 11: List of Fit Parameters for the SRL Triple-wall Equation (Aluminum Impactor)

The SRL equation was adjusted using approximately 200 impact tests on various dual- and triple-wall structures. For CFRP, approximately 90 impact tests were performed using six different sandwich panel configurations and an aluminum plate for the rear wall [17]. The tests were performed with impact velocities ranging from 2 to 8 km/s, at three different impact angles (0°, 45°, and 60°). For aluminum targets, about 110 impact experiments were used including both aluminum Whipple shields and honeycomb sandwich panels [18]. The impact experiments used representative space hardware for the rear wall structure (e.g., CFRP overwrapped pressure vessels, fuel pipes, heat pipes, etc.).

The validation overview is shown in Table 12.

	Validated for	Applied to	Comments
Bumper materials	CFRP, Aluminum	CFRP, Aluminum	For CFRP, use equivalent Al thicknesses.
Impact angles	0°, 45°, 60°	Normal, oblique	No limit angle specified.
Impact velocities	2–8 km/s	All	None.
Projectile diameters	0.08–0.5 cm	All	None.
Projectile materials	Aluminum	All	None.

Table 12: Valid Application of the SRL Triple-wall BLE

Triple wall

For triple-wall configurations (e.g., metallic triple-wall, sandwich panel, and pressure hull, etc.), the SRL triple-wall BLE is applied (see Figure 14).
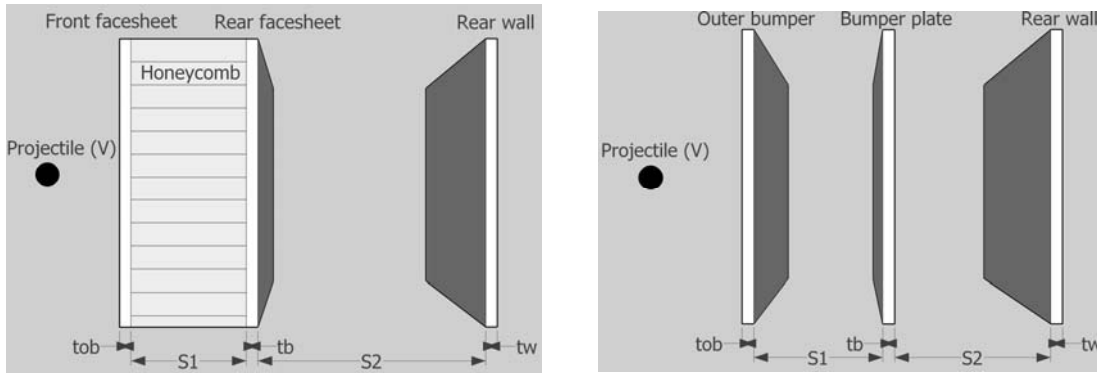
Figure 14: Applicable configurations for the SRL triple-wall BLE.

Assuming an equal thickness of the outer and inner bumper plates (i.e., $t_{ob} = t_b$), the performance of a triple-wall shield as described by the SRL equation improves as mass is concentrated in the rear wall (i.e., $t_b/t_w \rightarrow 0$). Similarly, as total spacing is biased more towards bumper spacing (i.e., $S_1/S_2 \rightarrow \infty$) the shield performance also increases (for $S_{total}/t_{total} \leq 30$). As the thicknesses of the inner bumper and rear wall are coupled in the SRL triple-wall equation for impacts at HV, the bumper plate is sized as a percentage of rear wall thickness, the lower limit of which is restricted based on available test data [20].

For CFRP bumper plates and an aluminum rear wall,

$$t_{ob} = t_b = c_b t_w \tag{61}$$

$$t_w = \left[0.866 \frac{d_p K_{3D}^{2/3} \rho_p^{1/3} \rho_{ob}^{1/9} V^{2/3} (\cos\theta)^\delta (70/\sigma_y)^{1/3}}{(c_b + K_{tw})^{2/3} S_1^{1/3} + K_{S2} S_2^\beta (\cos\theta)^{-\varepsilon}} \right]^{3/2} \tag{62}$$

where $c_b = 0.1$ and shield properties (t, σ, ρ) are for a reference aluminum.

For all-aluminum configurations, the rear wall design equation is complicated by the dependence of the t_w fit parameter in the hypervelocity regime (γ). Rear wall thickness is calculated using

$$t_w = \frac{-\frac{1}{2}\left(C_2 - \sqrt{C_2{}^2 + 4C_1C_3}\right)C_3 - \frac{\left(C_2 - \sqrt{C_2{}^2 + 4C_1C_3}\right)C_2{}^2}{2C_1} - C_2C_3}{C_1{}^2} \tag{63}$$

where $C_1 = 1.368 S_1{}^{1/3}$

$C_2 = K_{S2} S_2{}^\beta \left(\cos\theta\right)^{-\varepsilon}$

$C_3 = 0.866 \cdot d_p K_{3D}{}^{2/3} \rho_p{}^{1/3} \rho_{ob}{}^{1/9} V^{2/3} \left(\cos\theta\right)^\delta \left(70/\sigma_y\right)^{1/3}$

$$t_{ob} = t_b = c_b t_w \tag{64}$$

where $c_b = 0.1$

As a practical guideline, the accuracy of Eq. (62) is questionable for facesheet thicknesses below 0.04 cm for aluminum and 0.1 cm for CFRP (however, in this case, sizing is expected to be conservative). Eq. (62) is valid only for impacts in the HV regime, which is defined as velocities that are above 7, 8.4, and 10 km/s for impact of aluminum on aluminum, CFRP, and MLI, respectively.

For performance assessments, the SRL triple-wall equation is used (expressed for application on triple wall structures) as follows:

In the LV regime, $V/\cos\theta \leq V_{LV}$:

$$d_c = \left[\frac{\frac{\left(t_w{}^{1/2} + t_b\right)}{K_{3S}} \cdot \left(\frac{\sigma}{40}\right)^{1/2} + t_{ob}}{0.6\left(\cos\theta\right)^\delta \rho_p{}^{1/2} V^{2/3}}\right]^{18/19} \tag{65}$$

In the HV regime, $V/\cos\theta \geq V_{HV}$:

$$d_c = \frac{1.155\left(S_1{}^{1/3}\left(t_b + K_{tw} t_w\right)^{2/3} + K_{S2} S_2{}^\beta t_w{}^\gamma \left(\cos\theta\right)^{-\varepsilon}\right) \cdot \left(\frac{\sigma}{70}\right)^{1/3}}{K_{3D}{}^{2/3} \rho_p{}^{1/3} \rho_{ob}{}^{1/9} V^{2/3} \left(\cos\theta\right)^\delta} \tag{66}$$

For $V_{LV} < V/\cos\theta < V_{HV}$, linear interpolation is used; i.e.,

$$d_c = d_c\left(V_{LV}\right) + \frac{\left[d_c\left(V_{HV}\right) - d_c\left(V_{LV}\right)\right]}{V_{HV} - V_{LV}} \times \left(V - V_{LV}\right) \tag{67}$$

Impact regime transition velocities (V_{LV}, V_{HV}) are dependent on the outer bumper and projectile material. In [17], a one-dimensional shock impedance match analysis was performed to determine transition veloci-

ties for impact of aluminum on CFRP. An overview of the parameters that are applicable with the SRL triple-wall equation is given in Table 13.

Outer bumper	V_{LV}	V_{HV}	K_{3S}	K_{3D}	K_{tw}	K_{S2}	β	δ	ε	γ
Aluminum	3	7	1.4	0.4	1.5	0.1	2/3	4/3 if $45 \geq \theta \leq 65°$ 5/4 if $45 < \theta > 65°$	8/3 if $45 \geq \theta \leq 65°$ 10/4 if $45 < \theta > 65°$	1/3
CFRP	4.2	8.4	1.1	0.4	1	1	1/3	4/3	0	2/3

Table 13: List of Fit Parameters for the SRL Triple-wall Equation (Aluminum Impactor)

The SRL equation was adjusted using approximately 200 impact tests on various dual- and triple-wall structures. For CFRP, approximately 90 impact tests were performed using six different honeycomb sandwich panel (HC SP) configurations and an aluminum plate for the rear wall [17]. The tests were performed with impact velocities ranging from 2 to 8 km/s, at three different impact angles (0°, 45°, and 60°). For aluminum targets, about 110 impact experiments were used, including both aluminum Whipple shields and honeycomb sandwich panels [18]. The impact experiments used representative space hardware for the rear wall structure (e.g., CFRP overwrapped pressure vessels, fuel pipes, heat pipes, etc.). The validation overview is shown in Table 14.

	Validated for	Applied to	Comments
Bumper materials	CFRP, Aluminum	CFRP, Aluminum	For CFRP, use equivalent Al thicknesses.
Bumper configurations	HC SP, Whipple shield	HC SP, Whipple shield	For CFRP, honeycombs only configuration validated.
Impact angles	0°, 45°, 60°	Normal, oblique	No limit angle specified.
Impact velocities	2–8 km/s	All	None.
Projectile diameters	0.08–0.5 cm	All	None.
Projectile materials	Aluminum	All	None.

Table 14: Valid Application of the SRL Triple-wall BLE

Advanced configurations

Stuffed Whipple shield

The stuffed Whipple shield includes intermediate fabric layers (such as Nextel ceramic fiber or Kevlar® aramid fiber) between an outer aluminum bumper plate and an inner aluminum pressure wall, as shown in Figure 15. These intermediate layers (or stuffings) act to reduce the impulsive load of projectile fragments on the spacecraft pressure hull.
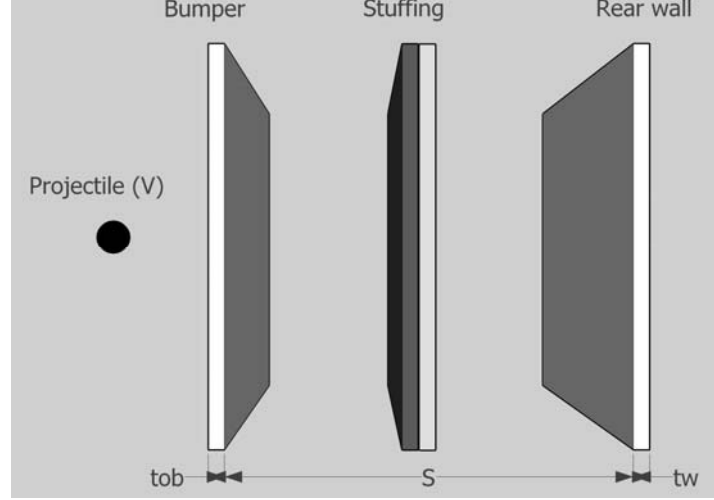
Figure 15: Stuffed Whipple shield configuration for application of the NASA JSC stuffed Whipple shield BLE.

For sizing of the stuffed Whipple shield, Christiansen [10] defines the following equations:

$$t_b = c_b d_p \, \rho_p / \rho_b \tag{68}$$

$$AD_{stuffing} = c_{stuffing} d_p \rho_p \tag{69}$$

$$AD_b = t_b \rho_b + AD_{stuffing} \tag{70}$$

$$t_w = c_w \left(\frac{AD_b}{c_0 d_p \rho_p} \right)^{-1.1} \frac{m_p \left(V \cos^{3/2} \theta \right)}{\rho_w S^2 \left(\sigma_w / 40 \right)^{1/2}} \tag{71}$$

The equation coefficients are given for impact of an aluminum particle on a Whipple shield with Kevlar®/Nextel stuffing. Other types of ceramic cloth are also suitable for use with the sizing equations. In the above equations, coefficient $c_b = 0.15$ {unitless}, $c_{stuffing} = 0.23$ {unitless}, $c_w = 8.8$ {s/km}, and $c_0 = 0.38$ {unitless}.

The Nextel/Kevlar® stuffing should be placed halfway between the bumper and plate and rear wall, and the fraction of Nextel to Kevlar® areal weight should be kept to: $AD_{Nextel} = 3AD_{Kevlar}$. No limits are placed on shield spacing.

The performance of a stuffed Whipple shield configuration at LV (i.e., $V \leq 2.6/(\cos \theta)^{0.5}$ km/s) is evaluated using

$$d_c = 2.35 \frac{\left(t_w \left(\sigma_y / 40 \right)^{0.5} + 0.37 AD_b \right)}{\left((\cos \theta)^{4/3} \rho_p^{0.5} V^{2/3} \right)} \tag{72}$$

In the HV regime, $V \geq 6.5/(\cos \theta)^{3/4}$,

26

$$d_c = 0.321 \frac{(t_w \rho_w)^{1/3} S^{2/3} (\sigma_y/40)^{1/6}}{\rho_p^{1/3} V^{1/3} (\cos \theta)^{1/2}} \tag{73}$$

For $2.6/(\cos \theta)^{0.5} < V < 6.5/(\cos \theta)^{3/4}$, linear interpolation is used; i.e.,

$$d_c = d_c(V_{LV}) + \frac{[d_c(V_{HV}) - d_c(V_{LV})]}{V_{HV} - V_{LV}} \times (V - V_{LV}) \tag{74}$$

Given its extensive application on the ISS, the stuffed Whipple shield configuration has been subject to extensive impact testing. Application of the stuffed Whipple shield BLE is not restricted by shield spacing to projectile diameter ratio (unlike the MS and mesh double-bumper equations), nor is a limit angle defined. The validation overview is shown in Table 15.

	Validated for	Applied to	Comments
Fabric materials	Kevlar®, Nextel	Nextel, Kevlar®	No distinction is made in the BLE for different materials.
Impact angles	0°, 15°, 45°, 60°	Normal, oblique	No limit angle.
Impact velocities	2.94–11.42 km/s	All	Higher-velocity impact testing performed with non-spherical projectiles (inhibited shaped charge launcher).
Projectile diameters	0.67–1.59 cm	All	For shaped, charged launcher projectiles, equivalent projectile diameter calculated.
Projectile materials	Aluminum	All	None.

Table 15: Valid Application of the Christiansen Stuffed Whipple Shield BLE

Multi-shock shield

There are three MS shielding configurations for which BLEs are considered (Figure 16) [4]:

- Four equally spaced ceramic fabric bumpers with a flexible rear wall
- Four equally spaced ceramic bumpers with an aluminum rear wall
- Two equally spaced ceramic bumpers with a two-sheet aluminum Whipple shield (hybrid Nextel/ aluminum MS shield). Spacing between the aluminum bumper and the aluminum rear wall is equal to twice the inter-bumper spacing.

The MS equations use a combined bumper plate areal density (AD_b) and total shield spacing (S) that are sized using the following:

For ceramic MS shield with a flexible rear wall,

$$AD_b = 0.19 d_p \rho_p \tag{75}$$

$$AD_w = K \cdot m_p (V \cos \theta)/S^2 \tag{76}$$

where $K = 43.6$ for Nextel, $K = 29.0$ for Kevlar®.
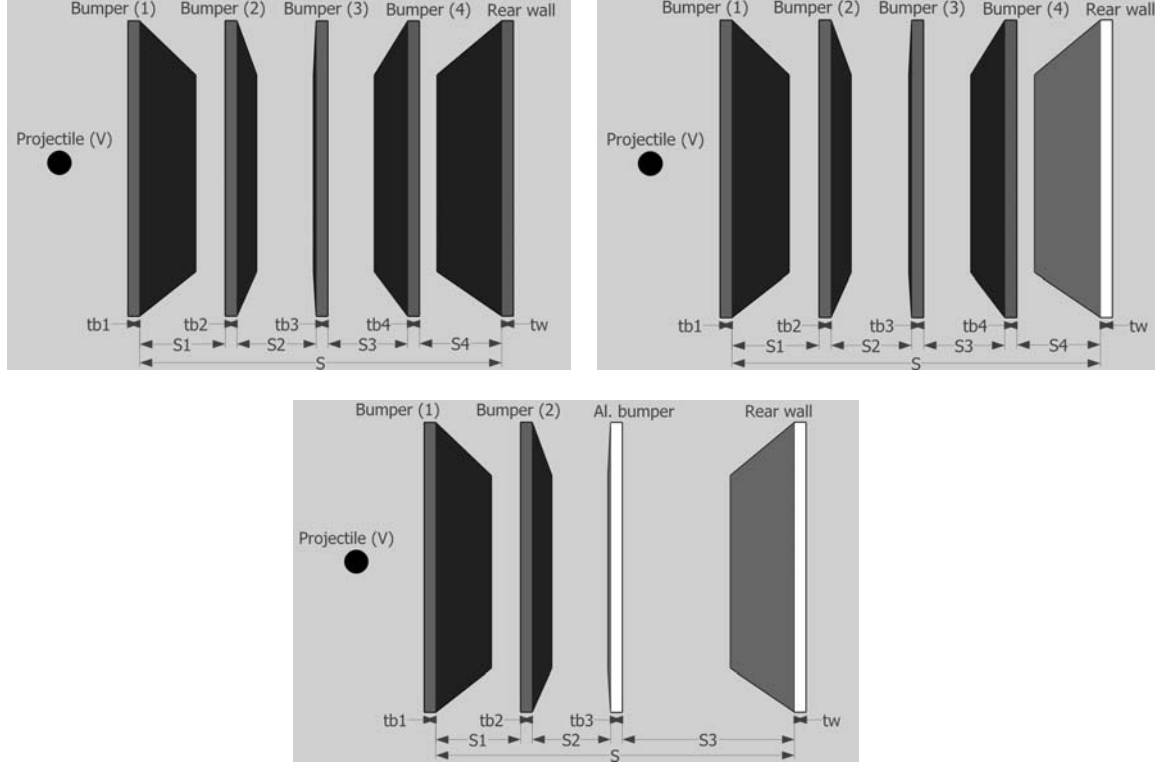
Figure 16: Configurations applicable for the NASA JSC MS BLEs. Clockwise from upper left: Nextel MS shield with a fabric rear wall, Nextel MS shield with an aluminum rear wall, and a hybrid ceramic/aluminum MS shield with an aluminum rear wall.

For the ceramic MS shield with an aluminum rear wall,

$$AD_b = 0.19 d_p \rho_p \tag{77}$$

$$AD_w = 41.7 m_p \left(V \cos \theta \right) / S^2 \left(40/\sigma_y \right)^{0.5} \tag{78}$$

For the hybrid ceramic/aluminum MS shield with an Aluminum rear wall,

$$AD_w = 0.269 \cdot d_p^{3/2} \rho_p^{1/2} \rho_A^{1/6} \left(V \cos \theta \right) S^{-1/2} \left(40/\sigma_y \right)^{1/2} \tag{79}$$

$$AD_A = 0.5 AD_w \tag{80}$$

$$AD_b = 0.5 AD_w \tag{81}$$

where   subscript "A" indicates the aluminum bumper.

For the Nextel MS shields, no limit angle is defined as the ceramic fabric bumpers are not considered to produce damaging fragments (unlike metallic structures). However, for the hybrid Nextel/aluminum MS shields, a limit incidence of 75° is defined.

The performance of the MS shield configurations is assessed over three velocity ranges, which are similar to those of the JSC Whipple shield equation.

For LV, $V \leq V_{LV}$ km/s:

For MS ceramic bumpers and a flexible rear wall,

$$d_c = 2.7 \frac{\left(0.50 AD_w + 0.37 AD_b\right)}{\left(\left(\cos\theta\right)^{4/3} \rho_p^{0.5} V^{2/3}\right)} \tag{82}$$

For MS ceramic bumpers and an aluminum rear wall,

$$d_c = 2 \frac{\left(t_w \left(\sigma_y/40\right)^{0.5} + 0.37 AD_b\right)}{\left(\left(\cos\theta\right)^{4/3} \rho_p^{0.5} V^{2/3}\right)} \tag{83}$$

For a hybrid ceramic/aluminum MS shield with an aluminum rear wall,

$$d_c = 2 \frac{\left(t_w \left(\sigma_y/40\right)^{0.5} + 0.37 AD_b\right)}{\left(\left(\cos\theta\right)^{\chi} \rho_p^{0.5} V^{2/3}\right)} \tag{84}$$

where $\chi = 7/3$ when $\theta \leq 45°$ and $\chi = 2$ when $\theta > 45°$.

In the HV regime, $V \geq V_{HV}$:

For MS ceramic bumpers and a flexible rear wall,

$$d_c = 1.24 \frac{AD_w^{1/3} S^{2/3}}{K^{1/3} \rho_p^{1/3} V^{1/3} \left(\cos\theta\right)^{1/3}} \tag{85}$$

where $K = 43.6$ for Nextel, $K = 29.0$ for Kevlar®.

For MS ceramic bumpers and an aluminum rear wall,

$$d_c = 0.358 \frac{\left(t_w \rho_w\right)^{1/3} S^{2/3} \left(\sigma_y/40\right)^{1/6}}{\rho_p^{1/3} V^{1/3} \left(\cos\theta\right)^{1/3}} \tag{86}$$

For hybrid ceramic/aluminum MS shield with an aluminum rear wall,

$$d_c = 2.4 \frac{\left(t_w \rho_w\right)^{2/3} S^{1/3} \left(\sigma_y/40\right)^{1/3}}{\rho_p^{1/3} \rho_A^{1/9} \left(V \cos\theta\right)^{2/3}} \tag{87}$$

29

For VLV < V < VHV, linear interpolation is used; i.e.,

$$d_c = d_c(V_{LV}) + \frac{[d_c(V_{HV}) - d_c(V_{LV})]}{V_{HV} - V_{LV}} \times (V - V_{LV}) \tag{88}$$

For Nextel MS shields, the impact regime transition velocities are defined as: $V_{LV} = 2.4/(\cos \theta)^{0.5}$ km/s; $V_{HV} = 6.4/(\cos \theta)^{0.25}$. For hybrid Nextel/aluminum MS shields, those transition velocities occur at: $V_{LV} = 2.7/(\cos \theta)^{0.25}$; $V_{HV} = 6.5/(\cos \theta)^{2/3}$.

The MS BLEs were developed from impact experiments that were performed with aluminum, ruby, and copper projectiles at velocities ranging from 2.5 to 7 km/s. The placement and areal weight of each bumper shield is expected to affect the capability of the MS shield. These BLEs are assumed to be equally spaced and of equal areal weight (with the exception of the aluminum bumper plate for the hybrid Nextel/aluminum configuration). The MS ballistic limit equation is only valid for configurations with a total standoff-to-projectile-diameter ratio (S/d_p) that is greater than 15. For values that are less than this, the equation may provide very conservative predictions. The validation overview is shown in Table 16.

	Validated for	Applied to	Comments
Rear bumper materials	Nextel, Aluminum	Nextel, Aluminum	None.
Rear wall materials	Nextel, Aluminum	Nextel, Aluminum	None.
Impact angles	0°, 15°, 30°, 45°, 60°, 75°	Normal, oblique	Nextel MS: no limit. Hybrid Nextel/Al MS: $d_c(\theta>75°)=d_c(\theta=75°)$.
Impact velocities	2.5–7 km/s	None	None.
Projectile diameters	Up to 1 cm	All	Equation is valid only for shields with a total standoff-to-projectile-diameter ratio (S/d_p) that is greater than 15.
Projectile materials	Aluminum	All	None.

Table 16: Valid Application of the NASA JSC MS Shield BLE

Mesh double-bumper shield

The mesh double-bumper (MDB) shield consists of an outer layer of aluminum mesh that is effectively followed by a stuffed Whipple shield. The only configuration that is considered for the MDB ballistic limit equation uses an aluminum plate as the second bumper (Figure 17).
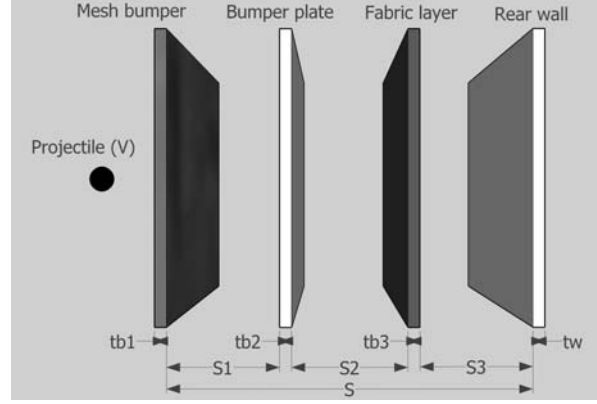
Figure 17: MDB shielding configuration for application with the NASA JSC MDB BLE.

Although other materials have been shown to perform as well or better than aluminum (e.g., graphite/epoxy, Nextel, etc.), the equation was derived for systems that were upgraded from typical metallic Whipple shield designs [21]. The mesh, second bumper plate and intermediate fabric layer are sized for optimal shielding capability and minimal weight in a manner similar to that of the bumper plate of a Whipple shield bumper plate. These components are sized in terms of their areal density.

$$AD_{mesh} = c_{mesh} d_p \rho_p \tag{89}$$

$$AD_{b2} = 0.093 d_p \rho_p \tag{90}$$

$$AD_b = AD_{mesh} + AD_{b2} \tag{91}$$

$$AD_f = c_f d_p \rho_p \tag{92}$$

$$AD_w = 9 m_p \left(V \cos \theta \right) \Big/ S^{3/2} \left(40 / \sigma_y \right)^{0.5} \tag{93}$$

The mesh sizing coefficient, c_{mesh}, can range from 0.035 to 0.057 without affecting the accuracy of the sizing equations for the remaining shield components. A larger value means that a higher percentage of the bumper areal mass is concentrated in the mesh bumper, with a subsequent reduction in the areal mass of the second bumper plate and intermediate fabric layer. The fabric sizing coefficient, c_f, is given as 0.064 for Kevlar® and Spectra®, and 0.095 for Nextel.

Equations (89)–(93) are valid for impact velocities above $6.4/(\cos \theta)^{1/3}$ and total shielding spacing to projectile diameter ratios (S/d_p) greater than 15. Internally, distribution of the shield bumpers should be made such that S_1 (mesh bumper to second plate) = $4d_p$, and S_3 (fabric layer to rear wall) = $4d_p$.

The performance of a MDB shield configuration is determined in the LV regime ($V \leq 2.8/(\cos \theta)^{0.5}$ km/s) using

$$d_c = 2.2 \frac{\left(t_w \left(\sigma_y / 40 \right)^{0.5} + 0.37 \left(AD_b + AD_f \right) \right)}{\left((\cos \theta)^{5/3} \rho_p^{0.5} V^{2/3} \right)} \tag{94}$$

In the HV regime, $V \geq 6.4/(\cos \theta)^{1/3}$ km/s:

$$d_c = 0.6 \frac{(t_w \rho_w)^{1/3} S^{1/2} (\sigma_y/40)^{1/6}}{\rho_p^{1/3} (V \cos \theta)^{1/3}} \qquad (95)$$

For $V_{LV} < V < V_{HV}$, linear interpolation is used; i.e.,

$$d_c = d_c(V_{LV}) + \frac{[d_c(V_{HV}) - d_c(V_{LV})]}{V_{HV} - V_{LV}} \times (V - V_{LV}) \qquad (96)$$

Over 100 HV impact tests have been performed by NASA JSC on MDB shield configurations. However, these tests included material and spacing investigations and, as such, were not all used for derivation and empirical adjustment of the BLE. The equations are validated for configurations using either Kevlar® or Spectra® for the intermediate fabric layer. Although the placement of the fabric layer was found to have a significant influence on shielding capability, the equation considers only the total spacing of the shield. The equation was derived using fabric layers that were located a short distance (three to four times the projectile diameter) from the rear wall. The validation overview is shown in Table 17.

	Validated for	Applied to	Comments
Fabric materials	Kevlar®, Spectra®	Nextel, Kevlar®, Spectra®	No distinction is made in the BLE for different fabric materials.
Impact angles	0°, 45°, 60°, 75°	Normal, oblique	No limit angle defined.
Impact velocities	2.63–7.53	All	None.
Projectile diameters	0.08–1 cm	All	None.
Projectile materials	Aluminum	All	None.

Table 17: Valid Application of the NASA JSC MDB BLE

Thermal Protection Systems

Ceramic tiles

Two types of ceramic tiles are used on board the shuttle: standard low (LI-900) and higher-density (LI-2200). The tiles are composed of compacted silica fibers that are fused with colloidal silica during a high-temperature sintering process. The tiles have a borosilicate coating on top and sides that is nominally 0.20 to 0.38 mm thick. The rear surface is bonded with room temperature vulcanizing ((RTV)) adhesive to a strain isolation pad (SIP) that is then bonded to the vehicle skin (monolithic plate or honeycomb sandwich panel; shown in Figure 18). For the case of an aluminum honeycomb sandwich panel structure wall, the effective thickness (t_w) is the sum of the facesheet thicknesses. Aluminum enhanced thermal barrier (AETB) tiles with toughened unipiece fibrous insulation (TUFI) coating were developed at NASA Ames Research Center as an improvement to the LI-900 tile. The AETB-8 tiles are also coated on the top and sides by a borosilicate glass layer, and are bonded to a 0.4-cm-thick SIP and a graphite-cyanate composite facesheeted sandwich panel.
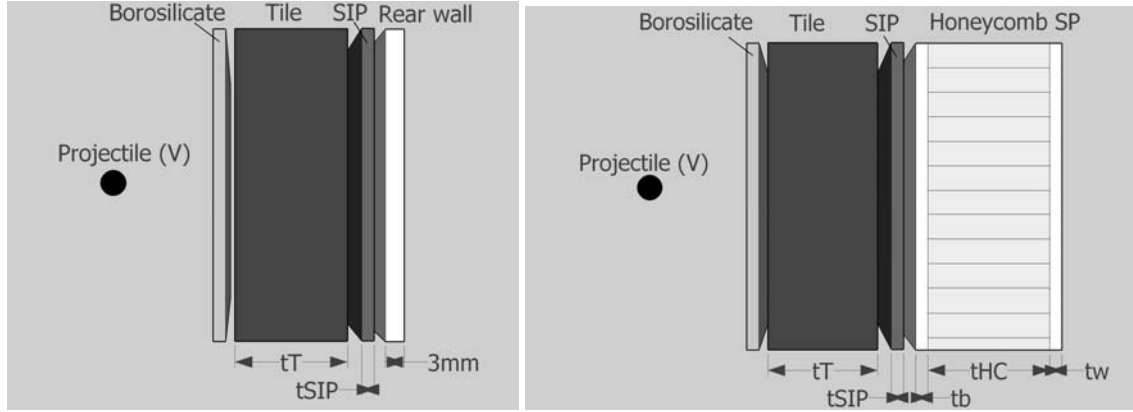
Figure 18: Shuttle thermal tile configurations for application of the NASA JSC general BLE for ceramic tiles.

The penetration depth into ceramic tiles that are bonded to a SIP and a substructure (monolithic plate or honeycomb sandwich panel) is calculated using (from [22])

$$P_\infty = 1.27 d_p \left(V \cos\theta \right)^{2/3} \left(\rho_p / \rho_T \right)^{0.5} \tag{97}$$

where ρ_T = nominal density of the ceramic tile (not including borosilicate glass coating or ceramic slurry used for densification).
ρ_T = 0.14/0.35 g/cm^3 for LI-900/2200 tile, respectively.

For stand-alone tiles, thickness is defined in terms of allowable penetration depth (as percentage of the tile thickness), P_c; i.e.,

$$t_T = \frac{1.27}{P_c} \cdot d_p \left(V \cos\theta \right)^{2/3} \left(\rho_p / \rho_T \right)^{0.5} \tag{98}$$

The ballistic performance of unsupported tiles is calculated by

$$d_c = P_c \cdot K \cdot d_p \left(V \cos\theta \right)^{-2/3} \left(\rho_p / \rho_T \right)^{-0.5} \tag{99}$$

For the LI-900 and LI-2200 tiles, general ballistic limit equations were derived in [22] to predict the critical projectile diameter resulting in the threshold perforation of a TPS tile and substructure (either monolithic plate or honeycomb sandwich panel). As the ceramic tiles are bonded to the SIP and metallic substructure, detached spallation from the rear of the tile is not applicable. As such, the onset of failure is defined once the penetration depth exceeds the thickness of the ceramic tile.

For LV impacts ($V_n \leq 2.5$ km/s), the ballistic performance of the tile configuration is calculated using

$$d_c = \frac{t_w \left(\sigma_y / 40 \right)^{0.5} + t_T \left(\rho_T / \rho_{AL} \right)^{0.5}}{0.55 \left(\cos\theta \right)^{5/3} \rho_p^{0.5} V^{2/3}} \tag{100}$$

33

For impacts at HV ($V_n \geq 7$ km/s),

$$d_c = 3\frac{(t_T + 0.5t_{HC})^{1/3}(t_{w+SIP})^{2/3}(\sigma_y/70)^{1/3}}{\rho_p^{1/3}(V\cos\theta)^{2/3}} \tag{101}$$

where $\quad t_{w+SIP} = t_w + AD_{SIP}/\rho_w$

For 3 km/s $< V_n <$ 7 km/s, linear interpolation is used; i.e.,

$$d_c = d_c(V_{LV}) + \frac{[d_c(V_{HV}) - d_c(V_{LV})]}{V_{HV} - V_{LV}} \times (V - V_{LV}) \tag{102}$$

For supported AETB-8 tiles, a ballistic limit equation was developed for a 5.1-cm-thick tile that is bonded to a 0.4-cm-thick SIP and a composite facesheeted honeycomb sandwich panel. This substructure configuration had 0.2-cm-thick graphite/cyanate facesheets and a total thickness of 3.8 cm. Failure is defined as any hole or through crack in the rear facesheet of the honeycomb sandwich panel. For LV impacts ($V_n \leq 2.5$ km/s),

$$d_c = 2.64\rho_p^{-1/2}(\cos\theta)^{-5/3}V^{-2/3} \tag{103}$$

For impacts at hypervelocity ($V_n \geq 7$ km/s),

$$d_c = 2.98\rho_p^{-1/3}(V\cos\theta)^{-2/3} \tag{104}$$

For 3 km/s $< V_n <$ 7 km/s, linear interpolation is used; i.e.,

$$d_c = d_c(V_{LV}) + \frac{[d_c(V_{HV}) - d_c(V_{LV})]}{V_{HV} - V_{LV}} \times (V - V_{LV}) \tag{105}$$

In addition to penetration, the size of non-penetrating craters in ceramic tiles is also of concern (particularly in the wake of the *Columbia* accident). During reentry, non-penetrating impact craters can grow until they reach the substructure (plate or honeycomb), effectively resulting in a penetration-type failure. For this, the maximum cavity diameter is of interest as it is generally larger in ceramic tiles than in the entry hole. Maximum cavity is calculated as (from [22])

$$D_c = 1.85d_p\rho_p^{1/3}V^{2/3}(1 + 0.25\sin\theta)^{2/3} \tag{106}$$

To evaluate the impact performance of ceramic TPS tiles when using maximum cavity size as a failure criterion, the critical projectile diameter is calculated in terms of a maximum allowable cavity diameter, $D_{c,max}$:

$$d_c = \frac{D_{c,max}}{1.85\rho_p^{1/3}V^{2/3}(1 + 0.25\sin\theta)^{2/3}} \tag{107}$$

The general penetration-based TPS ballistic limit equation was derived using test data from 12 impact experiments on TPS configurations with 4-mm-thick SIP bonded to aluminum plates and aluminum honeycomb sandwich panels. The impact tests were performed with aluminum and steel spheres, at different impact angles (0°, 30°, 45°, 60°) over a range of impact velocities from 2.65 to 7.42 km/s. The aluminum plate had a thickness of 0.25/0.13 cm, and the dimensions of the aluminum honeycomb sandwich panel were 0.064-cm-thick facesheets and a 2.5-cm-thick core. For entry hole diameter-based equations, additional impact tests (including some on tile samples that had no supporting substructure or borosilicate glass coating) were considered [23]. The ballistic limit equation for AETB tiles and substrate are significantly less widely validated, based on limited normal incidence testing on the X-38 crew return vehicle (CRV) TPS.

The validation overview is shown in Table 18.

	Validated for	Applied to	Comments
Impact angle	0°, 30°, 45°, 60°	Normal, oblique	None.
Impact velocities	2.65–7.42 km/s	All	None.
Projectile diameters	0.119–0.674	All	None.
Projectile materials	Aluminum, steel, Nylon	All	For configurations with Aluminum honeycomb backing plates, test data exist only for aluminum projectiles.

Table 18: Valid Application of the NASA JSC BLE for Shuttle Ceramic Tiles

Reinforced Carbon-Carbon

RCC is a structural composite that is used as the TPS for the high-temperature areas of the shuttle; i.e., the wing leading edge and the nose cap. To meet requirements for oxidation resistance and reusability, the RCC is coated with silicon carbide (SiC), as shown in Figure 19.
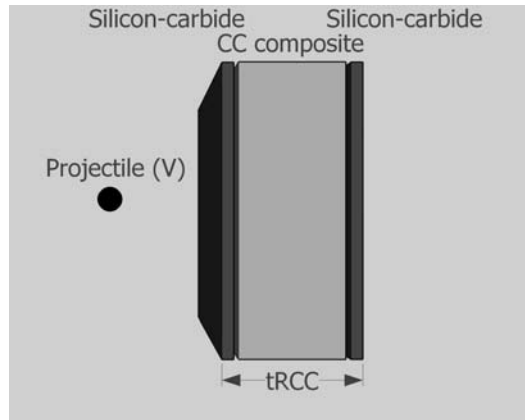
Figure 19: RCC TPS configuration for application of BLEs.

The ballistic limit of RCC is calculated using a cratering equation in which the penetration depth is determined using (from [22])

$$P_\infty = 0.61 d_p \left(V \cos\theta \right)^{2/3} \left(\rho_p / \rho_{RCC} \right)^{0.5} \tag{108}$$

Similar to the Cour-Palais cratering equation for metallic plates, the failure limits of RCC are determined by reducing the thickness of the semi-infinite plate applicable in Eq. (108). The required thickness of RCC to prevent failure can be calculated using

To prevent detached spallation: $\quad t_{RCC} \geq 4.5 P_\infty$ $\qquad\qquad$ (109)

To prevent perforation: $\qquad\quad t_{RCC} \geq 2.3 P_\infty$ $\qquad\qquad$ (110)

For assessing the performance of the RCC, the ballistic limit equation is defined as

$$d_c = 1.639 \frac{t_{RCC} \left(\rho_{RCC}/\rho_p\right)^{0.5}}{k \cdot \left(V \cos\theta\right)^{2/3}} \qquad (111)$$

where $\quad k$ defines the failure mode (2.3 for penetration, 4.5 for detached spallation).

The diameter of perforation holes in RCC is critical to its thermal protective capability. The hole diameter in completely perforated RCC panels is measured as the through-hole diameter (not entry or exit diameter, as shown in Figure 20) and is calculated using

$$D_h = 2.20 d_p \rho_p^{1/3} \left(V \cos\theta\right)^{1/3} - 0.36 \qquad (112)$$
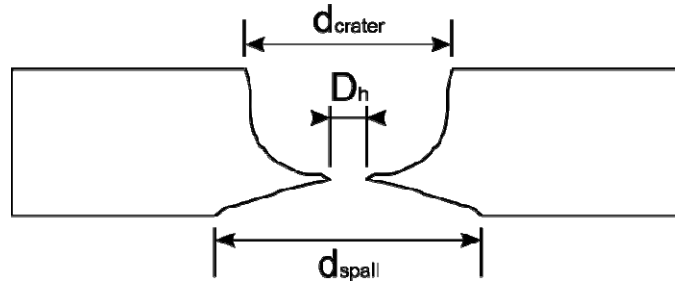
Figure 20: Clear hole diameter measurement in RCC panels.

For sizing of RCC panels that are based on the allowable clear hole diameter, Eq. (112) is solved for projectile diameter, d_p, in terms of $D_{h,max}$ which is then substituted into the sizing equation for no perforation; i.e.,

$$t_{RCC} = 1.342 \left(V \cos\theta\right)^{1/3} \left(\rho_p/\rho_{RCC}\right)^{0.5} \left(D_{h,\max} + 0.36\right) \rho_p^{-1/3} \qquad (113)$$

To evaluate the performance of an RCC panel over a range of impact conditions that is based on maximum allowable perforation hole diameter, a three-step procedure is used as follows:

1) The clear hole diameter (D_h) is calculated at the onset of perforation (i.e., $d_p = d_c$) over the range of relevant impact velocities using Eq. (111) and Eq. (112).

2) A maximum clear hole diameter ($D_{h,max}$) that is greater than those calculated in step 1) is defined for the range of impact velocities considered.

3) The critical projectile diameter is calculated for the range of impact velocities that is considered (i.e., ballistic limit curve) in terms of $D_{h,max}$:

$$d_c = \frac{D_{h,\max} + 0.36}{2.2 \cdot \rho_p^{1/3} \left(V \cos\theta\right)^{1/3}} \tag{114}$$

It should be noted that clear hole diameter characterization has been performed for 6.3-mm, nominally thick RCC panels (with 0.8-mm-thick SiC coating on the upper and lower surfaces). The effect of panel thickness on perforation hole diameter is unknown and, as such, application of hole diameter-based failure limits for structures with thicknesses other than 6.3 mm should be done with caution.

Eq. (108) has been developed from a series of nine impact tests [22]. Recent updates to RCC damage equations have been developed at NASA JSC as part of the shuttle return to flight investigation; however, these results have focused primarily on failure limits (i.e., allowable crater dimensions) rather than on penetration thresholds. The validation overview is shown in Table 19.

	Validated for	Applied to	Comments
Impact angle	0°, 30°, 45°, 80°	Normal, oblique	None.
Impact velocities	2.49–7.33 km/s	All	None.
Projectile diameter	0.39–6.28 cm	All	None.
Projectile materials	Aluminum, steel	All	None.
Target thicknesses	6.3 mm	All	Application of clear hole diameter-based failure criteria should be made with extreme caution for panels with thicknesses other than 6.3 mm.

Table 19: Valid Application of the NASA JSC RCC BLE

Ablative heat-shield

Penetration equations have been developed for two types of ablative shields: Avcoat and phenolic impregnated carbon ablator (PICA). Avcoat is low-density, glass-filled epoxy-novolac that was used as an ablative heat shield during the Apollo Program. PICA is combination of carbon fiberform and phenolic resin, and is a lightweight alternative to Avcoat (nominal density of 0.24 g/cm^3) (Figure 21). High-density PICA is also available, with a nominal density of 0.48 g/cm^3.
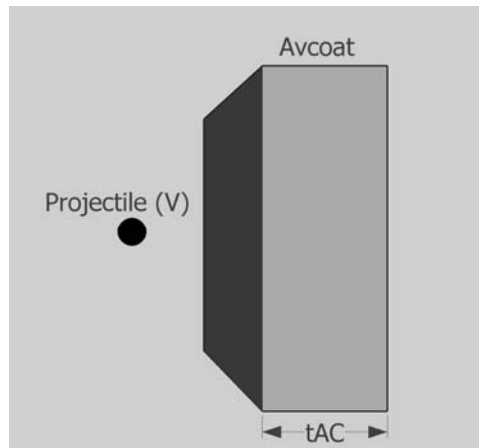
Figure 21: Avcoat ablative heat shield configuration for application with the NASA JSC ablative heat shield BLE.

Penetration into porous, low-density ablative materials by MMOD projectiles forms a central damage cavity; however, in some cases individual projectile fragments may penetrate beyond the central cavity. The depth of these individual fragment channels are not predicted by the penetration equations.

Allowable penetration limits into an ablative heat shield such as Avcoat are not fully characterized and may be mission dependent. As such, failure limits are defined by the user in terms of the failure coefficient k. The penetration into an Avcoat heat shield is calculated using (from [1])

$$P_\infty = K \cdot d_p^{\,19/18} \rho_p^{\,0.5} \left(V \cos \theta \right)^{2/3} \tag{115}$$

where $K = 1.61/1.25$ for Avcoat (for $\rho_p / \rho_{AC} > 4$ and $\rho_p / \rho_{AC} \leq 4$, respectively), and
         $K = 0.72$ for PICA

Design sizing is made as a function of user-defined failure coefficient k and penetration depth

$$t_s = k \cdot P_\infty \tag{116}$$

where $k = 100 / P_{allowable}$ and $P_{allowable}$ are expressed as a percentage of the ablator thickness.

The ballistic performance of an Avcoat ablative heat shield is calculated using

$$d_c = \left[\frac{t_s}{k \cdot K_{AC} \cdot \rho_p^{\,0.5} \left(V \cos \theta \right)^{2/3}} \right]^{18/19} \tag{117}$$

The Avcoat penetration equation was empirically adjusted from the general Cour-Palais cratering equation that was based on an extensive test program that was performed during the Apollo Program at NASA JSC, General Motors Defense Research Laboratory, AVCO, and the Naval Research Laboratory (NRL). PICA is being considered for use on the Orion CEV, for which test data are not publicly available.

The validation overview is shown in Table 20.

	Validated for	Applied to	Comments
Impact angle	0°	Normal, oblique	Avcoat was used in the Apollo command module heat shield, supported by a nylon phenolic honeycomb core. For similar configurations, penetration depths may be under predicted at oblique impact angles.
Impact velocities	~4.50–8.00 km/s	All	None.
Projectile energy	~20–1,000 J	All	None.
Projectile materials	Nylon, glass, polyethylene, copper, aluminum, Pyrex®, Delrin® (ρ_p = 1.0–8.90 g/cm³)	All	The density term ($\rho_p^{\,0.5}$) in the penetration depth equation is insufficient to generalize the equation for widely varying projectile materials. As such, the material constant K is included as a variable based on projectile density (for Avcoat).

Table 20: Valid Application of the NASA JSC BLE for an Ablative Heat Shield

Shape effects

All BLEs that were defined above are valid for the impact of solid spherical projectiles. Although it is generally considered that spherical projectiles can reasonably represent meteoroids, this is not true for orbital debris [24]. Rod- (L/D>1) and disk- (L/D<1) shaped projectiles have both been found to be more lethal on impact with a dual-wall shield at HV than a comparable spherical projectile [25]. This is because a considerable percentage of the projectile mass remains a lethal threat to the rear wall following perforation of the bumper plate. As such, current ballistic limit curves are effectively based on impact from the most benign of projectile shapes at normal orientation (i.e., not considering cylindrical projectiles inclined off their rotational axis). Thus, the equations that were presented in the preceding section may inherently provide a non-conservative estimation of penetration risk. Schaefer et al. [26] considered the effect of projectile shape on the penetration risk of metallic Whipple shields in terms of rotationally symmetrical ellipsoids (semi major axis a=b≠c). Thus, the projectile shape can be described in terms of a single parameter, f, which is effectively equal to the l/d ratio of a cylindrical projectile. A projectile is therefore described either as spherical (f = 1), oblate (f <1), or prolate (f >1) (Figure 22).
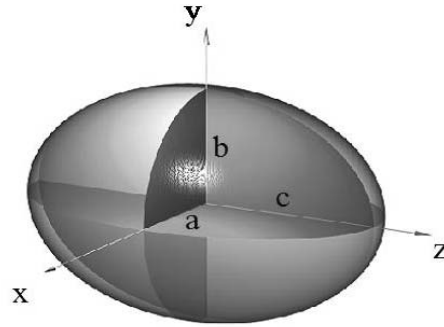
Figure 22: Ellipsoid with rotational symmetry.

For impact on a metallic Whipple shield, the shape effect is taken into account in the LV regime by incorporating the shape factor f^{a2} into the equation denominator. For example, in the LV regime (i.e., $V/\cos\theta \le 3 \cdot f^{a1}$ km/s), the shape factor-modified NASA JSC Whipple shield equation is expressed as

$$d_c = \left[\frac{t_w \left(\sigma_y/40 \right)^{0.5} + t_b}{0.6 \left(\cos\theta \right)^{5/3} \rho_p^{0.5} V^{2/3} f^{a1}} \right]^{18/19} \tag{118}$$

In the HV regime (i.e., $V/\cos\theta \ge 7 \cdot f^{b1}$ km/s), projectile shape is accounted for through the inclusion of a Gaussian function and shape factor f^{b1}

$$d_c = 3.918 \frac{t_w^{2/3} S^{1/3} \left(\sigma_y/70 \right)^{1/3}}{\rho_p^{1/3} \rho_b^{1/9} \left(V \cos\theta \right)^{2/3}} \cdot \frac{f^{b1}}{b3^{(f-1)^2/b2}} \tag{119}$$

For impact velocities in the transition regime, the effect of projectile shape is considered to vary the fragmentation behavior of the impacting projectile (i.e., the onset of projectile breakup and projectile melting). This effect is accounted for through the inclusion of the shape factor f^{a1} for V_{LV} and f^{b1} for V_{HV}, in addition to the empirically adjusted fit factors *a1* and *b1*:

$$d_c = d_c(V_{LV}) + \frac{[d_c(V_{HV}) - d_c(V_{LV})]}{V_{HV} - V_{LV}} \times (V - V_{LV})$$ (120)

An overview of the shape-effect coefficients that were used in Eq. (118)–(120) is given in Table 21 (from [26]). Although the baseline Whipple shield equation that was implemented in the program is the Reimerdes modified equation [11], validation of the shape effect factors was performed using the JSC Whipple shield equation on a shield that was below the recommended t_b/d_p cutoff (i.e. 0.25). Thus, the effects of an undersized bumper shield are incorporated in the JSC Whipple shield equation via the constants listed in Table 21 for the configurations described in [26].

Coefficient	Value
a1	0.08
a2	0.3
b1	0.25
b2	0.4
b3	1.4

Table 21: Set of Parameters for Use in Schaefer et al. Shape Effects BLE

Considering non-spherical projectiles, it is evident that the definition of critical projectile diameter is not directly applicable. More appropriately, failure limits that are based on projectile "critical mass" can be calculated from Eq. (118)–(120) as

$$m_c(v) = \rho_p \frac{\pi}{6} (d_c(v))^3$$ (121)

Nonetheless, current risk assessment software (e.g., BUMPER, ESABASE, etc.) requires ballistic limit equations that are expressed in terms of projectile diameter. Thus, for non-spherical particles, failure limits are expressed in terms of an equivalent-spherical diameter.

The ballistic limit modifications for unyawed ellipsoid projectiles were derived from experimental and numerical impact data using three different projectile volumes (equivalent to a 6-, 5-, and 4-mm aluminum sphere) with three different shape factors (f =0.42, 1.0, and 1.53). In total, 39 impact tests were performed, all at normal incidence, over impact velocities ranging between 0.85 and 6.76 km/s. Eight hydrocode simulations were performed that considered only the impact of the prolate ellipsoid (f =1.53) at impact velocities between 0.5 and 13.0 km/s. All impact tests and simulations were performed on aluminum Whipple shield targets. The validation overview is shown in Table 22.

	Validated for	Applied to	Comments
Impact angle	Unyawed projectiles	Normal	None
Impact velocities	0.85–6.76 km/s	All	Numerical simulations performed up to velocities of 13.0 km/s for prolate projectiles, unclear in [26] if used in validation.
Materials	Aluminum	All	Application with non-aluminum materials is not recommended and should not be used beyond a preliminary analysis tool.
Target configurations	Whipple shield	Whipple shield	Shape effect is primarily a result of debris cloud formation; thus, this modification is valid only for the metallic Whipple shield.

Table 22: Valid Application of Schaefer Unyawed Ellipsoid Shape Effects

Multilayer Insulation

In practice, MLI is included in the majority of shielding configurations either as an internal layer of the shield or placed externally on top of the front bumper plate. The presence of MLI can significantly affect, both positively and detrimentally, the impact performance of shielding configurations at hypervelocity [27]. There is currently no all-encompassing means to predict the effect of MLI on the performance of a debris shield. Indeed, most damage equations do not allow for the inclusion of MLI (Figure 23).
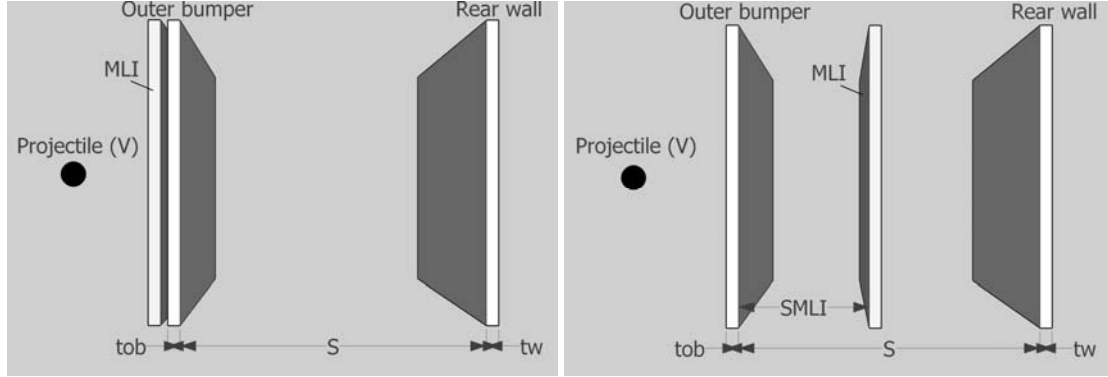
Figure 23: External (left) and internal (right) MLI configurations (shown with Whipple shield).

For MLI that is located on the exposed surface of a metallic monolithic shield, an increase in penetration limit is predicted based on cratering relationships (from [1]):

$$d_{c, with\,MLI} = 2.2 AD_{MLI}\rho_p^{-0.47} \left(V\cos\theta\right) - 0.63 + d_{c,\,without\,MLI} \tag{122}$$

For monolithic composite shields, Schaefer et al. [7] defined an increase in penetration limit corresponding to an effective increase in shield thickness as:

$$t_{b,eff} = t_b + K_{MLI}\frac{AD_{MLI}}{\rho_b} \tag{123}$$

where $K_{MLI} = 4.5$ for monolithic composites.

For MLI that is placed within Whipple shield configurations, Christiansen [16] proposes that the effect of MLI on shield performance should be evaluated in terms of its areal density (AD_{MLI}) and distance from the bumper plate (S_{MLI}).

$$\Delta_{MLI} = K_{MLI} AD_{MLI}\left(\frac{S_{MLI}}{S}\right)^{1/2} \tag{124}$$

where $K_{MLI} = 1.4$ cm^2.

The effect is included in the HV regime as a simple addition to critical projectile diameter. In the LV regime, MLI acts to shock the projectile a second time prior to impact on the rear wall, inducing fragmentation of the projectile at lower-impact velocities (decreased from to 2 km/s for aluminum-on-aluminum impacts).

For MLI that is placed on the outer surface of a single plate or multi-wall configurations, Schaefer et al. [7][18] conclude that the effect could be evaluated by increasing the effective thickness of the plate in the LV regime (only) according to the areal density of the MLI and a performance factor K_{MLI}.

$$t_{b,eff} = t_b + K_{MLI} \frac{AD_{MLI}}{\rho_b} \qquad (125)$$

where $K_{MLI} = 3.0$ for multi-wall configurations and 4.5 for single-wall shields (no units).

With caution, these approaches can be included in any of the single- and multi-wall ballistic limit equations (excluding the advanced configurations) that are presented in this paper for preliminary sizing or performance evaluation of an MMOD shield. However, their validity is not widely developed and, thus, predictions may be non-conservative (e.g., ATV-ICC [28]).

The validation overview is shown in Table 23.

	Validated for	Applied to	Comments
Impact angle	0°, 45°, 60°, 70°, 75°	Normal, oblique	MLI placed within Whipple shield configurations has been subject to extensive testing due to its application on the ISS Node 2/3 and U.S. Laboratory module. For externally placed MLI, test data have been used to validate the equations at 0°, 45°, and 60°.
Impact velocities	2–8 km/s	All	Internal MLI accounted for by the inclusion of Δ_{MLI} at HVs (only), and a lower low-shatter transition velocity (2 km/s). External MLI is only considered in the LV regime.
Target configurations	Internal MLI – metallic Whipple shields External MLI – CFRP plates, metallic Whipple shields, HC SPs, triple wall	Single-wall (external MLI only), Whipple shield, HC SP (external MLI only), triple-wall (external MLI only)	None.

Table 23: Guidelines for the Inclusion of Internal or External MLI in Shield Performance Assessments

Conclusions

A program has been developed that allows users to perform ballistic limit analyses of common MMOD shielding configurations. This program is presented in two modules: a design module for preliminary sizing of MMOD shields based on a pre-defined "design" particle, and a performance module that provides the failure limits of a defined shielding configuration over a range of impact velocities. The program is implemented as an add-in to Microsoft Excel$^©$, and is intended for use in MMOD shielding risk analysis procedures. The program applies the most widely accepted BLEs for each configuration that is represented, a summary of which is presented in this report. Validation of the program outputs has been made via a comparison with outputs from the NASA risk analysis software package BUMPER-II; variations between the outputs are discussed in the Appendix.

References

[1]   Anon. "ASM Handbook Volume 2 – Properties and Selection: Nonferrous Alloys and Special Purpose Materials." ASM International, ISBN 0871703785, 1990.

[2]   E.L. Christiansen, J. Arnold, B. Corsaro, A. Davis, F. Giovane, J. Hyde, D. Lear, J.C. Liou, F. Lyons, T. Prior, M. Ratliff, S. Ryan, G. Studor, "Handbook for Designing MMOD Protection." NASA Johnson Space Center, NASA/TM-2009-214785, 2009.

[3]   B.G. Cour-Palais. "Hypervelocity Impact Investigations and Meteoroid Shielding Experience Related to Apollo and Skylab." Orbital Debris Workshop, NASA CP-2360 (pp.247-275), Houston, August 27–29, 1982.

[4]   E.L. Christiansen. "Design and Performance Equations for Advanced Meteoroid and Debris Shields." *Int. J. Impact Eng.*, 14:145–156, 1993.

[5]   E.L. Christiansen, E Cykowski, J Ortega, "Highly Oblique Impacts into Thick and Thin Targets." *Int. J. Impact Eng.*, 14: 157-168, 1993.

[6]   J.M. Ratliff, E.L. Christiansen, C. Bryant, "Ballistic Limit Equation for Single Wall Titanium." 5th European Conference on Space Debris, JSC-17569, Darmstadt, May 30–April 2, 2009.

[7]   F. Schaefer, E. Schneider, M. Lambert. "Review of Ballistic Limit Equations for CFRP Structure Walls of Satellites." 5th International Symposium on Environmental Testing for Space Programmes, ESA SP-558, Noordwijk, June 15–17, 2004.

[8]   K. Edelstein. "Hypervelocity Impact Damage Tolerance of Fused Silica Glass." 43rd International Astronautical Congress, IAF 92-0334, Washington D.C., August 28–September 5, 1992.

[9]   R.R. Burt, E.L. Christiansen. "Hypervelocity Impact Testing of Transparent Spacecraft Materials." *Int. J. Impact Eng.*, 29:153–166, 2003.

[10] S. Ryan. Unpublished work, 2008.

[11] J.W. Gehring (Jr.), "Theory of Impact on Thin Targets and Shields and Correlation with Experiments", in: R. Kinslow (Ed.), High-Velocity Impact Phenomena, Academic Press, N.Y., 1970.

[12] H.G. Reimerdes, D. Noelke, F. Schaefer, "Modified Cour-Palais/Christiansen Damage Equations for Double-Wall Structures." *Int. J. Impact Eng.*, 33: 645-654, 2006.

[13] W.H. Press, S.A. Teukolsky, W.T. Vetterling, B.P. Flannery, "Numerical Recipes in FORTRAN." Second Edition, University of Cambridge, Melbourne, 1992.

[14]   C.J. Maiden, A.R. McMillan, R.E. Sennett III, "Thin Sheet Impact," General Motors Corporation, Santa Barbara, Calif., NASA CR-295, 1965.

[15]   A.J. Piekutowski, "Fragmentation-initiation Threshold for Spheres Impacting at Hypervelocity." *Int. J. Impact Eng.,* 29: 563-574, 2003.

[16]   E.L. Christiansen. "Meteoroid/Debris Shielding." NASA Johnson Space Center, Houston, NASA TP-2003-210788, 2003.

[17]   S. Ryan, F. Schaefer, R. Destefanis, M. Lambert. "A Ballistic Limit Equation for Hypervelocity Impacts on Composite Honeycomb Sandwich Panels Satellite Structures." *Adv. Space Res.*, 41(7):1152–1166, 2008.

[18]   F. Schaefer, S. Ryan, M. Lambert, R. Putzar. "Ballistic Limit Equation for Equipment Placed Behind Satellite Structure Walls." Hypervelocity Impact Symposium, Williamsburg, Va., September 23–27, 2007.

[19]   G. Drolshagen, J. Borde. "Meteoroid/Debris Impact Analysis (ESABASE/DEBRIS): Technical Description." Matra Espace, Report No. ESABASE-GD-01/1, 1992.

[20]   R. Putzar, F. Schaefer, O Rohmberg, H Stokes, A Heine, J. Zimmermann. "Vulnerability of Spacecraft Equipment to Space Debris and Meteoroid Impacts." Ernst-Mach-Institute, Freiburg, Germany, Report No. I-15/06, 2006.

[21]   E.L. Christiansen, J.H. Kerr. "Mesh Double-Bumper Shield: A Low-Weight Alternative for Spacecraft Meteoroid and Orbital Debris Protection." *Int. J. Impact Eng.*, 14(1–4):169–180, 1993.

[22]   E.L. Christiansen, L. Friesen,."Penetration Equations for Thermal Protection Materials." *Int. J. Impact Eng.*, 20:153–164, 1997.

[23]   E. Christiansen, J. Ortega. "Hypervelocity Impact Testing of Shuttle Orbiter Thermal Protection System Tiles." AIAA Space Programs and Technologies Conference, AIAA paper 90-3666, Huntsville, Ala., September 25–28, 1990.

[24]   B.G. Cour-Palais. "The Shape Effect of Non-Spherical Projectiles in Hypervelocity Impacts." *Int. J. Impact Eng.*, 26:129–143, 2001.

[25]   A.J. Piekutowski. "Debris Clouds Produced by the Hypervelocity Impact of Nonspherical Projectiles." *Int. J. Impact Eng.*, 26:613–624, 2001.

[26]   F. Schaefer, S. Hiermaier, E. Schneider. "Ballistic Limit Equation for the Normal Impact of Unyawed Ellipsoid-Shaped Projectiles on Aluminum Whipple Shields." 54th International Astronautical Congress, Bremen, Germany, IAC-03-IAA.5.3.06, 2003.

[27]   R. Destefanis, F. Schaefer, M. Lambert, M. Faraud, E. Schneider. "Enhanced Space Debris Shields for Manned Spacecraft." *Int. J. Impact Eng.*, 29: 215–226, 2003.

[28]   F. Schaefer, L. Guenther. "Impact Testing of the ATV-ICC Meteoroid and Debris Protection Shield." FhG Ernst-Mach-Institute (EMI), Freiburg, Germany, EMI Report E 28/2000, 2001.

Appendix: Validation of Program Output

Aluminum Single Wall (No Perforation)

BUMPERII VERSION 1.92f-EMU2   ** R E S P O N S E **
MAN-MADE DEBRIS ANALYSIS
ORDEM2000 DEBRIS ENVIRONMENT
MAN-MADE DEBRIS CONSTANT DENSITY (2.8 g/cm3)
METRIC UNITS
IMPACT ANGLE CUT-OFF (DEGREES)   =   60.0000

PROPERTY ID   1
SINGLE WALL
VESSEL WALL MATERIAL   = 6061-T6   ALUMINUM
COUR-PALAIS PENETRATION FUNCTION
PERFORATION FAILURE CRITERIA
VESSEL WALL THICKNESS (CM)   =   1.5000

Shield analysis program inputs					
Shield type: Single wall					
Analysis: No perforation					
Material: Al 6061-T6					
Parameter	*Units*	*Value*	*Parameter*	*Units*	*Value*
Sheet thickness	cm	1.5	Projectile density	g/cm^3	2.8
Sheet density	g/cm^3	2.713	Impact angle	deg	0/30/60
Brinell hardness	HB	73	Min. velocity	km/s	0.1
Sound speed	m/s	5.069	Max. velocity	km/s	15
MLI areal density	g/cm^2	0			
MLI standoff	cm	N/A			

Figure 1: Ballistic limit curves of a representative metallic single-wall MMOD shield calculated using BUMPER-II and the Ballistic Limit Analysis Program (SAP).

Aluminum Single Wall (No Detached Spall)

BUMPERII VERSION 1.92f-EMU2   ** R E S P O N S E **
MAN-MADE DEBRIS ANALYSIS
ORDEM2000 DEBRIS ENVIRONMENT
MAN-MADE DEBRIS CONSTANT DENSITY (2.8 g/cm3)
METRIC UNITS
IMPACT ANGLE CUT-OFF (DEGREES)   =   60.0000

PROPERTY ID   1
SINGLE WALL
VESSEL WALL MATERIAL   = 6061-T6   ALUMINUM
COUR-PALAIS PENETRATION FUNCTION
DETACHED SPALL FAILURE CRITERIA
VESSEL WALL THICKNESS (CM)   =   1.5000

Shield analysis program inputs

Shield type: Single wall
Analysis: No detached spall
Material: Al 6061-T6

Parameter	Units	Value	Parameter	Units	Value
Sheet thickness	cm	1.5	Projectile density	g/cm^3	2.8
Sheet density	g/cm^3	2.713	Impact angle	deg	0/30/60
Brinell hardness	HB	73	Min. velocity	km/s	0.1
Sound speed	m/s	5.069	Max. velocity	km/s	15
MLI areal density	g/cm^2	0			
MLI standoff	cm	N/A			

Figure 2: Ballistic limit curves of a representative metallic single-wall MMOD shield calculated using BUMPER-II and the Ballistic Limit Analysis Program (SAP).

Titanium Single Wall (No Perforation)

Source: E. Christiansen, J. Arnold, A. Davis, J. Hyde, D. Lear, J. Liou, F. Lyons, T. Prior, M. Ratliff, S. Ryan, F. Giovane, R. Corsaro, G. Studor, "Handbook for designing MMOD protection." NASA Johnson Space Center, NASA/TM-2009-214785, Houston, 2009.

Configuration data:
SHEET THICKNESS = 0.15 cm
SHEET DENSITY = 4.73 g/cm^3
BRINELL HARDNESS = 257 HB
SOUND SPEED = 4.26 km/s
MLI AREAL DENSITY = 0
MLI7 STANDOFF = N/A
PROJECTILE DENSITY = 2.8 g/cm^3
IMPACT ANGLE = 0°/45°/70°

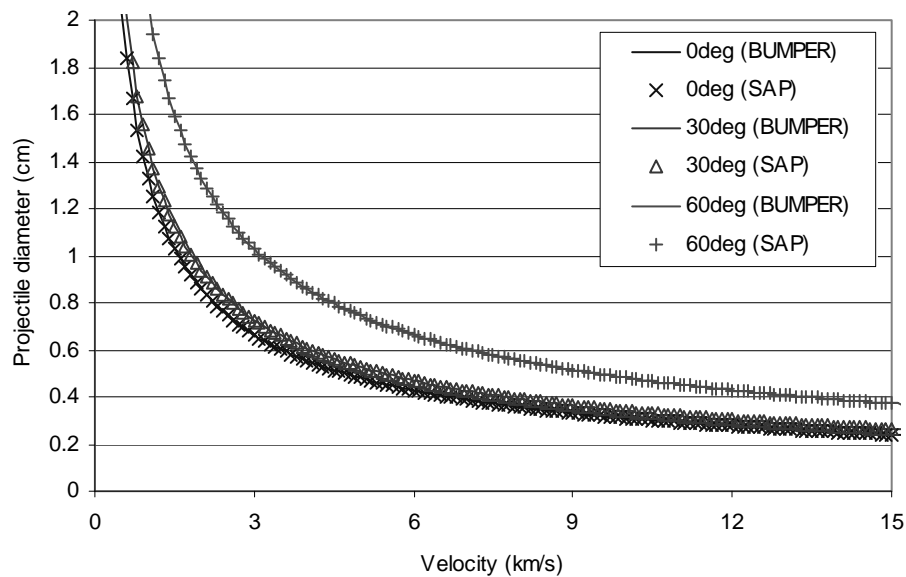| Shield analysis program inputs						
Shield type: Single wall						
Analysis: No perforation						
Material: Titanium						
Parameter	*Units*	*Value*		*Parameter*	*Units*	*Value*
Sheet thickness	cm	0.15		Projectile density	g/cm^3	2.8
Sheet density	g/cm^3	4.73		Impact angle	deg	0/45/70
Brinell hardness	HB	257		Min. velocity	km/s	0.1
Sound speed	km/s	4.26		Max. velocity	km/s	15
MLI areal density	g/cm^2	0				
MLI standoff	cm	N/A				

Figure 3: Ballistic limit curves of a representative titanium single-wall MMOD shield calculated using the published BLE and the Ballistic Limit Analysis Program (SAP).

47

Titanium Single Wall (No Attached Spall)

Source: E. Christiansen, J. Arnold, A. Davis, J. Hyde, D. Lear, J. Liou, F. Lyons, T. Prior, M. Ratliff, S. Ryan, F. Giovane, R. Corsaro, G. Studor, "Handbook for designing MMOD protection." NASA Johnson Space Center, NASA/TM-2009-214785, Houston, 2009.

Configuration data:
SHEET THICKNESS = 0.15 cm
SHEET DENSITY = 4.73 g/cm^3
BRINELL HARDNESS = 257 HB
SOUND SPEED = 4.26 km/s
MLI AREAL DENSITY = 0
MLI STANDOFF = N/A
PROJECTILE DENSITY = 2.8 g/cm^3
IMPACT ANGLE = 0°/45°/70°

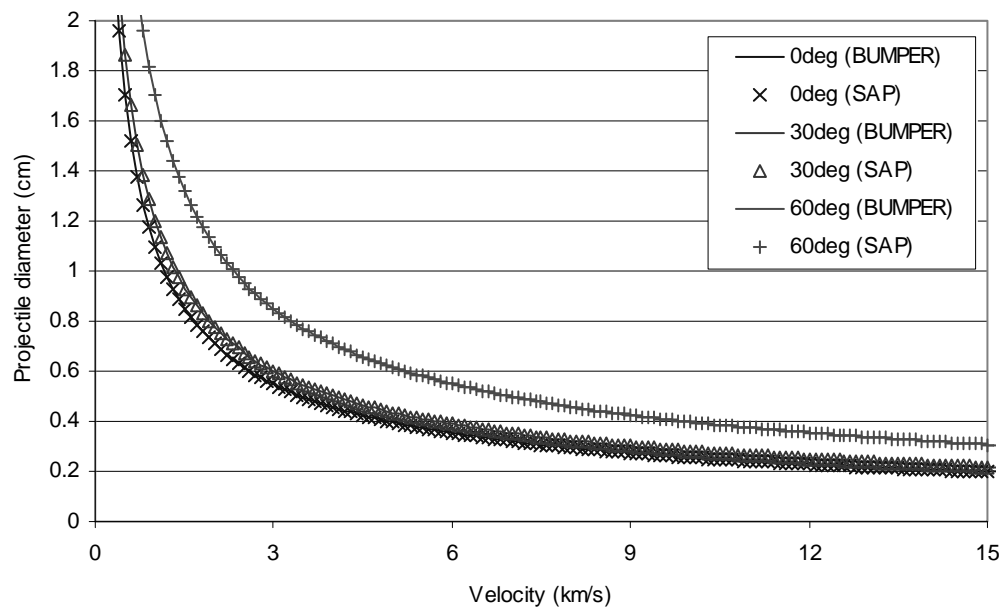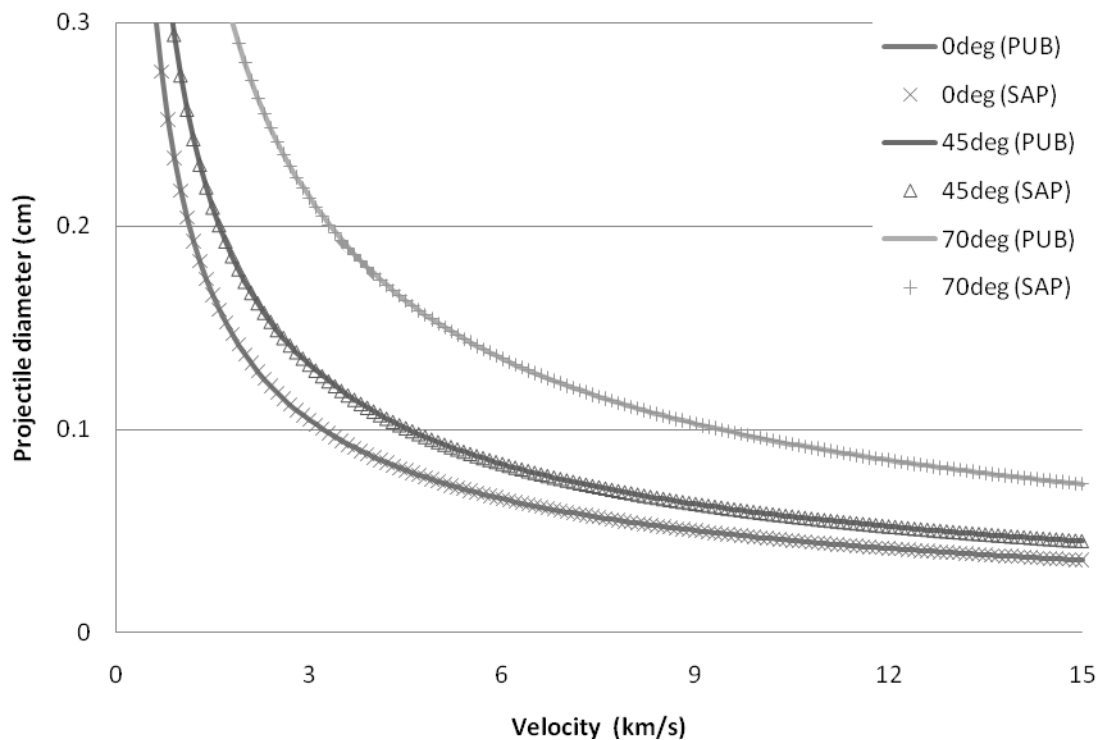| Shield analysis program inputs						
Shield type: Single wall						
Analysis: No incipient spall						
Material: Titanium						
Parameter	*Units*	*Value*		*Parameter*	*Units*	*Value*
Sheet thickness	cm	0.15		Projectile density	g/cm^3	2.8
Sheet density	g/cm^3	4.73		Impact angle	deg	0/45/70
Brinell hardness	HB	257		Min. velocity	km/s	0.1
Sound speed	km/s	4.26		Max. velocity	km/s	15
MLI areal density	g/cm^2	0				
MLI standoff	cm	N/A				

Figure 4: Ballistic limit curves of a representative titanium single-wall MMOD shield calculated using the published BLE and the Ballistic Limit Analysis Program (SAP).

48

Stainless-steel Single Wall (No Perforation)

Source: E. Christiansen, J. Arnold, A. Davis, J. Hyde, D. Lear, J. Liou, F. Lyons, T. Prior, M. Ratliff, S. Ryan, F. Giovane, R. Corsaro, G. Studor, "Handbook for designing MMOD protection." NASA Johnson Space Center, NASA/TM-2009-214785, Houston, 2009.

Configuration data:
SHEET THICKNESS = 0.2 cm
SHEET DENSITY = 7.8 g/cm^3
MLI AREAL DENSITY = 0 g/cm^2
MLI STANDOFF = N/A
PROJECTILE DENSITY = 2.8 g/cm^3
IMPACT ANGLE = 0°/45°/70°

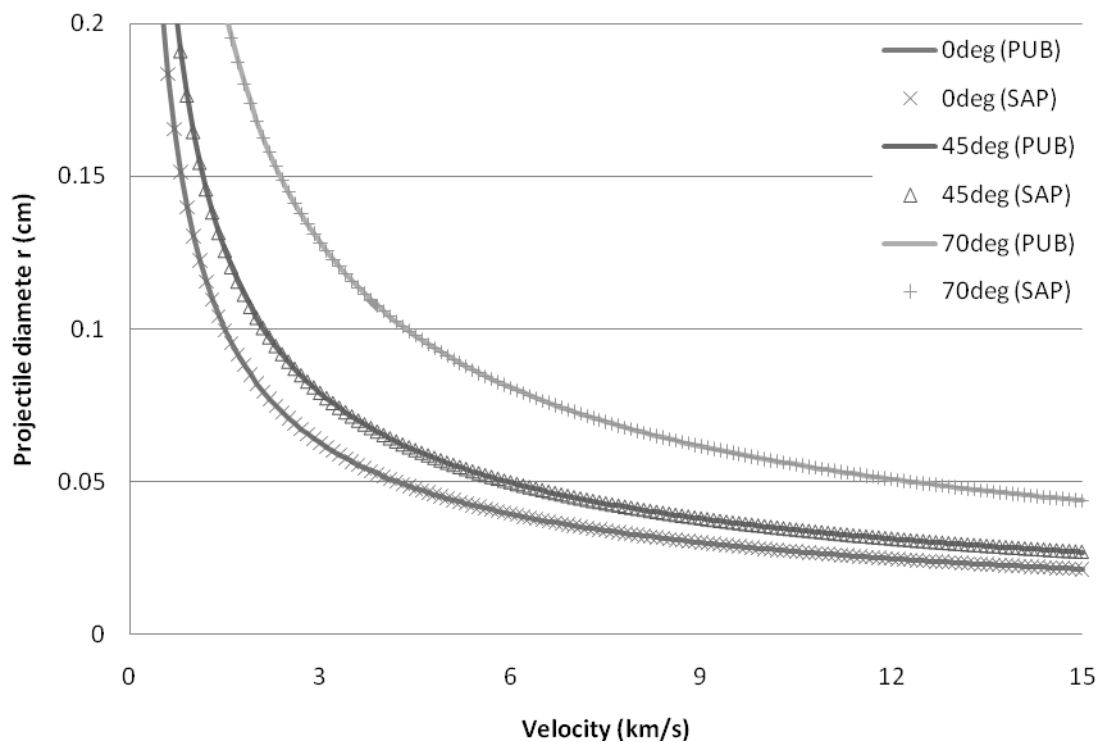| Shield analysis program inputs					
Shield type: Single wall					
Analysis: No perforation					
Material: Titanium					
Parameter	*Units*	*Value*	*Parameter*	*Units*	*Value*
Sheet thickness	cm	0.2	Projectile density	g/cm^3	2.8
Sheet density	g/cm^3	7.8	Impact angle	deg	0/45/70
Brinell hardness	HB	N/A	Min. velocity	km/s	0.1
Sound speed	km/s	N/A	Max. velocity	km/s	15
MLI areal density	g/cm^2	0			
MLI standoff	cm	N/A			

Figure 5: Ballistic limit curves of a representative stainless-steel single-wall MMOD shield calculated using the published BLE and the Ballistic Limit Analysis Program (SAP).

Stainless-steel Single Wall w/MLI (No Perforation)

Source: E. Christiansen, J. Arnold, A. Davis, J. Hyde, D. Lear, J. Liou, F. Lyons, T. Prior, M. Ratliff, S. Ryan, F. Giovane, R. Corsaro, G. Studor, "Handbook for designing MMOD protection." NASA Johnson Space Center, NASA/TM-2009-214785, Houston, 2009.

Configuration data:
SHEET THICKNESS = 0.2 cm
SHEET DENSITY = 7.8 g/cm^3
MLI AREAL DENSITY = 0.1 g/cm^2
MLI STANDOFF = N/A
PROJECTILE DENSITY = 2.8 g/cm^3
IMPACT ANGLE = 0°/45°/70°

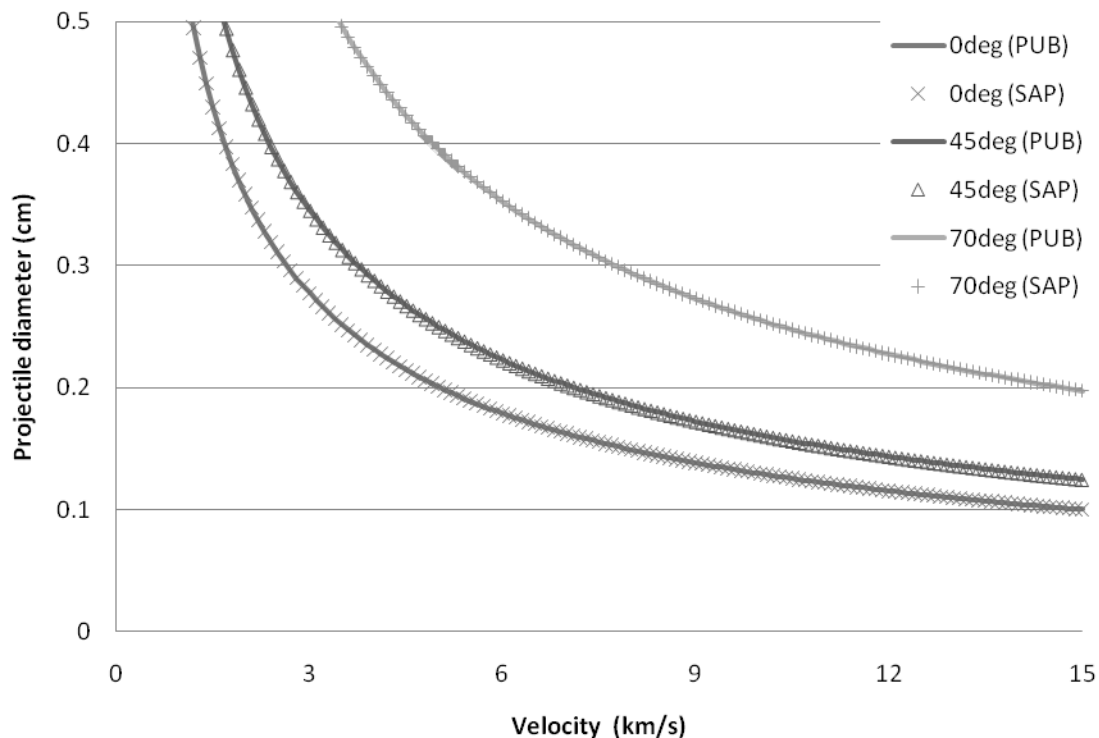| **Shield analysis program inputs**					
Shield type: Single wall					
Analysis: No perforation					
Material: Titanium					
Parameter	*Units*	*Value*	*Parameter*	*Units*	*Value*
Sheet thickness	cm	0.2	Projectile density	g/cm^3	2.8
Sheet density	g/cm^3	7.8	Impact angle	deg	0/45/70
Brinell hardness	HB	N/A	Min. velocity	km/s	0.1
Sound speed	km/s	N/A	Max. velocity	km/s	15
MLI areal density	g/cm^2	0.1			
MLI standoff	cm	N/A			
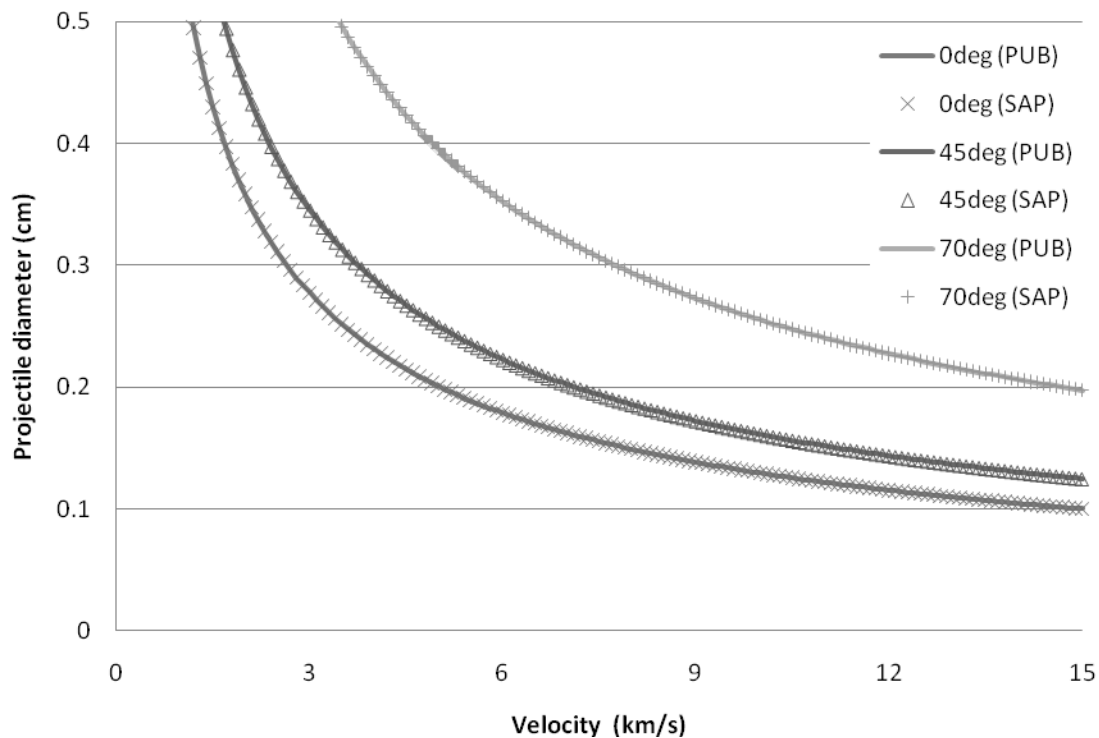
Figure 6: Ballistic limit curves of a representative stainless-steel single wall (with MLI) MMOD shield calculated using the published BLE and the Ballistic Limit Analysis Program (SAP).

50

Fused Silica Single Wall (No Perforation)

BUMPER-STS SHUTTLE VERSION 2.41   STANDARD RISK ANALYSIS OPTION
MAN-MADE DEBRIS ANALYSIS
ORDEM2000 DEBRIS ENVIRONMENT
MAN-MADE DEBRIS CONSTANT DENSITY (2.8 g/cm3)
METRIC UNITS
IMPACT ANGLE CUT-OFF (DEGREES)   =   89.90

PROPERTY ID   1
SINGLE WALL
VESSEL WALL MATERIAL   = FUSED SILICA
PERFORATION FAILURE CRITERIA
WALL THICKNESS (CM)   =   1.4200

Shield analysis program inputs						
Shield type: Single wall						
Analysis: No perforation						
Material: Silica						
Parameter	*Units*	*Value*		*Parameter*	*Units*	*Value*
Sheet thickness	cm	1.5		Projectile density	g/cm^3	2.8
				Impact angle	deg	0/30/60
				Min. velocity	km/s	0.1
				Max. velocity	km/s	15

Figure 7: Ballistic limit curves of a representative fused silica glass single-wall MMOD shield calculated using BUMPER-II and the Ballistic Limit Analysis Program (SAP).

Fused Silica Single Wall (No Detached Spall)

BUMPER-STS SHUTTLE VERSION 2.41   STANDARD RISK ANALYSIS OPTION
MAN-MADE DEBRIS ANALYSIS
ORDEM2000 DEBRIS ENVIRONMENT
MAN-MADE DEBRIS CONSTANT DENSITY (2.8 g/cm3)
METRIC UNITS
IMPACT ANGLE CUT-OFF (DEGREES)   =   89.90

PROPERTY ID   1
SINGLE WALL
VESSEL WALL MATERIAL   = FUSED SILICA
DETACHED SPALL FAILURE CRITERIA
WALL THICKNESS (CM)   =   1.4200

Shield analysis program inputs					
Shield type: Single wall					
Analysis: No spall					
Material: Silica					
Parameter	*Units*	*Value*	*Parameter*	*Units*	*Value*
Sheet thickness	cm	1.5	Projectile density	g/cm^3	2.8
			Impact angle	deg	0/30/60
			Min. velocity	km/s	0.1
			Max. velocity	km/s	15
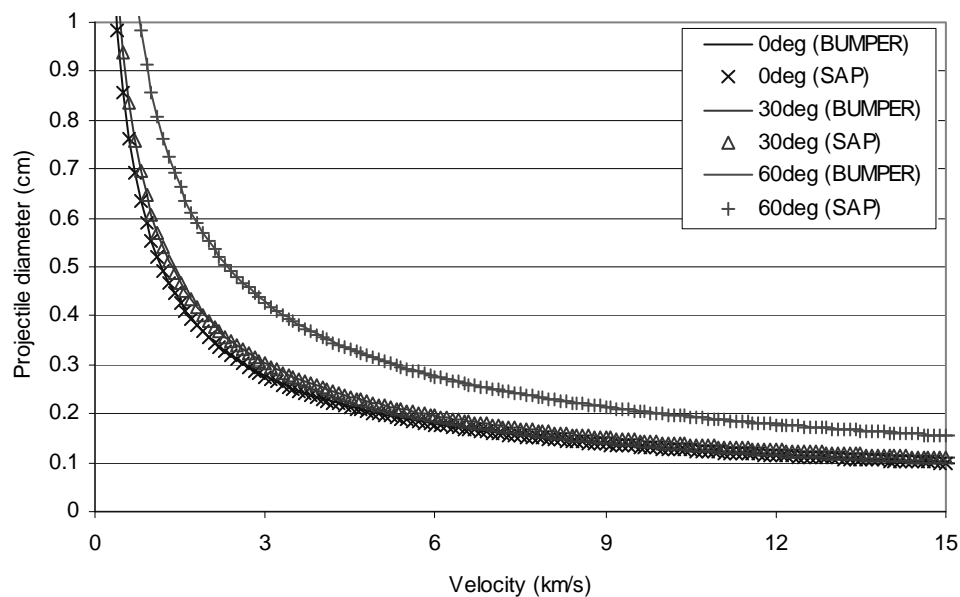
Figure 8: Ballistic limit curves of a representative fused silica glass single-wall MMOD shield calculated using BUMPER-II and the Ballistic Limit Analysis Program (SAP).

Fused Quartz Single Wall (No Perforation)

Source: Unpublished.

Configuration data:
SHEET THICKNESS = 1.5 cm
PROJECTILE DENSITY = 2.8 g/cm^3
IMPACT ANGLE = 0°/45°/70°
NO PERFORATION FAILURE CRITERIA (k = 2.0)

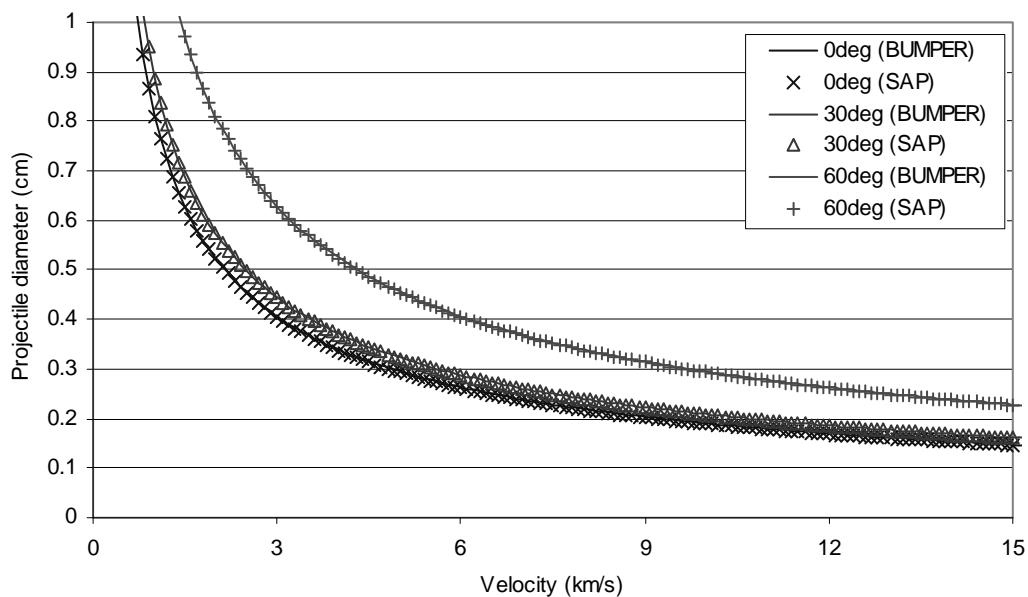| Shield analysis program inputs					
Shield type: Single wall					
Analysis: Penetration based					
Failure criteria: No perforation					
Material: Fused quartz glass					
Parameter	*Units*	*Value*	*Parameter*	*Units*	*Value*
Sheet thickness	cm	1.5	Projectile density	g/cm^3	2.8
			Impact angle	deg	0/45/70
			Min. velocity	km/s	0.1
			Max. velocity	km/s	15
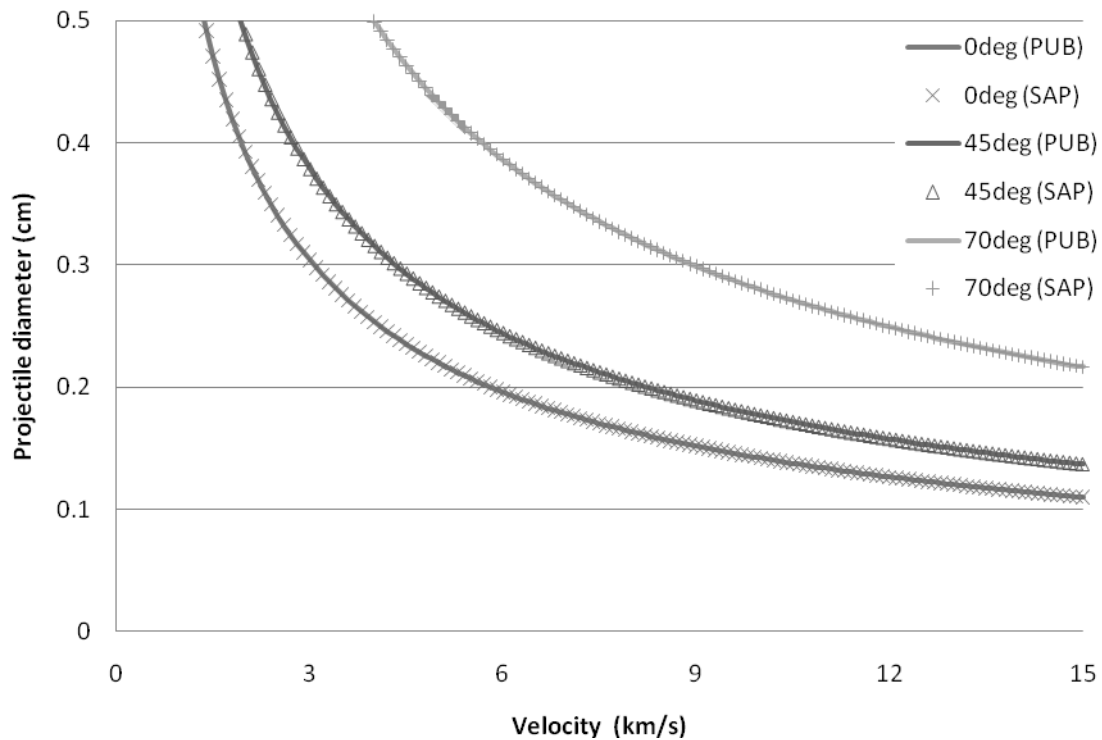
Figure 9: Ballistic limit curves of a representative fused quartz glass single-wall MMOD shield calculated using the BLE and the Ballistic Limit Analysis Program (SAP).

Fused Quartz Single Wall (Maximum crater diameter)

Source: Unpublished.

Configuration data:
SHEET THICKNESS = 1.5 cm
PROJECTILE DENSITY = 2.8 g/cm^3
IMPACT ANGLE = 0°/45°/70°
MAX CRATER DIAMETER = 3.0 cm

Shield analysis program inputs
Shield type: Single wall
Analysis: Cratering based
Max crater diameter: 3 cm
Material: Fused quartz glass

| Parameter	Units	Value	Parameter	Units	Value
Sheet thickness	cm	1.5	Projectile density	g/cm^3	2.8
			Impact angle	deg	0/45/70
			Min. velocity	km/s	0.1
			Max. velocity	km/s	15
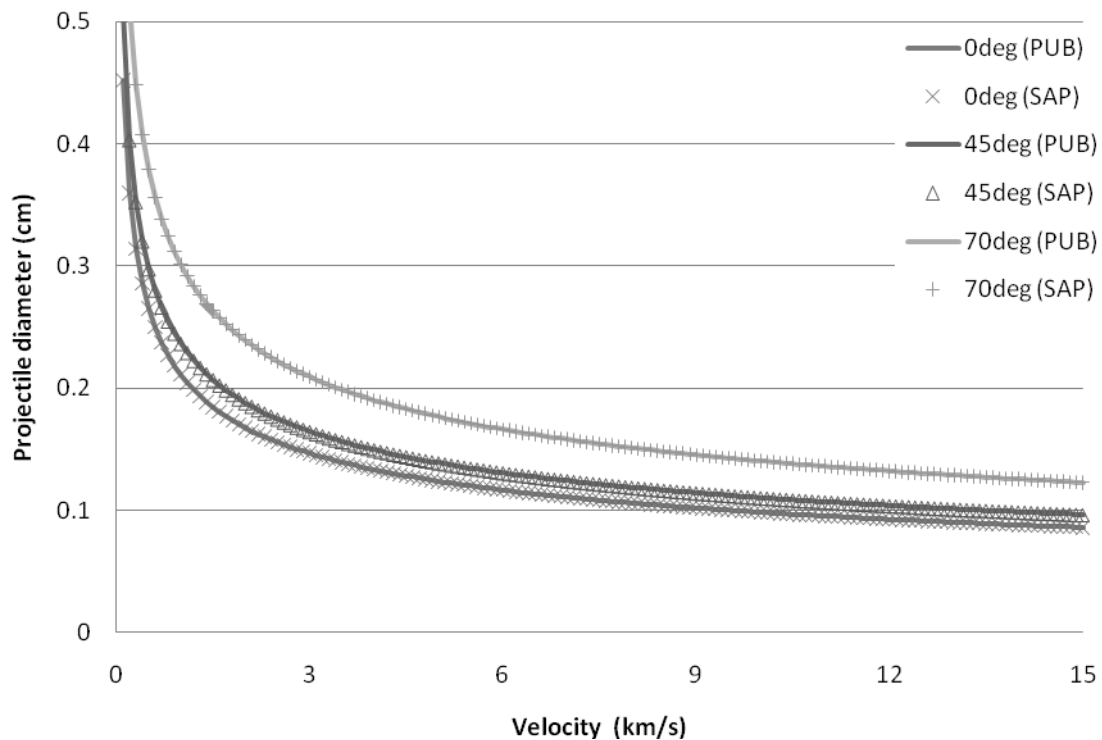
Figure 10: Ballistic limit curves of a representative fused quartz glass single-wall MMOD shield calculated using the BLE and the Ballistic Limit Analysis Program (SAP).

54

Polycarbonate Single Wall (No Perforation)

Configuration data:
SHEET THICKNESS = 0.95 cm
PROJECTILE DENSITY = 2.8 g/cm^3
IMPACT ANGLE = 0°/45°/75°
NO PERFORATION FAILURE CRITERIA

Shield analysis program inputs

Shield type: Single wall
Analysis: Penetration based
Failure criteria: No perforation
Material: Polycarbonate

| Parameter	Units	Value	Parameter	Units	Value
Sheet thickness	cm	0.95	Projectile density	g/cm^3	2.8
			Impact angle	deg	0/45/75
			Min. velocity	km/s	0.1
			Max. velocity	km/s	15
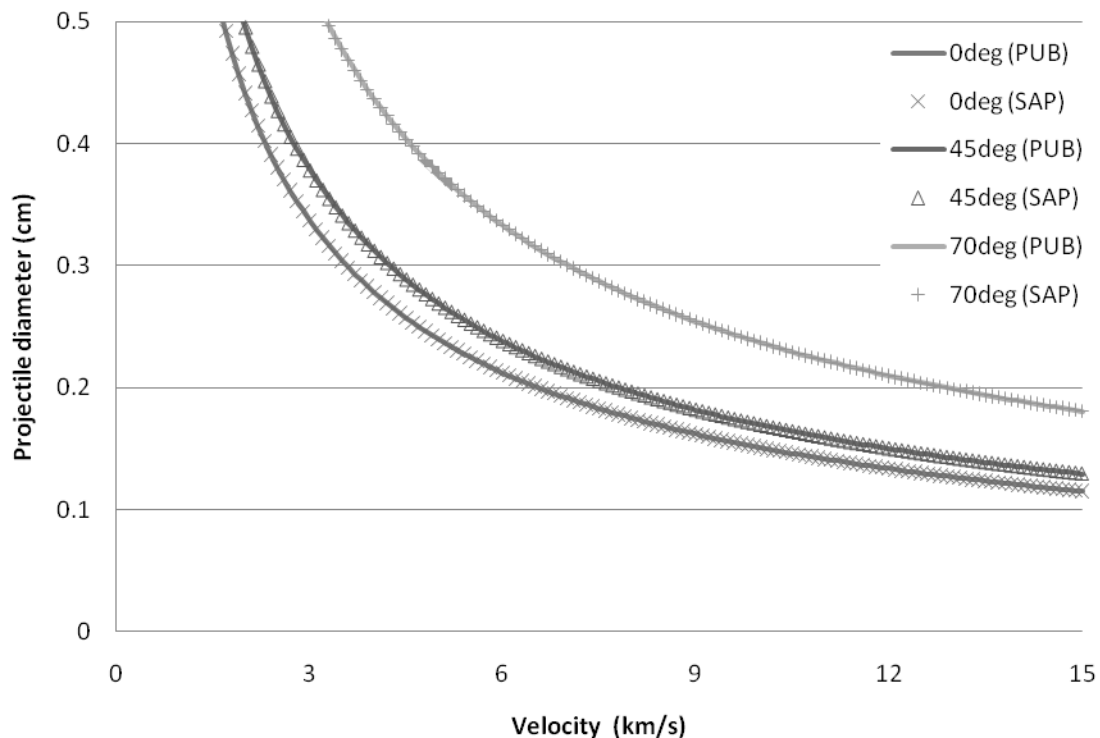
Figure 11: Ballistic limit curves of a representative polycarbonate single-wall MMOD shield calculated using the published BLE and the Ballistic Limit Analysis Program (SAP).

Polycarbonate Single Wall (No Detached Spall)

Source: E. Christiansen, J. Arnold, A. Davis, J. Hyde, D. Lear, J. Liou, F. Lyons, T. Prior, M. Ratliff, S. Ryan, F. Giovane, R. Corsaro, G. Studor, "Handbook for designing MMOD protection." NASA Johnson Space Center, NASA/TM-2009-214785, Houston, 2009.

Configuration data:
SHEET THICKNESS = 0.95 cm
PROJECTILE DENSITY = 2.8 g/cm^3
IMPACT ANGLE = 0°/45°/75°
NO DETACHED SPALL FAILURE CRITERIA

Shield analysis program inputs

Shield type: Single wall
Analysis: Penetration based
Failure criteria: No detached spall
Material: Polycarbonate

| Parameter	Units	Value	Parameter	Units	Value
Sheet thickness	cm	0.95	Projectile density	g/cm^3	2.8
			Impact angle	deg	0/45/75
			Min. velocity	km/s	0.1
			Max. velocity	km/s	15
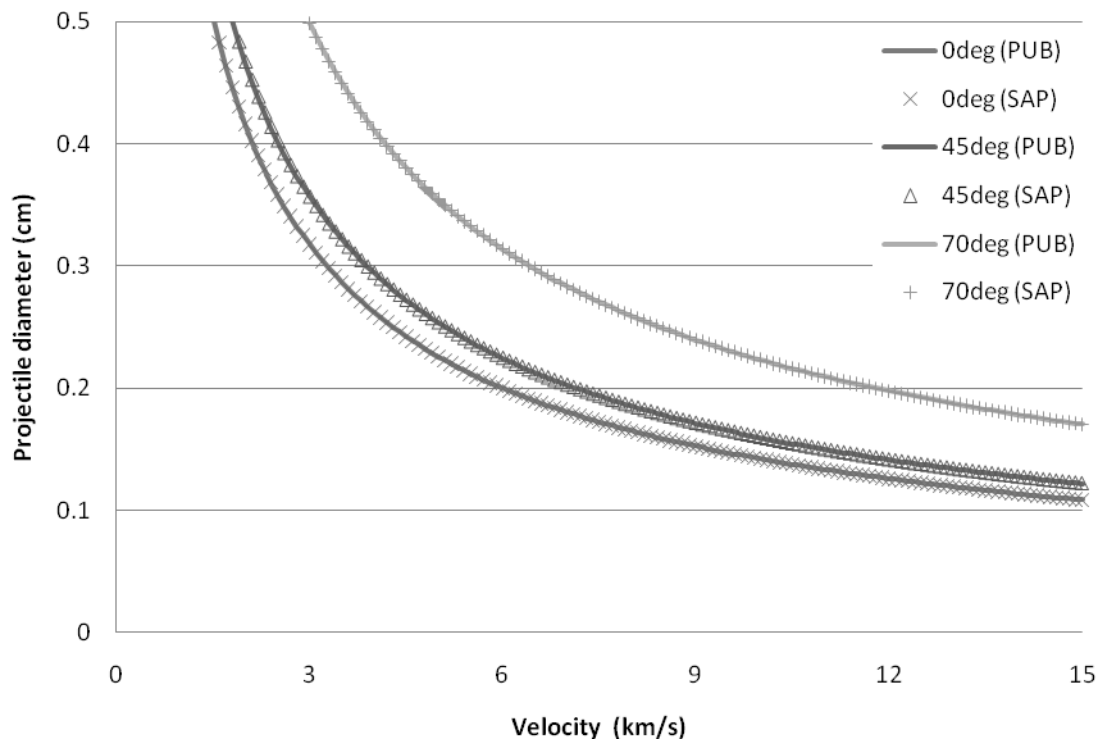
Figure 12: Ballistic limit curves of a representative polycarbonate single-wall MMOD shield calculated using the published BLE and the Ballistic Limit Analysis Program (SAP).

CFRP Single Wall

Source: F.K. Schaefer, E. Schneider, M. Lambert. "Review of Ballistic Limit Equations for CFRP Structure Walls of Satellites."
5th International Conference on Environmental Testing for Space Programs, ESA SP-558, Noordwijk, June 15–17, 2004.

Data from publication:
CFRP PLATE THICKNESS = 0.38 cm
DENSITY OF CFRP = 1.8 g/cm^3
MLI AREAL DENSITY = 0/0.058 g/cm^2
PROJECTILE DENSITY = 2.7 g/cm^3
IMPACT ANGLE = 0°
FAILURE PARAMETER, k = 1.8/3.0 (No Perforation/No Spall)

Shield analysis program inputs

Shield type: Single wall
Analysis: No perforation/No spall
Material: CFRP

Parameter	Units	Value	Parameter	Units	Value
Sheet thickness	cm	0.38	Projectile density	g/cm^3	2.7
Sheet density	g/cm^3	1.8	Impact angle	deg	0
MLI areal density	g/cm^2	0/0.058	Min. velocity	km/s	0.1
MLI standoff	cm	N/A	Max. velocity	km/s	15

Figure 13: Ballistic limit curves of a representative CFRP single-wall MMOD shield calculated from publication (PUB) and using the Ballistic Limit Analysis Program (SAP).

57

Fiberglass Single Wall

Source: E. Christiansen, J. Arnold, A. Davis, J. Hyde, D. Lear, J. Liou, F. Lyons, T. Prior, M. Ratliff, S. Ryan, F. Giovane, R. Corsaro, G. Studor, "Handbook for designing MMOD protection." NASA Johnson Space Center, NASA/TM-2009-214785, Houston, 2009.

Configuration data:
FIBERGLASS PLATE THICKNESS = 0.8 cm
DENSITY OF FIBERGLASS = 1.8 g/cm^3
MLI AREAL DENSITY = 0 g/cm^2
PROJECTILE DENSITY = 2.8 g/cm^3
IMPACT ANGLE = 0°/45°/70°

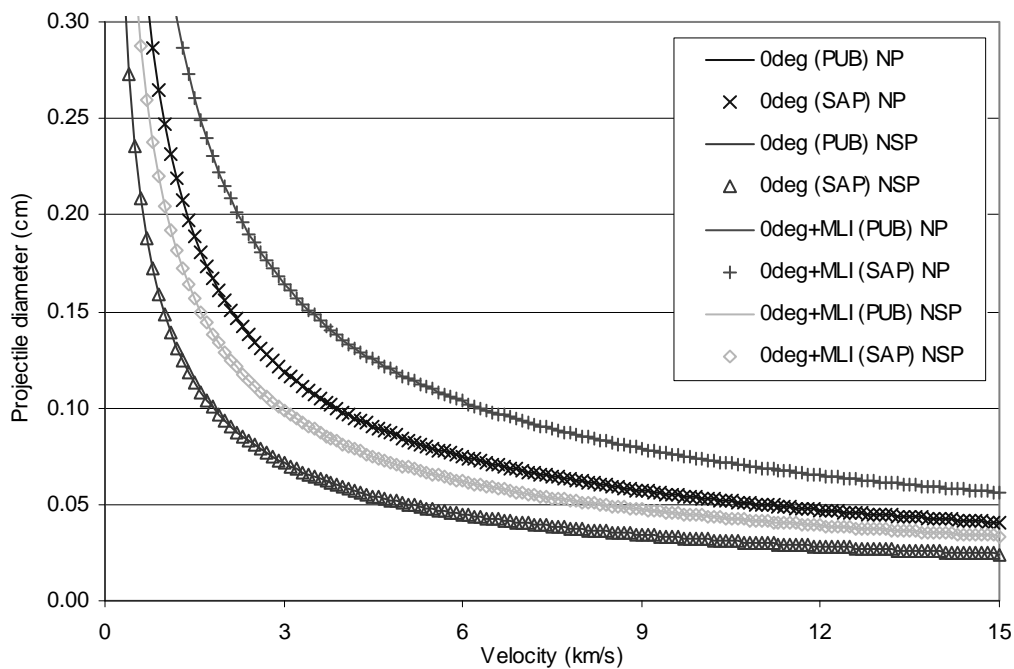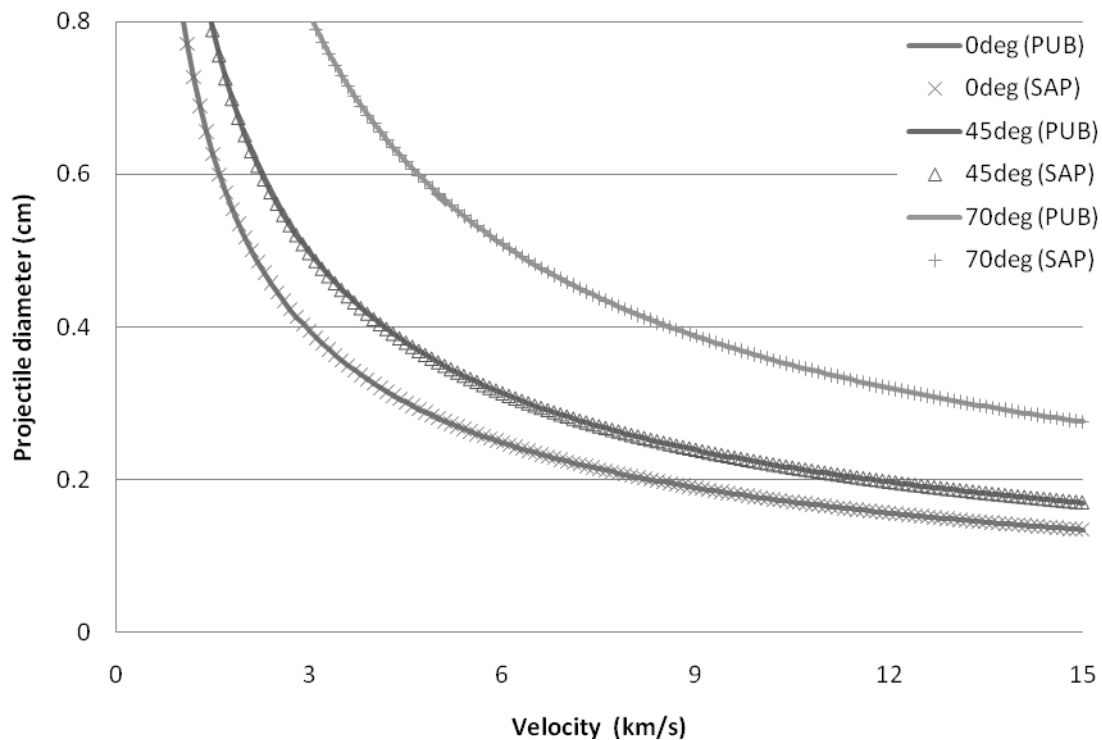| Shield analysis program inputs						
Shield type: Single wall						
Analysis: No perforation						
Material: Fiberglass						
Parameter	*Units*	*Value*		*Parameter*	*Units*	*Value*
Sheet thickness	cm	0.8		Projectile density	g/cm^3	2.8
Sheet density	g/cm^3	1.8		Impact angle	deg	0/45/70
MLI areal density	g/cm^2	0		Min. velocity	km/s	0.1
MLI standoff	cm	N/A		Max. velocity	km/s	15

Figure 14: Ballistic limit curves of a representative CFRP single-wall MMOD shield calculated from publication (PUB) and using the Ballistic Limit Analysis Program (SAP).

Metallic Whipple Shield (No Perforation)

BUMPER-CEV VERSION 1.65r2   ANALYSIS DATE: 22-JUL-09
RESPONSE MODULE SUMMARY FILE
STANDARD RISK ANALYSIS OPTION
MAN-MADE DEBRIS ANALYSIS
ORDEM2000 DEBRIS ENVIRONMENT
 MAN-MADE DEBRIS CONSTANT DENSITY OPTION (2.80 g/cm^3)

PROPERTY ID NUMBER = 1
REIMERDES
UNMODIFIED
SHIELD MATERIAL = 6061-T6
SHIELD THICKNESS (CM) = 0.0500
SHIELD STANDOFF (CM) = 10.0000
REAR WALL MATERIAL = 6061-T6
REAR WALL THICKNESS (CM) =   0.4000
BALLISTIC LIMIT SCALING FACTOR = 1.0000

Shield analysis program inputs

Shield type: Dual-wall
Analysis: No perforation
Configuration: Whipple shield
Bumper material: Al 6061-T6
Rear wall material: Al 6061-T6

Parameter	Units	Value	Parameter	Units	Value
Bumper thickness	cm	0.05	Projectile density	g/cm^3	2.8
Rear wall thickness	cm	0.4	Impact angle	deg	0/30/60/75
Spacing	cm	10	Min. velocity	km/s	0.1
Bumper density	g/cm^3	2.713	Max. velocity	km/s	15
Rear wall yield strength	ksi	35	Shape factor	-	1
MLI areal density	g/cm^2	0			
MLI standoff	cm	N/A			

PROPERTY ID NUMBER = 3
REIMERDES
UNMODIFIED
SHIELD MATERIAL = 6061-T6
SHIELD THICKNESS (CM) = 0.2000
SHIELD STANDOFF (CM) = 10.0000
REAR WALL MATERIAL = 6061-T6
REAR WALL THICKNESS (CM) =   0.4000
BALLISTIC LIMIT SCALING FACTOR = 1.0000

Shield analysis program inputs

Shield type: Dual-wall
Analysis: No perforation
Configuration: Whipple shield
Bumper material: Al 6061-T6
Rear wall material: Al 6061-T6

Parameter	Units	Value	Parameter	Units	Value
Bumper thickness	cm	0.2	Projectile density	g/cm^3	2.8
Rear wall thickness	cm	0.4	Impact angle	deg	0/30/60/75
Spacing	cm	10	Min. velocity	km/s	0.1
Bumper density	g/cm^3	2.713	Max. velocity	km/s	15
Rear wall yield strength	ksi	35	Shape factor	-	1
MLI areal density	g/cm^2	0			
MLI standoff	cm	N/A			

Figure 15: Ballistic limit curves of a metallic Whipple shield calculated using BUMPER-II and the Ballistic Limit Analysis Program (SAP) (property ID = 1).
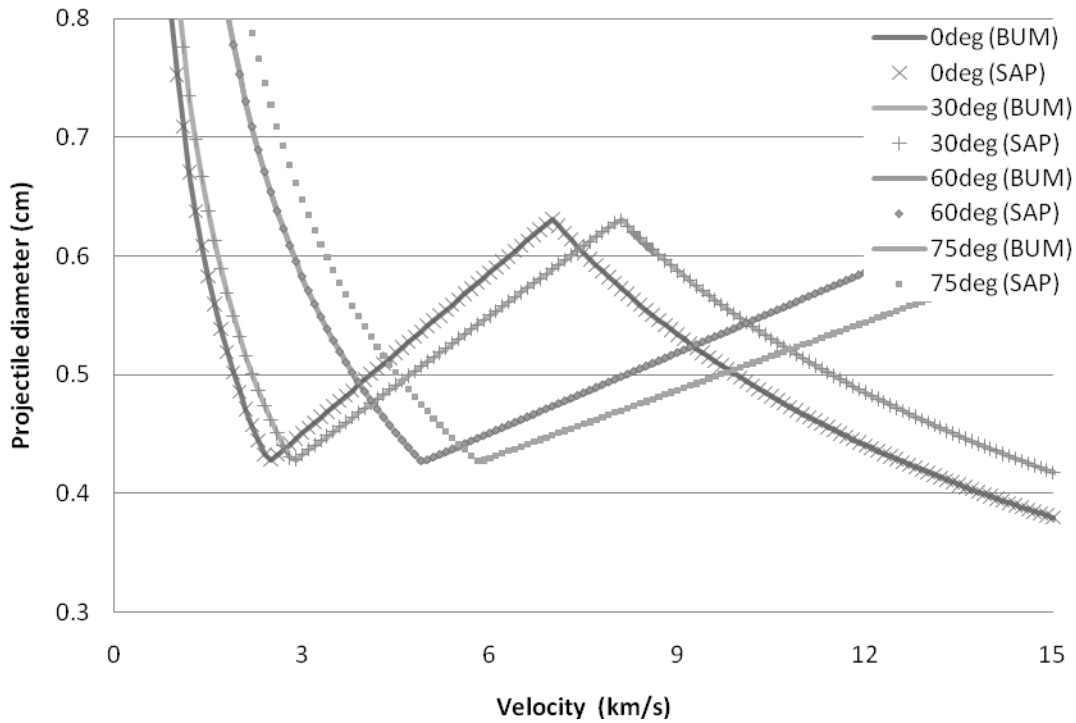
Figure 16: Ballistic limit curves of a metallic Whipple shield calculated using BUMPER-II and the Ballistic Limit Analysis Program (SAP) (property ID = 3).

There is a variation in the calculated performance of a metallic Whipple shield at 75°. Currently, the Reimerdes equation is implemented in BUMPER-II without a cutoff angle. Furthermore, the applied release of BUMPER-II defines a cut-off angle for the new non-optimum equation at 60°. In the Ballistic Limit Analysis Program, the cut-off angle for the new non-optimum equation is set at 65°, according to the validation limits that are defined in [4].

CFRP/Al Honeycomb Sandwich Panel (No Perforation)

Data from publication:
FRONT FACESHEET THICKNESS = 0.145 cm
REAR FACESHEET THICKNESS = 0.145 cm
MLI AREAL DENSITY = 0 g/cm^2
HONEYCOMB THICKNESS = 5.06 cm
CFRP DENSITY = 1.8 g/cm^3
PROJECTILE DENSITY = 2.7 g/cm^3
IMPACT ANGLE = 0°/45°/60°

Shield analysis program inputs					
Shield type: Dual-wall					
Analysis: No perforation					
Configuration: HC SP					
Facesheet material: CFRP					
Parameter	*Units*	*Value*	*Parameter*	*Units*	*Value*
Bumper thickness	cm	0.145	MLI areal density	g/cm^2	0
Rear wall thickness	cm	0.145	MLI standoff	cm	N/A
Spacing	cm	5.06	Projectile density	g/cm^3	2.7
Bumper density	g/cm^3	1.8	Impact angle	deg	0/45/60
Rear wall density	g/cm^3	1.8	Min. velocity	km/s	0.1
Rear wall yield strength	ksi	59.5	Max. velocity	km/s	15

Figure 17: Ballistic limit curves of a honeycomb sandwich panel with CFRP facesheets calculated from publication (PUB) and using the Ballistic Limit Analysis Program (SAP).

Aluminum Honeycomb Sandwich Panel (No Perforation)

Source: M. Lambert, F.K. Schaefer, T. Geyer. "Impact Damage on Sandwich Panels and Multi-Layer Insulation." *Int. J. Impact Eng.*, 26:369–380, 2001.

Data from publication (ATV honeycomb sandwich panel):
FRONT FACESHEET THICKNESS = 0.16 cm
REAR FACESHEET THICKNESS = 0.16 cm
MLI AREAL DENSITY = 0/0.015 g/cm^2
HONEYCOMB THICKNESS = 5 cm
FACESHEET DENSITY = 2.7 g/cm^3
PROJECTILE DENSITY = 2.7 g/cm^3
FACESHEET YIELD STRENGTH = 63.09 ksi
IMPACT ANGLE = 0°/30°/45°/60°/70°

Shield analysis program inputs

Shield type: Dual-wall
Analysis: No perforation
Configuration: HC SP
Facesheet material: Al 2024-T4

Parameter	Units	Value	Parameter	Units	Value
Bumper thickness	cm	0.16	Projectile density	g/cm^3	2.7
Rear wall thickness	cm	0.16	Impact angle	deg	0/30//45/60/70
Spacing	cm	5	Min. velocity	km/s	0.1
Bumper density	g/cm^3	2.7	Max. velocity	km/s	15
Rear wall density	g/cm^3	2.7			
Rear wall yield strength	ksi	63.09			
MLI areal density	g/cm^2	0			
MLI standoff	cm	N/A			

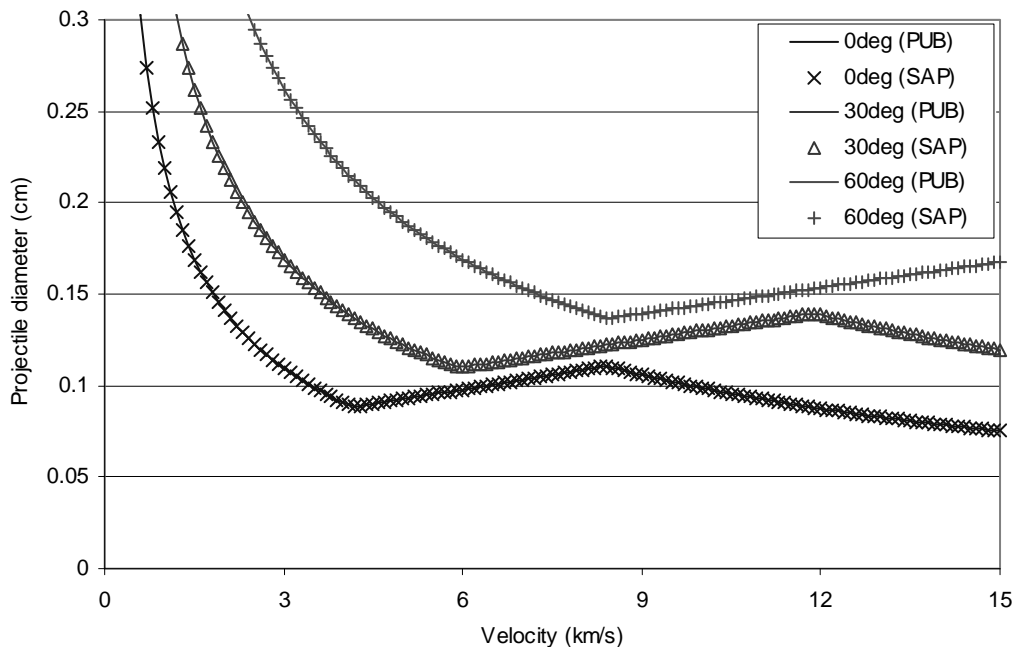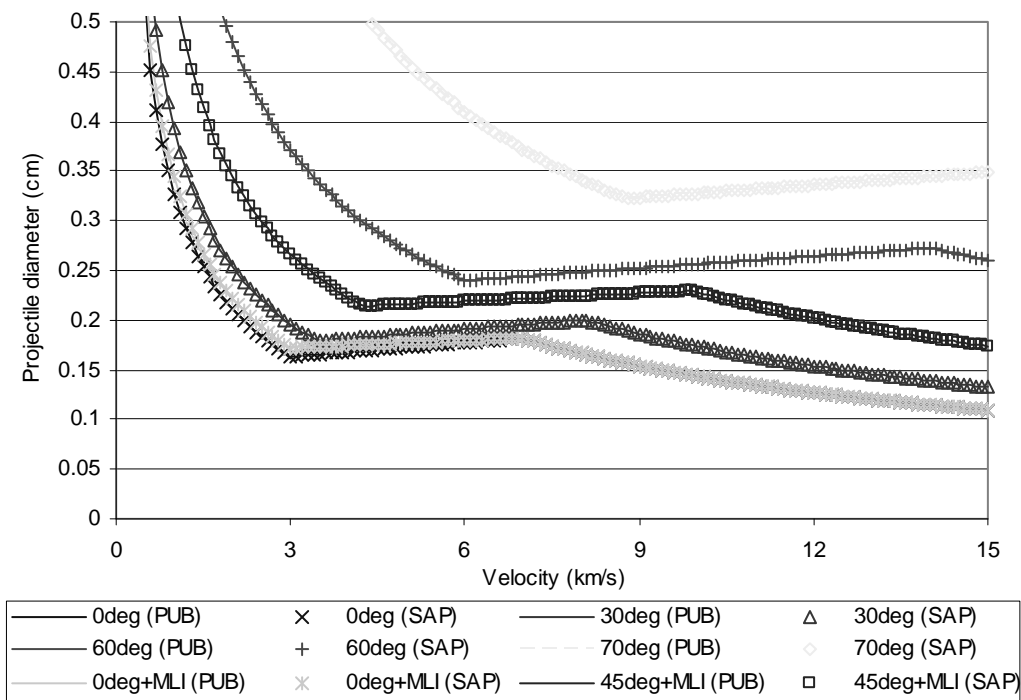**Figure 18:** Ballistic limit curves of an Aluminum honeycomb sandwich panel calculated from publication (PUB) and using the Ballistic Limit Analysis Program (SAP).

Triple wall w/CFRP/Al HC SP (No Perforation)

Source: S. Ryan, F.K. Schaefer, R. Destefanis, M. Lambert. "A Ballistic Limit Equation for Hypervelocity Impacts on CFRP/Al HC Satellite Structures." *Adv. Space Res.*, 41:1152–1166, 2008.

Data from publication:
FRONT FACESHEET THICKNESS = 0.16 cm
REAR FACESHEET THICKNESS = 0.16 cm
REAR WALL THICKNESS = 0.15 cm
MLI AREAL DENSITY = 0 g/cm^2
HONEYCOMB THICKNESS = 5.06 cm
REAR FACESHEET TO REAR WALL SPACING = 10 cm
FACESHEET DENSITY = 1.8 g/cm^3
REAR WALL DENSITY = 2.78 g/cm^3
FACESHEET YIELD STRENGTH = 59.5 ksi
PROJECTILE DENSITY = 2.7 g/cm^3
IMPACT ANGLE = 0°/45°

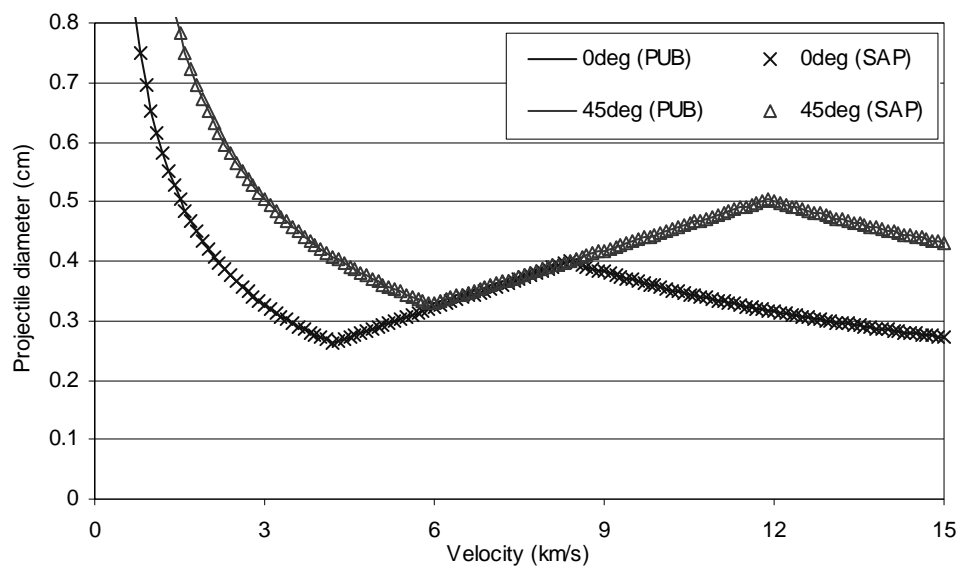| Shield analysis program inputs					
Shield type: Triple wall					
Analysis: No perforation					
Bumper configuration: HC SP					
Outer bumper material: CFRP					
Bumper material: CFRP					
Rear wall material: Al 2024-T4					
Parameter	*Units*	*Value*	*Parameter*	*Units*	*Value*
Outer bumper thickness	cm	0.145	Rear wall yield strength	ksi	59.5
Bumper thickness	cm	0.145	MLI areal density	g/cm^2	0
Rear wall thickness	cm	0.15	MLI standoff	cm	N/A
Outer bumper density	g/cm^3	1.8	Projectile density	g/cm^3	2.7
Bumper density	g/cm^3	1.8	Impact angle	deg	0/30//45/60/70
Rear wall density	g/cm^3	2.78	Min. velocity	km/s	0.1
Spacing (S1)	cm	5.06	Max. velocity	km/s	15
Spacing (S2)	cm	10			

Figure 19: Ballistic limit curves of a triple wall MMOD shield (CFRP/Al HC SP bumper) calculated from publication (PUB) and the Ballistic Limit Analysis Program (SAP).

Triple Wall w/Al HC SP (No Perforation)

Source: F.K. Schaefer, S. Ryan, M. Lambert, R. Putzar. "Ballistic Limit Equation for Equipment Placed Behind Satellite Structure Walls." *Int. J. Impact Eng.*, 35:1784–1791, 2008.

Data from publication (METOP SP + E-box):
FRONT FACESHEET THICKNESS = 0.041 cm
REAR FACESHEET THICKNESS = 0.041 cm
REAR WALL THICKNESS = 0.15 cm
MLI AREAL DENSITY = 0.0447 g/cm^2
HONEYCOMB THICKNESS = 3.5 cm
REAR FACESHEET TO REAR WALL SPACING = 0/10/30 cm
FACESHEET DENSITY = 2.7 g/cm^3
REAR WALL DENSITY = 2.7 g/cm^3
FACESHEET YIELD STRENGTH = 36.26 ksi
PROJECTILE DENSITY = 2.7 g/cm^3
IMPACT ANGLE = 0°/45°

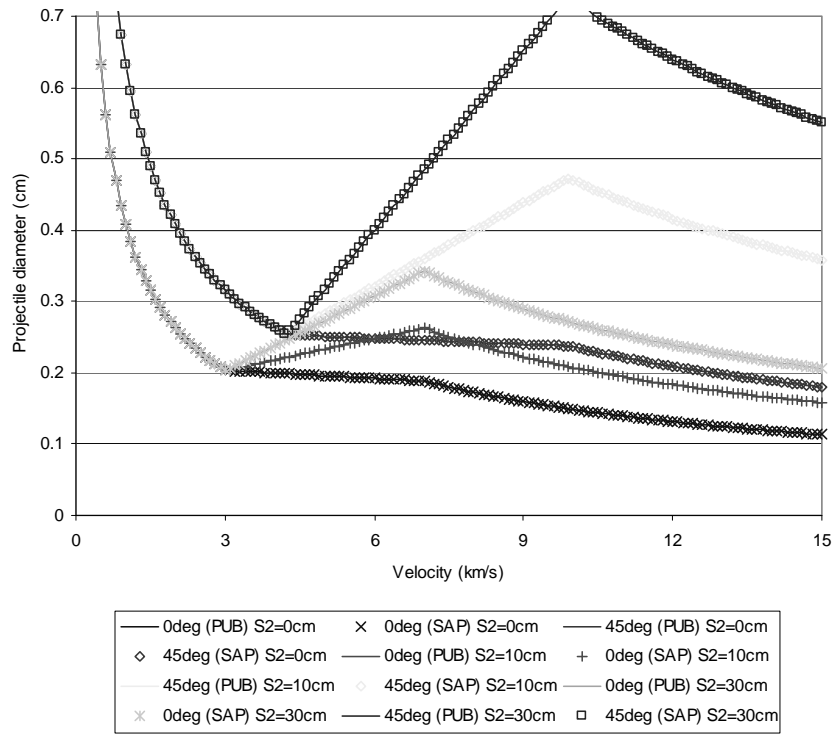| Shield analysis program inputs					
Shield type: Triple wall					
Analysis: No perforation					
Bumper configuration: HC SP					
Outer bumper material: Al 1100-H14					
Bumper material: Al 1100-H14					
Rear wall material: Al 1100-H14					
Parameter	*Units*	*Value*	*Parameter*	*Units*	*Value*
Outer bumper thickness	cm	0.041	Rear wall yield strength	ksi	36.26
Bumper thickness	cm	0.041	MLI areal density	g/cm^2	00447
Rear wall thickness	cm	0.15	MLI standoff	cm	N/A
Outer bumper density	g/cm^3	2.7	Projectile density	g/cm^3	2.7
Bumper density	g/cm^3	2.7	Impact angle	deg	0/45
Rear wall density	g/cm^3	2.7	Min. velocity	km/s	0.1
Spacing (S1)	cm	3.5	Max. velocity	km/s	15
Spacing (S2)	cm	0/10/30			

Figure 20: Ballistic limit curves of a triple wall MMOD shield (Al HC SP bumper) calculated from publication (PUB) and using the Ballistic Limit Analysis Program (SAP).

Nextel Multi-shock Shield w/Aluminum Rear Wall (No Perforation)

BUMPERII VERSION 1.93a ** R E S P O N S E **
MAN-MADE DEBRIS ANALYSIS
ORDEM2000 DEBRIS ENVIRONMENT
MAN-MADE DEBRIS CONSTANT DENSITY (2.8 g/cm3)
METRIC UNITS
IMPACT ANGLE CUT-OFF (DEGREES)   =   89.9000

PROPERTY ID   1
MULTI-WALL
MULTI-SHOCK PENETRATION FUNCTION (89 DEG)
TOTAL SHIELD AREAL DENSITY (G/CM^2) = 0.6000
VESSEL WALL MATERIAL = 2219-T87
VESSEL WALL THICKNESS (CM) = 0.4800

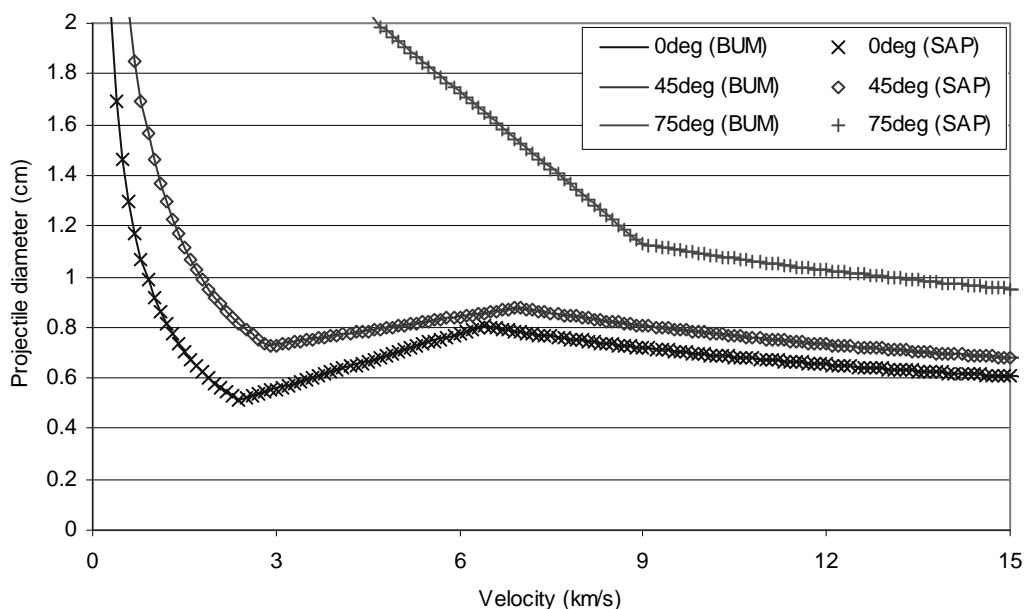| Shield analysis program inputs					
Shield type: Advanced					
Analysis: No perforation					
Configuration: Nextel multi-shock (Aluminum rear wall)					
Rear bumper material: Nextel					
Rear wall material: Al 2219-T87					
Parameter	*Units*	*Value*	*Parameter*	*Units*	*Value*
Total bumper areal density	g/cm^2	0.60	Projectile density	g/cm^3	2.8
Total bumper spacing	cm	6	Impact angle	deg	0/45/75
Rear wall thickness	cm	0.48	Min. velocity	km/s	0.1
Rear wall density	g/cm^3	2.851	Max. velocity	km/s	15
Rear wall yield strength	ksi	52			

Figure 21: Ballistic limit curves of a Nextel MS MMOD shield (w/aluminum rear wall) calculated using BUMPER-II (BUM) and the Ballistic Limit Analysis Program (SAP).

Hybrid Nextel/Aluminum Multi-shock Shield (No Perforation)

BUMPERII VERSION 1.93a ** R E S P O N S E **
MAN-MADE DEBRIS ANALYSIS
ORDEM2000 DEBRIS ENVIRONMENT
MAN-MADE DEBRIS CONSTANT DENSITY (2.8 g/cm3)
METRIC UNITS
IMPACT ANGLE CUT-OFF (DEGREES)   =   89.9000

PROPERTY ID   1
MULTI-WALL
NEXTEL-AL HYBRID PENETRATION FUNCTION (89 DEG)
ALUMINUM WHIPPLE MATERIAL = 6061-T6
SHIELD MATERIAL = NEXTEL – ALUMINUM
TOTAL SHIELD AREAL DENSITY (G/CM^2) = 0.7510
VESSEL WALL MATERIAL = 2219-T87
VESSEL WALL THICKNESS (CM) = 0.4800

Shield analysis program inputs					
Shield type: Advanced					
Analysis: No perforation					
Configuration: Hybrid Nextel/Aluminum multi-shock					
Rear bumper material: Al6061-T6					
Rear wall material: Al 2219-T87					
Parameter	*Units*	*Value*	*Parameter*	*Units*	*Value*
1st bumper areal density	g/cm^2	0.20	Projectile density	g/cm^3	2.8
2nd bumper areal density	g/cm^2	0.20	Impact angle	deg	0/45/60/75
Aluminum bumper areal density	g/cm^2	0.351	Min. velocity	km/s	0.1
Total bumper spacing	cm	6	Max. velocity	km/s	15
Rear wall thickness	cm	0.48			
Rear wall density	g/cm^3	2.851			
Rear wall yield strength	ksi	52			

Figure 22: Ballistic limit curves of a hybrid Nextel/aluminum MS MMOD shield calculated using BUMPER-II (BUM) and the Ballistic Limit Analysis Program (SAP).

There is a discrepancy between the performance of a hybrid Nextel/aluminum MS shield that is calculated using BUMPER-II and the Ballistic Limit Analysis Program for impacts at 45° obliquity (see Figure 22). In the LV regime (i.e., $V \leq VLV$), the angle dependence in the hybrid MS BLE is 7/3 for $\theta \leq 45°$ and 2 for $\theta > 45°$. Numerical rounding errors in BUMPER-II result in the angle-dependence transition occurring when θ should be equal to 45°.

Stuffed Whipple Shield (No Perforation)

BUMPERII VERSION 1.93a ** R E S P O N S E **
MAN-MADE DEBRIS ANALYSIS
ORDEM2000 DEBRIS ENVIRONMENT
MAN-MADE DEBRIS CONSTANT DENSITY (2.8 g/cm3)
METRIC UNITS
IMPACT ANGLE CUT-OFF (DEGREES)   =   89.9000

PROPERTY ID   1
MULTI-WALL
STUFFED WHIPPLE PENETRATION FUNCTION
GENERIC STUFFED WHIPPLE
TOTAL SHIELD AREAL DENSITY (G/CM^2) = 1.3780
VESSEL WALL MATERIAL = 2219-T87
VESSEL WALL THICKNESS (CM) = 0.4800
TOTAL BUMPER SPACING (CM) = 11.4300

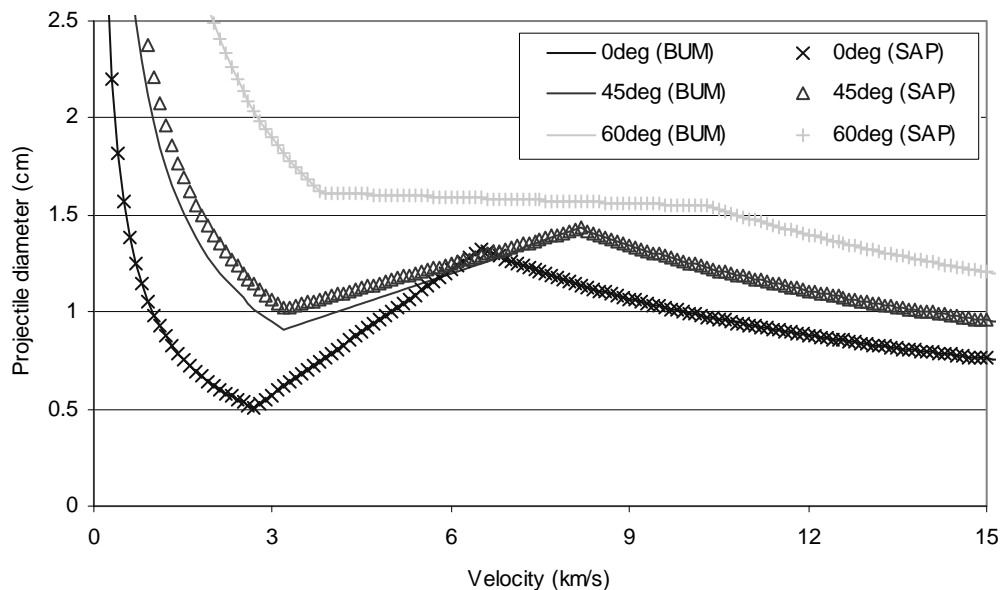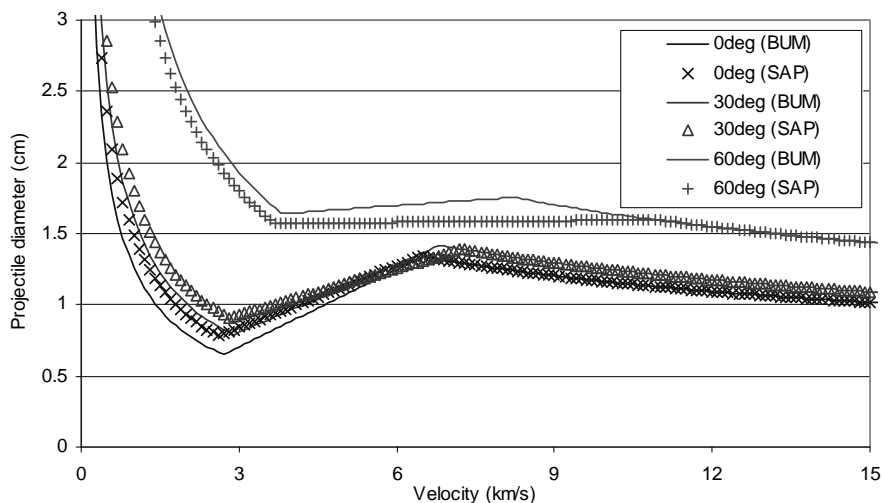| Shield analysis program inputs					
Shield type: Advanced					
Analysis: No perforation					
Configuration: Stuffed Whipple					
Bumper material: Al 2219-T87					
Rear wall material: Al 2219-T87					
Parameter	*Units*	*Value*	*Parameter*	*Units*	*Value*
Bumper thickness	cm	0.20	MLI areal density	g/cm^2	0
Rear wall thickness	cm	0.48	Projectile density	g/cm^3	2.8
Total spacing	cm	11.43	Impact angle	deg	0/30/60
Bumper density	g/cm^3	2.851	Min. velocity	km/s	0.1
Rear wall density	g/cm^3	2.851	Max. velocity	km/s	15
Rear wall yield strength	ksi	52			
Nextel areal density	g/cm^2	0.4039			
Kevlar areal density	g/cm^2	0.4039			

Figure 23: Ballistic limit curves of a Nextel/Kevlar® stuffed Whipple shield calculated using BUMPER-II (BUM) and the Ballistic Limit Analysis Program (SAP).

The performance of a stuffed Whipple shield calculated in BUMPER-II varies from that evaluated in the Ballistic Limit Analysis Program (see Figure 23). For normal and low-obliquity impacts ($\theta <$ ~45°), BUMPER-II predicts a lower critical projectile diameter in the low and intermediate regimes. At higher angles of obliquity, the performance that is predicted in BUMPER-II exceeds that predicted by the Ballistic Limit Analysis Program. This version of BUMPER-II uses an unpublished stuffed Whipple shield ballistic limit equation that varies in LV angle dependence, LV scaling coefficient, and the transition velocities (low-intermediate and intermediate-HV) from that used in the Ballistic Limit Program.

Ceramic Tile (LI-900) Thermal Protection System w/Substructure (No Perforation)

BUMPERII-S VERSION 2.32f1 ** R E S P O N S E **
MAN-MADE DEBRIS ANALYSIS
ORDEM2000 DEBRIS ENVIRONMENT
MAN-MADE DEBRIS CONSTANT DENSITY (2.8 g/cm3)
METRIC UNITS
IMPACT ANGLE CUT-OFF (DEGREES)   =   60.0000

PROPERTY ID   1
SINGLE WALL
VESSEL WALL MATERIAL = 6061-T6 ALUMINUM
TPS PENETRATION FUNCTIONS
TPS THICKNESS (CM) = 3.0000
TPS DENSITY (G/CM^2) = 0.2400
HONEYCOMB THICKNESS (CM) = 1.5000
VESSEL WALL THICKNESS (CM) = 1.5000
% PENETRATION DEPTH (CM) = 100.00

Shield analysis program inputs

Shield type: TPS
Analysis: No perforation
Configuration: LI-900
Skin type: Honeycomb sandwich panel
Skin material: Al 6061-T6

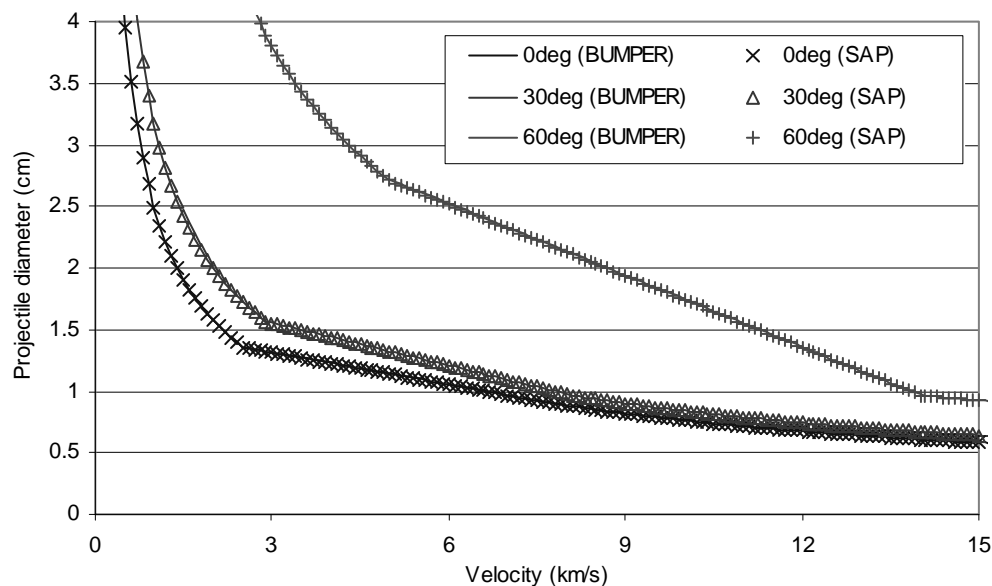| Parameter	Units	Value	Parameter	Units	Value
Tile thickness	cm	3.0	Projectile density	g/cm^3	2.8
Tile density	g/cm^3	0.24	Impact angle	deg	0/30/60
SIP areal density	g/cm^2	0.18	Min. velocity	km/s	0.1
Skin thickness	cm	0.75	Max. velocity	km/s	15
Skin density	g/cm^3	2.713			
Honeycomb sandwich panel thickness	cm^3	1.5			
Skin yield strength	ksi	35			

Figure 24: Ballistic limit curves of a ceramic tile TPS (w/honeycomb sandwich panel skin) calculated using BUMPER-II and the Ballistic Limit Analysis Program (SAP).

Ceramic Tile (LI-2200) Thermal Protection System (No Perforation)

Source: E. Christiansen, J. Arnold, A. Davis, J. Hyde, D. Lear, J. Liou, F. Lyons, T. Prior, M. Ratliff, S. Ryan, F. Giovane, R. Corsaro, G. Studor, "Handbook for designing MMOD protection." NASA Johnson Space Center, NASA/TM-2009-214785, Houston, 2009.

Configuration data:
MAXIMUM PENETRATION DEPTH = 0.75 cm
TILE DENSITY = 0.24 g/cm^3
PROJECTILE DENSITY = 2.8 g/cm^3
IMPACT ANGLE = 0°/45°/70°

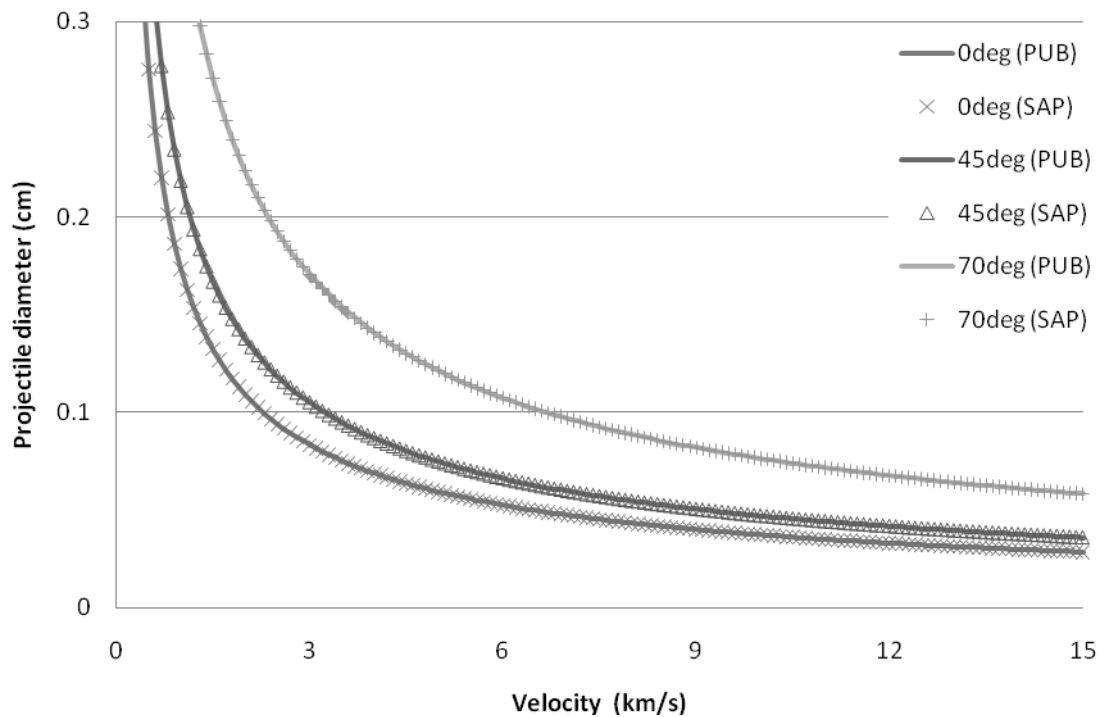| Shield analysis program inputs					
Shield type: TPS					
Analysis: No perforation					
Configuration: LI-2200					
Skin type: None					
Skin material:					
Allowable pen. depth (%): 25					
Parameter	*Units*	*Value*	*Parameter*	*Units*	*Value*
Tile thickness	cm	3.0	Projectile density	g/cm^3	2.8
Tile density	g/cm^3	0.24	Impact angle	deg	0/45/70
SIP areal density	g/cm^2	N/A	Min. velocity	km/s	0.1
Skin thickness	cm	N/A	Max. velocity	km/s	15
Skin density	g/cm^3	N/A			
Honeycomb sandwich panel thickness	cm^3	N/A			
Skin yield strength	ksi	N/A			

Figure 25: Ballistic limit curves of an AETB ceramic tile TPS (no substructure) calculated using the published BLE and the Ballistic Limit Analysis Program (SAP).

73

Ceramic Tile (AETB-8) Thermal Protection System (No Perforation)

Source: E. Christiansen, J. Arnold, A. Davis, J. Hyde, D. Lear, J. Liou, F. Lyons, T. Prior, M. Ratliff, S. Ryan, F. Giovane, R. Corsaro, G. Studor, "Handbook for designing MMOD protection." NASA Johnson Space Center, NASA/TM-2009-214785, Houston, 2009.

Configuration data:
MAXIMUM PENETRATION DEPTH = 0.75 cm
TILE DENSITY = 0.24 g/cm^3
PROJECTILE DENSITY = 2.8 g/cm^3
IMPACT ANGLE = 0°/45°/70°

Shield analysis program inputs

Shield type: TPS
Analysis: No perforation
Configuration: AETB-8
Skin type: Honeycomb sandwich panel
Skin material: Graphite-Cyanate composite
Allowable pen. depth (%): N/A

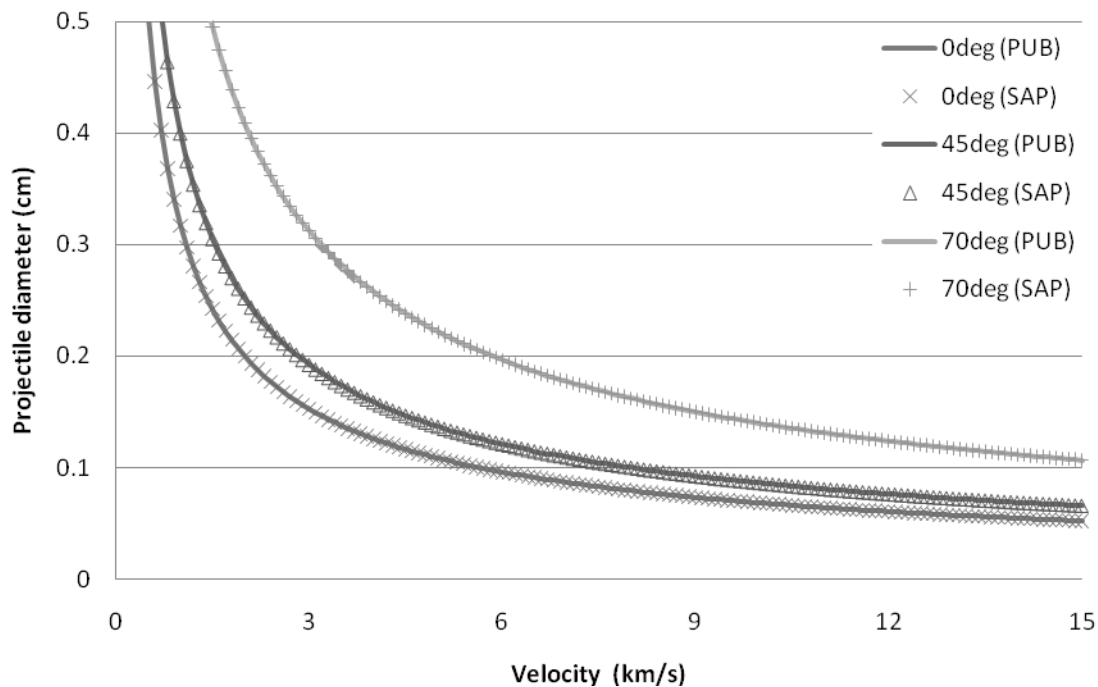| Parameter	Units	Value	Parameter	Units	Value
Tile thickness	cm	5.1	Projectile density	g/cm^3	2.8
Tile density	g/cm^3	0.24	Impact angle	deg	0/45/70
SIP areal density	g/cm^2	0.18	Min. velocity	km/s	0.1
Skin thickness	cm	0.2	Max. velocity	km/s	15
Skin density	g/cm^3	1.564			
Honeycomb sandwich panel thickness	cm^3	3.4			
Skin yield strength	ksi	450			

Figure 26: Ballistic limit curves of a LI-2200 ceramic tile TPS (no substructure) calculated using the published BLE and the Ballistic Limit Analysis Program (SAP).

Ceramic Tile (AETB-8) TPS w/Substructure (No Perforation)

Source: E. Christiansen, J. Arnold, A. Davis, J. Hyde, D. Lear, J. Liou, F. Lyons, T. Prior, M. Ratliff, S. Ryan, F. Giovane, R. Corsaro, G. Studor, "Handbook for designing MMOD protection." NASA Johnson Space Center, NASA/TM-2009-214785, Houston, 2009.

Configuration data:
PROJECTILE DENSITY = 2.8 g/cm^3
NO SUBSTRUCTURE PERFORATION FAILURE MODE

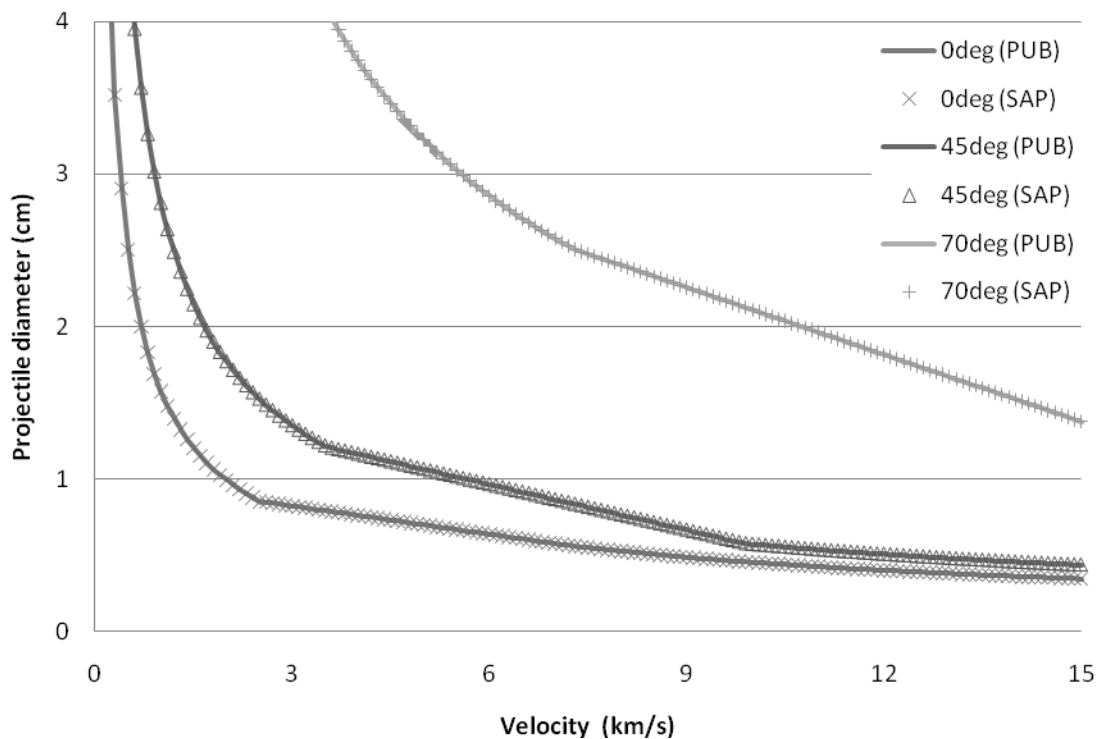| **Shield analysis program inputs**					
Shield type: TPS					
Analysis: No perforation					
Configuration: AETB-8					
Skin type: None					
Skin material: N/A					
Allowable pen. depth (%): 25					
Parameter	*Units*	*Value*	*Parameter*	*Units*	*Value*
Tile thickness	cm	5.1	Projectile density	g/cm^3	2.8
Tile density	g/cm^3	0.24	Impact angle	deg	0/45/70
SIP areal density	g/cm^2	N/A	Min. velocity	km/s	0.1
Skin thickness	cm	N/A	Max. velocity	km/s	15
Skin density	g/cm^3	N/A			
Honeycomb sandwich panel thickness	cm^3	N/A			
Skin yield strength	ksi	N/A			

Figure 27: Ballistic limit curves of a LI-2200 ceramic tile TPS (graphite-cyanate face-sheeted honeycomb sandwich panel substructure) calculated using the published BLE and the Ballistic Limit Analysis Program (SAP).

RCC Thermal Protection System (No Perforation)

BUMPER-STS SHUTTLE VERSION 2.41   STANDARD RISK ANALYSIS OPTION
MAN-MADE DEBRIS ANALYSIS
ORDEM2000 DEBRIS ENVIRONMENT
MAN-MADE DEBRIS CONSTANT DENSITY (2.8 g/cm3)
METRIC UNITS
IMPACT ANGLE CUT-OFF (DEGREES)   =   89.9000

PROPERTY ID   1
SINGLE WALL
RCC THRESHOLD PERFORATION FAILURE CRITERIA
VESSEL WALL MATERIAL = RCC
VESSEL WALL THICKNESS (CM) = 0.7000
RCC PERFORATION THRESHOLD (CM) = 0.3040

Shield analysis program inputs

Shield type: TPS
Analysis: No perforation
Configuration: RCC

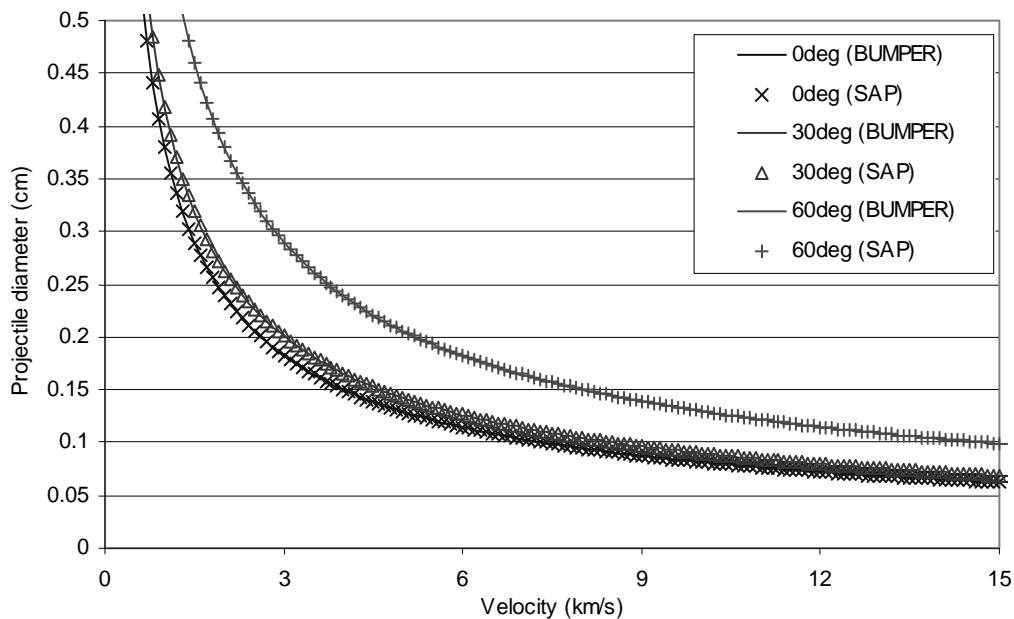| Parameter	Units	Value	Parameter	Units	Value
RCC thickness	cm	0.7	Projectile density	g/cm^3	2.8
RCC density	g/cm^3	1.62	Impact angle	deg	0/30/60
			Min. velocity	km/s	0.1
			Max. velocity	km/s	15

Figure 28: Ballistic limit curves of an RCC panel calculated using BUMPER-II and the Ballistic Limit Analysis Program (SAP).

Avcoat Ablative Heat Shield (No Perforation)

BUMPER-CEV VERSION 1.62-BETA1   STANDARD RISK ANALYSIS OPTION
MAN-MADE DEBRIS ANALYSIS
ORDEM2000 DEBRIS ENVIRONMENT
MAN-MADE DEBRIS CONSTANT DENSITY (2.8 g/cm3)

PROPERTY ID   1
AVCOAT ABLATOR
ABLATOR THICKNESS (CM) = 3.1000
DEPTH OF CRITICAL PENETRATION INTO ABLATOR (%) = 25.0000
BALLISTIC LIMIT SCALING FACTOR = 1.0000

Shield analysis program inputs
Shield type: TPS
Analysis: No perforation
Configuration: Avcoat
Allowable pen. depth (%): 25

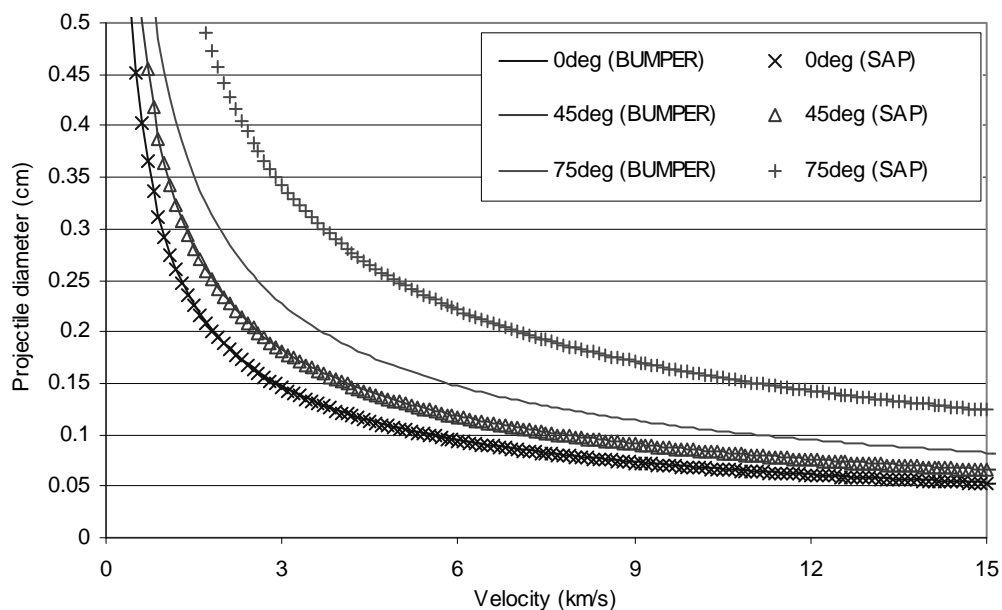| Parameter	Units	Value	Parameter	Units	Value
Avcoat thickness	cm	3.1	Projectile density	g/cm^3	2.8
Avcoat density	g/cm^3	0.5	Impact angle	deg	0/45/75
			Min. velocity	km/s	0.1
			Max. velocity	km/s	15

Figure 29: Ballistic limit curves of an Avcoat ablative heat shield calculated using BUMPER-II and the Ballistic Limit Analysis Program (SAP).

In the version of BUMPER-II that was used to calculate the ballistic limit curves for the Avcoat ablator that was shown in Figure 29, a cutoff angle of 60° is applied. As a result, the Ballistic Limit Analysis program predicts a significantly higher ballistic limit for impact at 75° (shown in Figure 29). In the upcoming releases of BUMPER-II, the angle dependence will be removed.

PICA Ablative Heat Shield (No Perforation)

Source: E. Christiansen, J. Arnold, A. Davis, J. Hyde, D. Lear, J. Liou, F. Lyons, T. Prior, M. Ratliff, S. Ryan, F. Giovane, R. Corsaro, G. Studor, "Handbook for designing MMOD protection." NASA Johnson Space Center, NASA/TM-2009-214785, Houston, 2009.

Configuration data:
ABLATOR THICKNESS = 5.1 cm
ABLATOR DENSITY = 0.24 g/cm^3

PROJECTILE DENSITY = 2.8 g/cm^3
IMPACT ANGLE = 0°/45°/70°
DEPTH OF CRITICAL PENETRATION INTO ABLATOR (%) = 25.0000

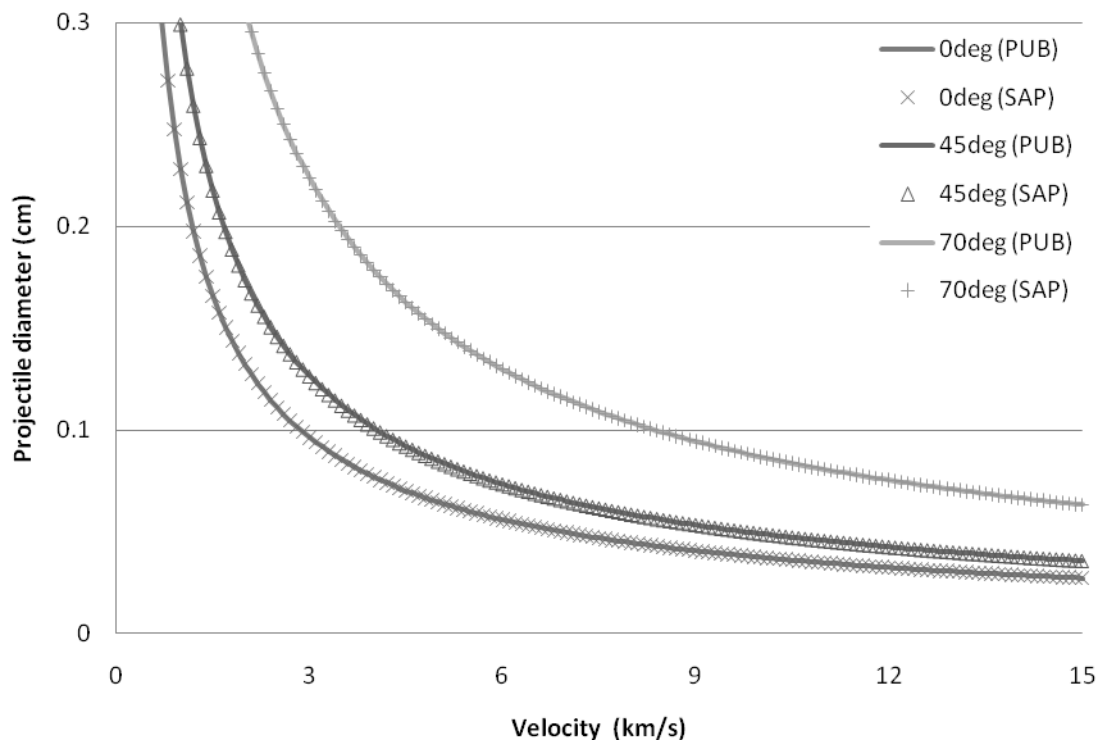| **Shield analysis program inputs**					
Shield type: TPS					
Configuration: Ablator					
Material: PICA					
Allowable pen. depth (%): 25					
Parameter	*Units*	*Value*	*Parameter*	*Units*	*Value*
Ablator thickness	cm	5.1	Projectile density	g/cm^3	2.8
Ablator density	g/cm^3	0.24	Impact angle	deg	0/45/70
			Min. velocity	km/s	0.1
			Max. velocity	km/s	15

Figure 30: Ballistic limit curves of a PICA ablative heat shield calculated from the published BLE and the Ballistic Limit Analysis Program (SAP).

1. AGENCY USE ONLY *(Leave Blank)*	2. REPORT DATE September 2009	3. REPORT TYPE AND DATES COVERED Technical Memorandum	

4. TITLE AND SUBTITLE Micrometeoroid and Orbital Debris (MMOD) Shield Ballistic Limit Analysis Program		5. FUNDING NUMBERS
6. AUTHOR(S) Shannon Ryan*; Eric L. Christiansen**		

7. PERFORMING ORGANIZATION NAME(S) AND ADDRESS(ES) *USRA Lunar and Planetary Institute, NASA Johnson Space Center; **Lyndon B. Johnson Space Center, Houston	8. PERFORMING ORGANIZATION REPORT NUMBERS S-1043
9. SPONSORING/MONITORING AGENCY NAME(S) AND ADDRESS(ES) National Aeronautics and Space Administration Washington, DC 20546-0001	10. SPONSORING/MONITORING AGENCY REPORT NUMBER TM-2009-214789

11. SUPPLEMENTARY NOTES *NASA Johnson Space Center

12a. DISTRIBUTION/AVAILABILITY STATEMENT Unclassified/Unlimited Available from the NASA Center for AeroSpace Information (CASI) 7115 Standard Drive Hanover, MD 21076-1320 Category: 61	12b. DISTRIBUTION CODE

13. ABSTRACT *(Maximum 200 words)*

A software program has been developed that enables the user to quickly and simply perform ballistic limit calculations for shield configurations that are subject to hypervelocity meteoroid/orbital debris (MMOD) impacts. This analysis program consists of two core modules: a design module and a performance module. The design module enables a user to calculate preliminary dimensions of a shield configuration (e.g., thicknesses/areal densities, spacing, etc.) for a "design" particle (diameter, density, impact velocity, incidence). The performance module enables a more detailed shielding analysis, providing the performance of a user-defined shielding configuration over the range of relevant in-orbit impact conditions.

14. SUBJECT TERMS computer programs, software engineering; shielding; micrometeoroids; space debris; hypervelocity projectiles; impact damage; meteoritic damage	15. NUMBER OF PAGES 94	16. PRICE CODE

17. SECURITY CLASSIFICATION OF REPORT Unclassified	18. SECURITY CLASSIFICATION OF THIS PAGE Unclassified	19. SECURITY CLASSIFICATION OF ABSTRACT Unclassified	20. LIMITATION OF ABSTRACT Unlimited